CCMS-86-04

VIRGINIA TECH

CENTER FOR COMPOSITE MATERIALS AND STRUCTURES

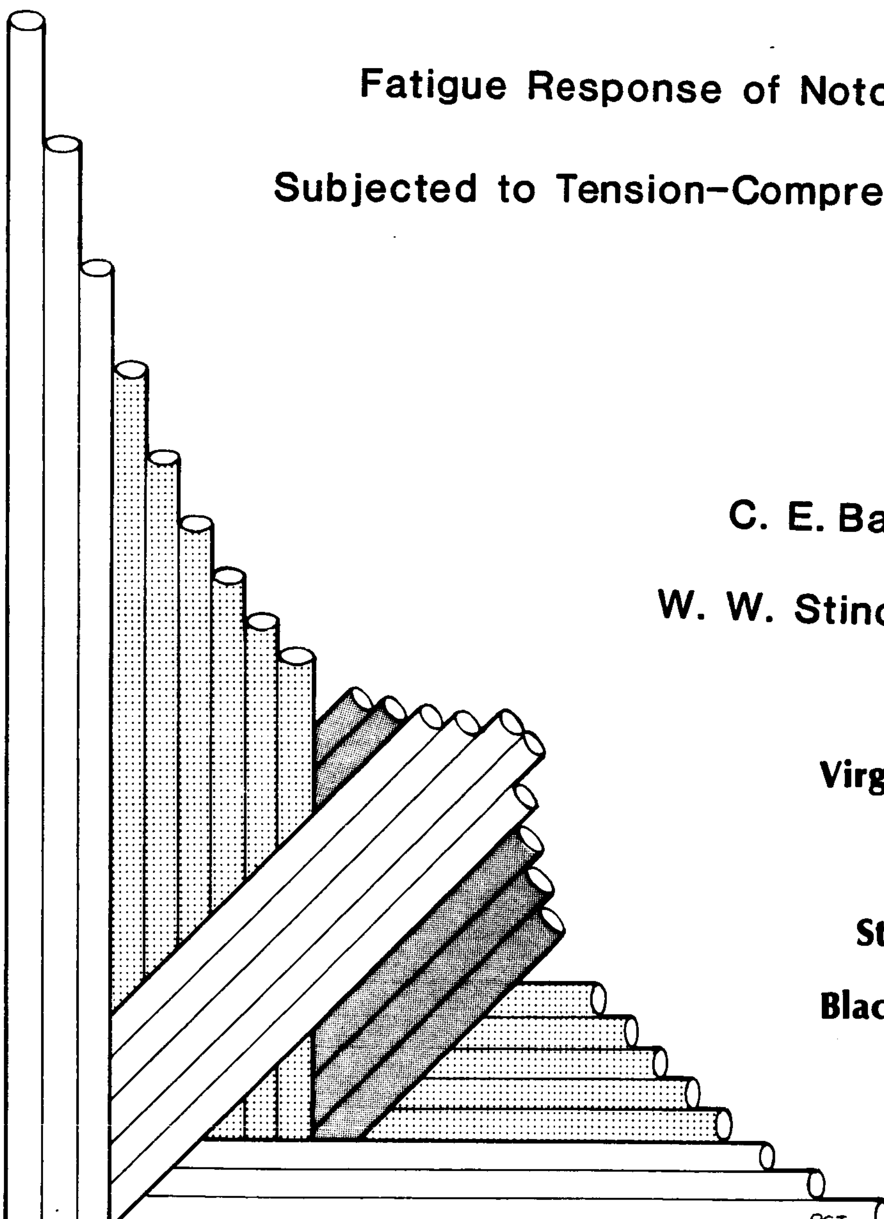

Fatigue Response of Notched Laminates Subjected to Tension-Compression Cyclic Loads

C. E. Bakis

W. W. Stinchcomb

Virginia Polytechnic Institute and State University
Blacksburg, Virginia 24061

(NASA-CR-179804) FATIGUE RESPONSE OF NOTCHED LAMINATES SUBJECTED TO TENSION-COMPRESSION CYCLIC LOADS Interim Report (Virginia Polytechnic Inst. and State Univ.) 201 p CSCL 11D G3/24

N87-10183

Unclas 44300

June 1986

FATIGUE RESPONSE OF NOTCHED LAMINATES SUBJECTED TO TENSION-COMPRESSION CYCLIC LOADS

C. E. Bakis[1] and W. W. Stinchcomb[2]
Materials Response Group
Virginia Polytechnic Institute and State University
Blacksburg, VA, USA 24061-4899

Interim Report
Grant Number NAG-1-343
NASA Langley Research Center
Hampton, Virginia 23665

[1]Graduate Project Assistant
[2]Professor

ABSTRACT

The fatigue response of a $[(0/45/90/-45)_s]_4$ T300-5208 graphite-epoxy laminate with a drilled center-hole subjected to various components of tensile and compressive cyclic loads was investigated. Damage evaluation techniques such as stiffness monitoring, penetrant-enhanced X-ray radiography, C-scan, laminate deply and residual strength measurement were used to establish the mechanisms of damage development as well as the effect of such damage on the laminate strength, stiffness and life. Damage modes consisted of transverse matrix cracks, initiating at the hole, in all plies, followed by delamination between plies of different orientation. Matrix cracks had a significant effect on delamination initiation and growth. Certain ply interfaces, appearing at regular intervals through the laminate's thickness, displayed earlier delamination initiation and a greater delamination growth rate when located closer to the laminate's surface. A characteristic stiffness response during cyclic loading at two load levels was identified and utilized a more reliable indicator of material and residual properties than accumulated cycles. For the load ratios of tension-compression loading used in this investigation, residual tensile strength increased significantly above the virgin strength early in the fatigue life and remained approximately constant to near the end of life. Failure was always precipitated by large delaminations that disabled the laminate's ability to sustain the compressive load. A simple technique developed for predicting delamination initiation sites along the hole boundary correlated well with experimental evidence.

TABLE OF CONTENTS

LIST OF FIGURES

Figure

page

Chapter I

INTRODUCTION AND LITERATURE SURVEY

The study of fiber-reinforced composite materials has been an active area of research in the fields of solid mechanics and materials science for the past fifteen years. Much of this research is driven by the needs of the aerospace industries, where the special structural properties of composites enable high performance, lightweight designs. For example, weight savings of 20 percent (over metals) have already been achieved in current production military aircraft components, and up to 40 percent savings in spacecraft structures [1]. Faced with the uncertainty of fuel costs, land and sea transportation industries are also searching for ways to travel longer distances and carry more payload with less fuel consumption. Fiber-reinforced composites are ideal for applications such as these because their strength and elastic properties can be tailored to meet specific design requirements. These structural properties are often superior to those of commonly available materials when material density is considered. Particular thermal and moisture expansion characteristics can be designed into a structure as well.

A composite material, by definition, consists of more than one constituent material. One commonly recognizes these constituent materials as being separate on the macroscopic scale, as opposed to the microscopic or molecular scale. An important reason for using structural composites is that a combination of at least two materials may have more desirable properties and may be more economical than any of the same materials taken alone. Designers long ago realized the advantages of reinforcing materials that were readily obtainable but lacking in durability and strength. As examples, consider the composites of mud and straw for building applications, and more recently, steel reinforced concrete for a variety of structural applications.

In this study, the material considered is of the lightweight, high strength and stiffness family of fiber reinforced polymers. In particular, these are composites of unidirectional, high strength and stiffness graphite fibers held together with a relatively compliant matrix of epoxy resin. These units, each called a lamina, can be stacked on top of each other at any orientation and in any sequence to achieve specific structural properties in the final assembly, called the laminate.

As with any other structural material, the strength, stiffness and life characteristics of graphite-epoxy composites must be established with a high degree of confidence before their great advantages can be safely and economically realized. At the same time, the states of stress and strain within the composite must be well known in order to carry out efficient design. These turn out to be especially challenging questions because of the infinite number of laminate configurations conceivable and the complicated manner in which subcritical damage develops in fiber-reinforced materials. Each configuration, or stacking sequence, produces different states of stress within each ply, which alters damage development under long term loading and makes laminate analysis more complicated than homogeneous material analysis.

1.1 OBJECTIVES

The primary objectives of the present study are to determine the mechanisms of damage development in a thick graphite-epoxy laminate with an unloaded center-hole by cyclic tension-compression loading and to establish the influence of such damage on the strength, stiffness and life of the laminate. An extensive experimental investigation was initiated and carried out using a 32-ply quasi-isotropic laminate. Non-destructive and destructive techniques were used to evaluate the response of the material to the mechanical loading. Among these are stiffness monitoring, X-ray radiography, C-scan, laminate deply, and residual strength measurement. A secondary objective is to evaluate the applicability of a simple model of delamination initiation to the laminate used in this study.

1.2 FAILURE PREDICTION

Within certain geometrical limitations, in-plane stresses can be easily predicted in uniform regions of a laminate using classical laminated plate theory. Several strength theories are available in the literature to predict static failure of laminates once the state of stress is known. Among these are the Maximum Stress, Maximum Strain, Tsai-Hill, and Tsai-Wu Tensor Polynomial theories [2]. These vary in complexity, with the higher order theories that account for interaction of stresses generally providing the most accurate prediction of failure. None of these schemes taken alone accounts for the complex damage state that develops in laminates prior to the final failure event. The state-of-the-art in fatigue life prediction is not well developed at this time, although several promising schemes have been proposed [3].

A failure theory based on the mechanics of materials approach requires a complete knowledge of the states of stress and strength in the material. In regions of the laminate near a free edge or stress concentrator, the stress state cannot be determined by classical plate theory. This is due to the presence of interlaminar stresses and/or stress gradients. The nature of these stresses determines the nature of the failure mode and strength. Several techniques addressing failure in these regions will be presented next.

1.2.1 Unnotched Laminates

Unnotched coupons are a starting point for the study of failure mechanisms of composite laminates. In the laboratory, test specimens generally are of compact dimensions and therefore influenced by edge effects. Without stress concentrators (notches), the effects of free edges can be more easily isolated. As an example of the importance of edge effects, simply changing the thickness of plies in a particular laminate or changing their stacking sequence not only changes the strength and fatigue life, but may also alter the mode of failure from a purely matrix one to a mixed one involving both the matrix and fibers [4,5,6]. This type of behavior has been attributed to interlaminar stresses in test coupons that arise from the mismatch of lamina elastic properties [7,8]. Analytical models of the stress state generally rely on numerical schemes such as finite elements or finite difference to solve complicated systems of equations that invariably arise in this type of problem [9-12]. It is has been suggested that there is a mathematical singularity of the stress state at a free edge, making any numerical approximation dependent on the amount of discretization utilized.

Interlaminar normal and shear stresses are suspected to have different importances in static and fatigue failure in delamination-prone graphite-epoxy laminates. Analytical predictions of such an effect are based on the strain energy release rate of a propagating delamination dominated by mode I (normal) or mode II (forward shear) crack opening [13]. Experiments performed with double cantilever beam (DCB) and cracked lap shear (CLS) specimens were used by Wilkins, et al. in [14] to formulate a power-law for crack growth rate. The mode I crack growth rate exponent found via the DCB specimens was relatively high, meaning that delaminations with high mode I components will grow rapidly to specimen failure only if the load is very close to the critical load for monotonic failure. At lower loads, the growth rate is much less, suggesting that mode I dominated delamination is more likely to be a cause of static failure as opposed to subcritical load failure (as in fatigue). On the other hand, the growth rate exponent for cracks in cracked lap shear specimens was much lower and comparable to aluminum. This indicates that at lower loads, such as during fatigue cycling, mode II delamination is more likely to be the dominant failure mechanism.

1.2.2 Notched Laminates

Geometrical discontinuities can induce severe stress gradients and concentrations in a material and therefore must be understood thoroughly for efficient design. Notches such as holes or cracks make up a special class of stress concentrators that are effectively free edges disturbing the uniform stress field of the material. The most common occurrence of these types of notches is a bolt-hole drilling for a structural component.

Drilling and bolting remains the most common method of attaching composite structures to each other, despite the promise of better performance by using adhesives, stitching, or co-curing. The necessity of inspections and repairs in certain applications guarantees that bolting will be used in the foreseeable future as well. This investigation considers only unloaded, circular through-holes, which are simpler to work with and analyze than pin- or bolt-loaded holes. Rosenfeld and Gause [15] have observed that the clamping constraint provided by idle fasteners placed in the notch of graphite-epoxy laminates can cause an increase in tension-compression fatigue life. Loaded holes are an entirely different problem, and will not be addressed here.

There are some characteristics of notches in orthotropic materials, such as laminated composites, that may seem unusual to those more familiar with notched behavior in homogeneous, isotropic materials. For example, consider a unidirectional graphite-epoxy plate of infinite extent. The maximum normal stress along the boundary of a circular cutout in such a material loaded along the fiber-direction is nearly 700 percent of the remote stress [16]. When loaded along a direction perpendicular to the fibers, the maximum stress concentration factor drops to about 250 percent [17]. In comparison, the stress concentration factor for uniaxial loading of a large isotropic plate with a circular cutout is 300 percent.

Several investigators have found that the strength of some notched graphite-epoxy laminates actually increases by up to 40 percent after some period of cyclic loading [18-23]. This type of behavior is not thoroughly understood, but has been suggested to be due to a reduction of the stress concentration by material "softening" in the vicinity of the notch. The softening generally begins with matrix cracking followed by delamination, which is not necessarily part of the eventual fracture surface at failure. In notched boron-epoxy laminates, contradictory results have been reported. Reifsnider, et al. [24] observed residual strength increases, while Roderick and Whitcomb [25] observed little or no increase in residual strength of orthotropic or quasi-isotropic laminates. This behavior seemed to depend on the direction of damage propagation in a particular laminate.

Schemes for predicting static notched strength have been published by several investigators. Most of these do not account for the interlaminar stresses that arise at the free surface of the notch; therefore, they cannot predict interlaminar failure modes. It has been shown that open notches in the interior of a laminate develop interlaminar stresses for the same reasons that straight edges do [26,27]. In an article by Whitney and Kim [28], it is argued that the effect of altered stacking sequence on laminate strength is in fact diminished by the stress concentration due to notch geometry. Experimental evidence is presented to justify this claim. Hence, the notched strength should be independent of stacking sequence. In contrast, Daniel et. al. [29] and Kress [18] observed experimentally that variations in stacking sequence could affect the tensile notched strength, life and/or failure mode of some laminates. Harris and Morris [30], on the other hand, concluded that for the thick laminates they investigated, stacking sequence did not strongly affect the compression-compression fatigue life. Despite these differences, the commonly used notched failure criteria can predict static failure loads with engineering accuracy and minimal computational effort, and thus deserve mention here.

Two closely related notched-material failure criteria proposed by Whitney and Nuismer are based on the introduction of a characteristic distance parameter to predict failure [31]. To use either criterion, the unnotched laminate strength as well as the maximum normal stress distribution extending away from the discontinuity must be known. The "point stress" failure criterion assumes failure when the normal stress over some distance away from the discontinuity equals or exceeds the strength of the unnotched material. This distance is assumed to be characteristic of the material at hand, independent of laminate geometry and stress distribution. The "average stress" criterion assumes that failure occurs when the average stress over a characteristic distance (not necessarily the same distance as that in the point stress criterion) equals or exceeds the unnotched strength. Both techniques provide reasonable agreement with experimental data, but cannot rigorously account for different strengths of different layups. Poe and Sova [32] and Cruse [33] have developed notched laminate strength prediction schemes based on fracture mechanics principles that also predict failure loads quite well, but independently of stacking sequence. In yet another notched laminate failure scheme that does not involve stacking sequence, Lo et. al. make use of the tensor polynomial failure criterion in conjunction with an iterative modification of lamina stiffness properties to reflect non-critical damage occurrences before the final failure event [34]. This method also agrees well with published experimental data. All of these schemes require a knowledge of the stress field away from the notch and are therefore most suitable for use in conjunction with a closed-form, full-field stress solution, although a numerical solution is adequate. To predict compressive strengths of laminates, the structural stability problem must also be considered along with a failure criterion.

1.3 DAMAGE DEVELOPMENT

Analytical modeling of composite material behavior becomes increasingly complex when changes in the state of the material are to be considered. During static or cyclic loading, graphite-epoxy composites commonly develop matrix cracks parallel to the fibers, disbonding of fiber-matrix interfaces, matrix crazing, delamination of adjacent laminae, and fiber fracture or microbuckling. Collectively, these events that cause changes in laminate life, stiffness and strength are called "damage". Initiation and accumulation of damage is dependent on load history, load rate, method of load introduction, laminate material, stacking sequence and stress concentrators [35,36].

Environmental factors such as temperature and moisture have been shown to affect fatigue damage development by altering the material properties and the chronology of damage events leading to failure [37]. Concurrent high temperature and high moisture content degrades the integrity of the matrix material in graphite-epoxy laminates. Since compressive properties such as strength and buckling load (stiffness) are sensitive to matrix-related damage such as delamination and fiber microbuckling, they will be affected by the environment more than tensile properties. An adverse environment can either increase or decrease scatter in fatigue data, depending on stacking sequence and load history.

The effects of frequency of load cycling in notched graphite-epoxy laminates has been investigated by Sun and Chan in [38]. They found that fatigue life of a matrix-dominated laminate, $[\pm 45]_{2s}$, is highly frequency and temperature dependent. If no temperature rise results as a consequence of higher cycle frequency, the fatigue life will be longer than at a lower frequency. If the temperature does rise near the notch, the fatigue life will be less. In support of this observation are Rosenfeld and Gause [15], who observed that the compressive fatigue behavior of notched $[0/\pm 45]_{3s}$ graphite-epoxy laminates was improved at 1 Hz as opposed to 3 Hz. Neither of these frequencies was high enough to cause an appreciable rise of temperature in the laminate.

Using Moire fringe patterns to measure in-plane displacement in unnotched [39] and notched [18] laminates, it has been shown that strain redistribution takes place in laminates as load-induced damage occurs. It thus follows that stress redistribution and concentration must also occur in order for the material to transfer load around the discontinuities [40]. With the aid of scanning electron microscopy, this concept is indeed supported by the presence of clusters of fiber breaks in plies adjoining a transverse crack [41]. The stress state around a matrix crack embedded in a laminate has been analytically studied by several investigators [13,42,43]. The results indicate that significant interlaminar and intralaminar stress disturbances evolve in the plies surrounding the crack. Considering that delamination and fiber fracture are predisposed to occur in such regions, it is postulated that matrix cracks may act as catalysts for subsequent forms of damage initiation [35,41].

Depending on the three-dimensional stress state at an edge of a laminate, matrix cracking may precede or succeed delamination in the chronological development of damage [44]. This behavior has been predicted using a technique employing finite element stress and energy methods by Wang, et al. [45] for unnotched $[\pm\theta/90_n]_s$ laminates. Whitcomb [20] and Ratwani and Kan [26] concluded that knowledge of the full stress state around a circular hole in laminates was sufficient to predict only initiation of delamination. Growth direction was more difficult to predict due to the changing stress state in the damaged material.

Along with the redistribution of stress and strain that accompanies damage, a change of global stiffness properties must also occur. These changes can be directly measured in a laboratory with minimal instrumentation, making them convenient indicators of damage accumulation. Reliable correlations between stiffness and damage as revealed by destructive and nondestructive evaluation have been achieved experimentally [46,47]. Reifsnider, et al. have noticed that there is a regular spacing of matrix cracks called the characteristic damage state (CDS) that occurs during the damage development process in a particular unnotched laminate subject to either static or cyclic loading. Predictions of this characteristic damage state and the resultant change of stiffness using a simple one-dimensional shear-lag (equilibrium element) analysis [48] and finite element energy methods [49] agree quite well with experimental data. To date, there has not been much success in adapting these analytical schemes to notched laminates.

Several articles concerning delamination in graphite-epoxy laminates and its effects on global stiffness properties have been published by O'Brien. His technique, based on a strain energy release rate concept, yields reliable predictions of delamination onset strain and location as well as the resulting change in stiffness in certain laminates [50]. A variation of this same technique has been used to predict delamination onset at a circular hole in a quasi-isotropic laminate [51]. Chapter Four will deal with this topic in greater detail. The three components of the strain energy release rate of a delamination, such as normal crack opening (I), forward shear (II), and parallel shear (III), have been shown to influence delamination growth in graphite-epoxy laminates with different material brands [52]. For example, Narmco T300-5208 graphite-epoxy was sensitive to the mode I component, while a tougher resin material, Hexcel C6000/H205, was sensitive to the sum of the three components. Influence of matrix cracks on delamination onset strain and location can also be accommodated with this technique. Strain level for delamination onset is predicted to be reduced by the presence of extensive matrix cracking, which is in agreement with published data for $[\pm 25/90_n]_s$ laminates [44].

1.4 NOTCHED, THICK LAMINATES

In engineering applications, there is often a need for holes or other cutouts in principle load-bearing composite structures. This structure may be subjected to either tensile or compressive loads and may be significantly thicker than many of the laboratory test coupons investigated to date. A wealth of information concerning fatigue behavior of notched composite laminates in various configurations has been published in the literature, particularly in the "Special Technical Publication" series by the American Society for Testing and Materials. Common types of fatigue loadings used in the laboratory are tension-tension (T-T), tension-compression (T-C), compression-compression (C-C), or some combination of these.

Experiments involving compressive load components are very sensitive to alignment and constraint conditions. Misalignment of the load axis with respect to the material axis of elastic symmetry causes excessive out-of-plane deflection and perhaps premature buckling. Increased amount of constraint, as in anti-buckling supports, delays buckling onset. Considering that such supports must apply force laterally to the specimen in order to be effective, there must be some complicated out-of-plane stresses induced in the material. This could bias damage development, and ultimately, the test results. Out-of-plane deformation causes premature specimen failure and/or unsymmetric damage development through the test specimen thickness. While this type of damage may be worthy of study in the laboratory, studies of the fundamental nature of damage in laminates subject to compressive loads should start with simple compression. Meaningful comparisons of results from different tests can only take place after all the above variables are considered.

Phillips investigated the effects of anti-buckling constraint on the fatigue life of notched laminates subjected to predominantly compressive loading [53]. It was determined that a smaller "window" of unsupported area around the notch retarded the development of fatigue damage, especially at higher compressive loads. Saff [54] provides an extensive review of literature concerning compression testing methodology. For compression-dominated loading, experimental results suggest that failure is primarily matrix-related. This implies matrix cracking, fiber-matrix debonding, delamination, and fiber buckling in regions of degraded matrix or stress concentration, which reduces the laminate's ability to sustain compressive load [15,19,22,30,53,55-57]. Delamination and matrix cracking also occur in laminates subject to quasi-static tension and T-T cyclic loading, but the final event leading to failure is thought to be fiber fracture in the principle load-bearing plies [3,22,35,36].

Increased thickness has been shown by Harris and Morris [58] to change the mode of tensile fracture of notched graphite-epoxy laminates. Thin laminates with a narrow, transverse slit loaded quasi-statically to failure were observed to have large-scale delaminations at the fracture surface. Thick laminates fabricated of repeating units of this same stacking sequence delaminated only near the surface in a manner similar to their thin counterparts. Farther in the interior of the laminate, the fracture surface appeared self-similar with the starter notch.

In another article on thickness effects by Harris and Morris [30], C-C fatigue-induced delaminations were observed to occur first near the surface of unnotched $[(90/45/0/-45)_n]_s$ and $[(45/0/-45/90)_n]_s$ laminates. Later in the life of the specimen, similar interfaces through the thickness delaminated. This type of behavior was supported by an analytical investigation by Whitcomb and Raju [59], where it was shown that interlaminar stresses (suspected to influence delamination initiation) are actually not uniform through the thickness of such laminates in the undamaged condition. In addition, examples were provided whereby it was shown that delaminations are more likely to occur near the surface of the laminates used by Harris, based on the strain energy release rate technique. The earliest delamination initiation sites generally had a high interlaminar shear stress combined with a tensile interlaminar normal stress. Delaminations later initiated at locations of high interlaminar shear and compressive normal stresses computed for the undamaged condition. Harris and Morris also investigated the same laminates as above with a circular hole drilled through the center. Essentially no difference in fatigue life was noted for the two laminates (as opposed to a significant difference observed in the unnotched case). There was also no strong effect of thickness on life, although the longest lives were obtained with the thickest laminates (at the same stress level). It was concluded that the stress concentration at the hole was more important to fatigue behavior than stacking sequence.

Not all thick laminates are subject to damage initiation on the surface. Black [19] investigated the C-C fatigue behavior of two thick, notched graphite-epoxy laminates with different symmetric stacking sequences. In a 42-ply laminate fabricated with two non-repeating halves, it was reported that delamination development through the thickness was quite uniform, if not slightly favoring the center. The other laminate, fabricated with repeating (but not symmetric) sub-units, displayed damage initiation at the surface in a manner similar to that observed in [30]. A finite element analysis of these two laminates by Ratwani and Kan [60] indicated that delaminations first initiated at interfaces of highest interlaminar shear stress. The laminate with lower interlaminar shear stresses did not delaminate as extensively as the other, and was not subject to fatigue failures unless cycled at maximum compressive stresses close to its static compressive strength.

There is much debate in the literature concerning the relative importance of load characteristics to fatigue-load induced damage. A combination of tensile and compressive components in the load cycle is generally considered to represent the most severe load case for composite laminates since their respective (and perhaps competitive) damage mechanisms are both active [3,15,22,36,57,61]. This is partly due to the coupling of damage modes induced separately in the compressive and tensile load excursions. Matrix cracking induced during the tensile portion of the load can act as a delamination catalyst during compression in certain laminates. Once delaminations are present in the material, the tensile strength may not be affected significantly, while compressive strength is highly dependent on delamination extent and location through the thickness. Ramani and Williams [23] concluded that load spectra containing a positive mean stress extended the fatigue life of notched laminates. Walter, et. al. [62] observed that fatigue life for T-C loading was about the same as for C-C with equal maximum compressive load in unnotched, impact-damaged graphite-epoxy laminates. All considered, there seems to be no certain consensus on generic response of composites to mixed tensile and compressive loads.

In another study of relevance to the present work, Ryder and Walker [22] investigated notched and unnotched fatigue behavior of a laminate constructed of ply groups similar to the one used in this study ($[0/45/90/-45]_s$). In contrast to the present study, however, the laminate was only half as thick (16 plies), and was fabricated with Thornel T300 graphite fibers in Fiberite 934 epoxy resin. The laminates subjected to compressive strength measurements had full face supports to prevent out-of-plane deflection, and those subjected to T-C fatigue were supported by two anti-buckling guides that reduced the effective column length. Extensive fatigue tests were carried out in T-T and many load ratios between -1 and zero to determine the effects of compressive load components on material properties such as strength and life. Environmental conditions such as high temperature and humidity were considered. Mechanisms of damage development, were not presented in great detail. Summarizing results for both notched and unnotched laminates, the damage modes in the two load cases were similar, but the T-C tests had to be terminated sooner than the T-T tests due to delaminations that reduced the coupon's ability to sustain compressive load excursions. Thus, the critical damage in T-C was delamination. The effects of compression with varying amounts of tension was not significant at high tensile loads; but at low tensile loads, the compressive load significantly shortened life. This effect was more pronounced with higher compressive loads. Higher temperature and moisture caused delamination to occur sooner and reduced notched and unnotched lives by factors of ten and three, respectively. In the unnotched laminates, fatigue damage in T-T or T-C decreased the residual tensile and compressive strengths. Tensile residual strength of the notched laminate increased during fatigue, and did not decrease before failure in T-C loading. Tension-tension fatigue failures were, however, realized in the notched laminate at peak loads greater than or equal to 73 percent of the undamaged static ultimate. Notched compressive residual strength data were not consistent. Overall, higher tensile residual strengths were measured with T-T than T-C fatigue. No residual strength data were presented for laminates cycled at fully reversed (R=-1) tension-compression. Residual strength increase was less with a hot and humid environment.

Ulman, et al. [57] also investigated fully reversed (R=-1) T-C fatigue behavior of center-drilled, thick laminates constructed of the same ply groups as those in the present investigation. The laminate was 48 plies thick, enabling compression loads to be accommodated without anti-buckling supports. The material system was Hercules AS1/3502. In the notched coupons, predominant damage modes were matrix cracking and delamination in the vicinity of the hole. T-T fatigue at 90 percent of the static ultimate did not produce fatigue failures due to a large increase in tensile residual strength. The tensile strength of such a highly damaged specimen was about 95 percent of the undamaged, unnotched strength of the ligaments of material between the notch and the straight edge, or 130 percent of the undamaged notched strength. No residual strength data were presented for fully reversed T-C loading. In T-C and C-C fatigue, fatigue failures were caused by severe delamination-induced laminate instability. Transverse matrix cracks appeared throughout the laminate during T-T and T-C fatigue. In C-C fatigue, there were no such cracks away from the hole. The fatigue behavior of this same laminate with a two zero deg. ply terminations in the interior region was also investigated, but will not be discussed here.

There are many parameters to vary in T-C fatigue tests, such as maximum stress, minimum stress, stress range and min/max stress ratio, as well as the constraint conditions.

The literature in this area of fatigue study needs to be supplemented in order to establish a broader understanding of the generic response of composites with various stacking sequences, load histories and constraint conditions.

In the following chapters, the relevant information pertaining to a primarily experimental investigation of fatigue damage in a notched composite laminate subject to T-C loading will be presented. Chapter Two contains the specimen design process and test methodology. Comparisons to related experiments in the literature are made. In Chapter Three, experimental results of this investigation are discussed. Analytical schemes for delamination prediction and their application to the laminate in this study are presented in Chapter Four. Conclusions are given in Chapter Five.

Chapter II

EXPERIMENTAL INVESTIGATION

2.1 TEST SPECIMEN DESIGN AND DESCRIPTION

This experimental program was conducted using test specimens fabricated with a graphite-epoxy material system called T300-5208 (Rigidite) by its manufacturer, Narmco Materials Inc. The material is widely used by aerospace industries today, and has been subjected to extensive testing since its introduction in the mid 1970's. In the "as received" state, the raw material consists of an essentially continuous length of Union Carbide's unidirectional Thornel T300 graphite fibers impregnated with Narmco's 5208 epoxy resin to form a 12 in. wide strip. Sheets of this unidirectional material, called pre-preg, were cut and layed-up at NASA Langley Research Center to the desired stacking sequence of $[(0/45/90/-45)_s]_4$ (Figure 1). The sign convention of ply orientations is such that 0 deg. is aligned with the loading axis and positive angles are measured clockwise, which is consistent with proposed additions to ASTM D3878 definitions [63]. The panels were then cut at NASA's facilities to a specimen width of 1.50 inches (38.1mm) and a preliminary length of 8 inches (203mm) using a circular saw with a diamond wheel. Average thickness of the cured specimens is

.164 inches (4.17mm). A hole of .375 inches (9.53mm) diameter was drilled through the center of each specimen. Nondestructive inspection of the specimens with an ultrasonic C-scan unit at VA. Tech documented the uniformity of the material and the quality of machining. After the time of fabrication and during testing, the specimens were stored in ambient laboratory conditions.

The choice of a moderately thick laminate accomplishes several test design tasks at once. First, compressive loads can be accommodated with or without side supports, depending on which suits the investigator's needs. Second, the damage patterns through the thickness can be observed to determine whether or not a third dimension of damage development exists. Finally, the high loads required to study very thick laminates are avoided, thus facilitating laboratory testing.

The balanced, symmetric laminate chosen for this study has in-plane (but not out-of-plane) stiffness properties resembling those of an isotropic material and is thus commonly called "quasi-isotropic". The particular laminate elastic and geometric properties chosen enable quick and economical analysis of the states of stress and strain using closed-form solutions for an isotropic or orthotropic plate of infinite extent and containing a circular hole [17,64].

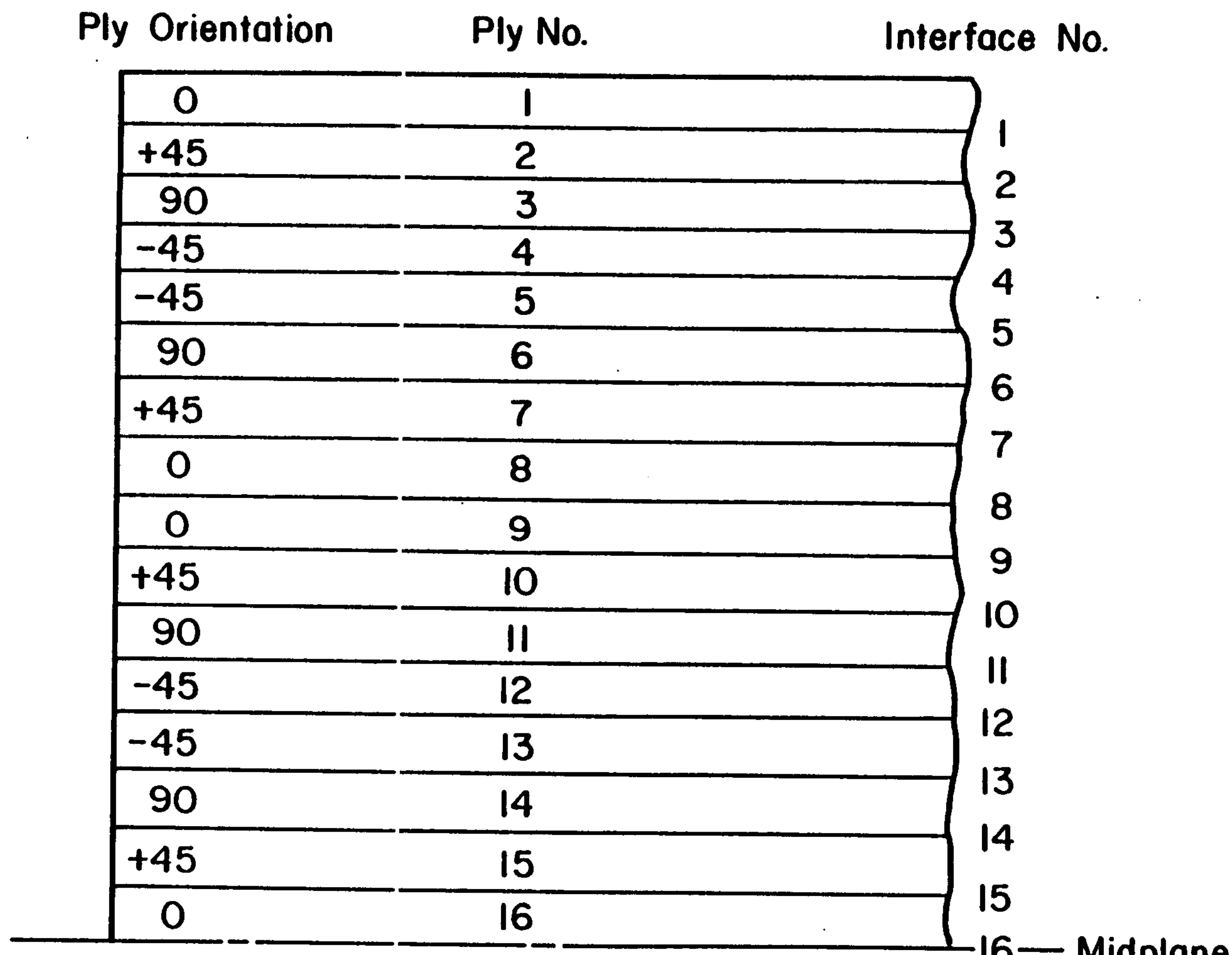

$[(0/45/90/-45)_s]_4$ Laminate

Figure 1: 32-Ply Layup Configuration

Interlaminar stresses at the straight edge are also minimized, allowing the dominant damage location to be located at the hole.

In order to design a laboratory test specimen that can sustain compressive load excursions, one must consider buckling. The primary interest in this investigation is the determination of fundamental mechanisms of damage development in T-C fatigue, without the peculiarities induced by laminate buckling or the complicated stresses induced by anti-buckling supports. Therefore, a preliminary test sequence was performed to evaluate the effects of specimen unsupported length (UNSL) on static and cyclic behavior. Details of these tests will be presented in Section 2.3. To summarize, the final length of the specimens was determined to be optimum at 4.75 inches (120.7 mm). This overall length corresponds to an unsupported or ungripped length of nominally 2.375 inches (60.3 mm), which allows for access to the specimen for attaching instrumentation and also minimizes out-of-plane deflection during the anticipated compressive load excursions. As the specimen becomes highly damaged during fatigue tests, however, the compressive stiffness may decrease such that significant out-of-plane deflection occurs within the cyclic load limits. Test specimen dimensions are depicted in

Figure 2, while coordinates and quadrant notation are defined in Figure 3.

2.2 MECHANICAL TESTING

2.2.1 Test Program

A mechanical test program must be conceived to determine the material properties of and induce damage initiation and growth mechanisms in the aforesaid laminates. A particular combination of geometry and constraint conditions must be chosen so that a consistent base of information can be gathered that is applicable to a wide range of engineering situations. The program should also be designed such that the investigator can continuously evaluate parameters that provide significant information regarding the state of the material before the final failure event. Without this type of data, it is quite difficult to determine the long-term response to mechanical loading.

A preliminary set of static tests were carried out to determine the laminate's undamaged tensile and compressive properties. The majority of fatigue tests in this investigation had a load ratio (R) of -1, corresponding to fully reversed T-C fatigue. Two load levels were chosen such that most fatigue lives were between 100 thousand (100K) and one million (1M) cycles. Several specimens were

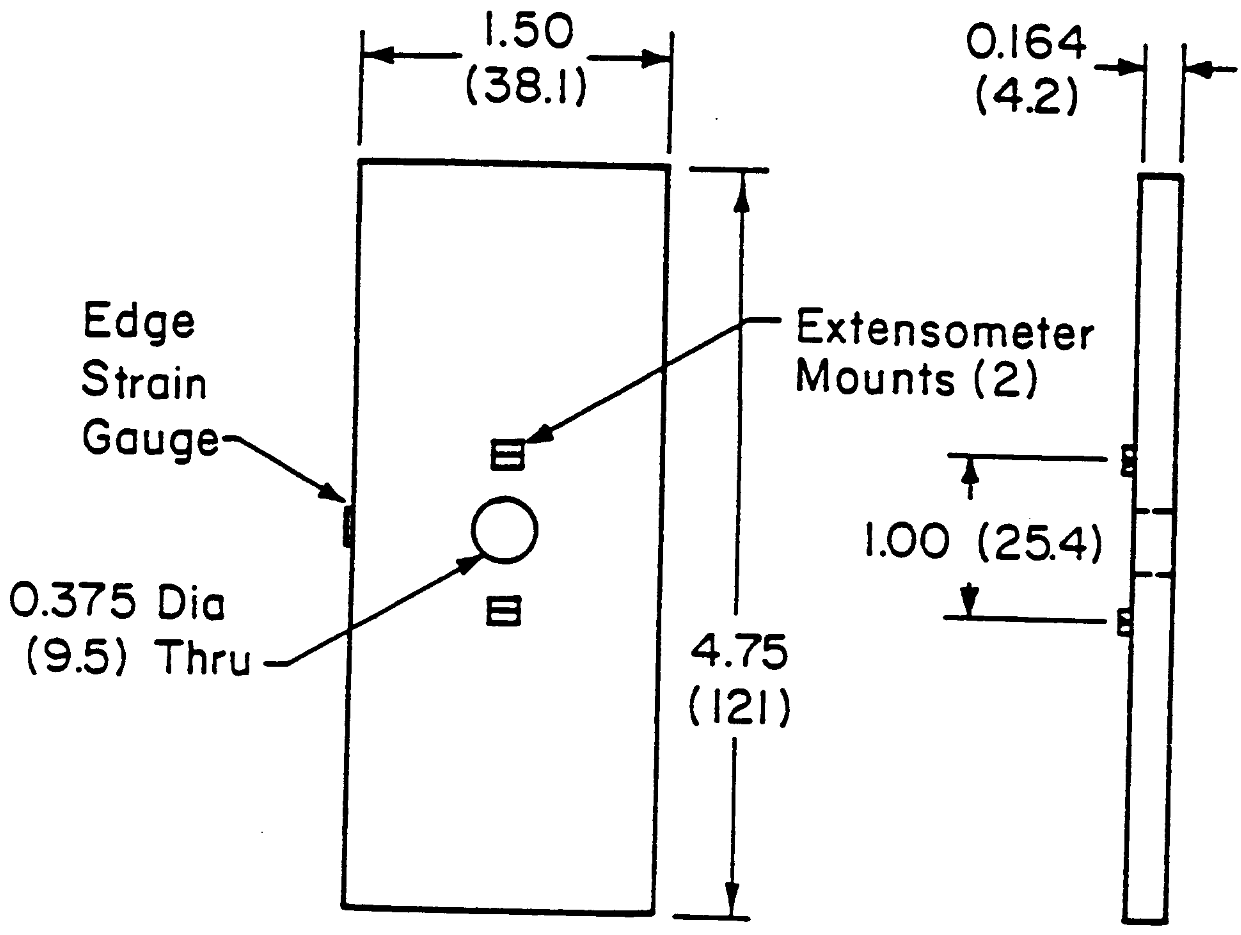

Figure 2: Test Specimen Dimensions

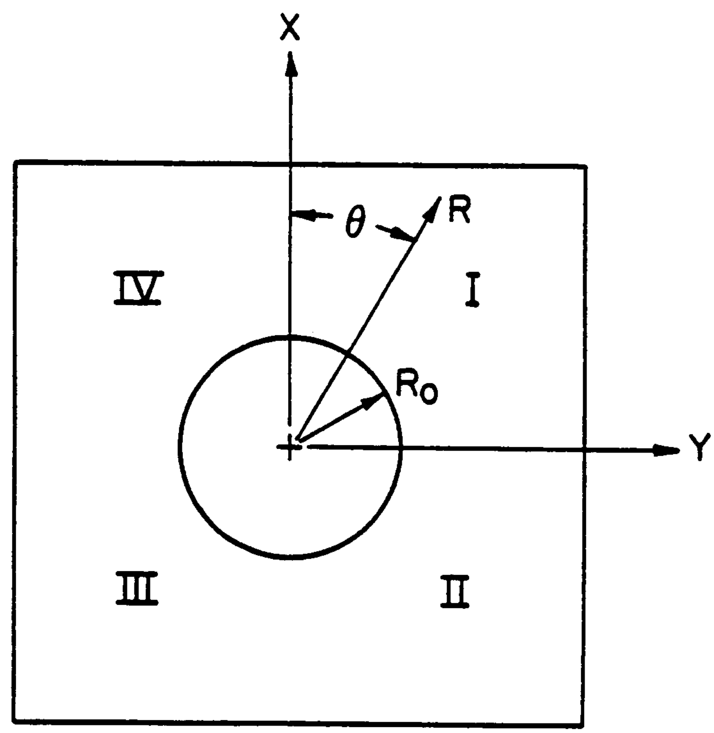

Figure 3: Specimen Coordinate and Quadrant Notation

cycled to failure at these load levels to establish a correlation between stiffness behavior and damage documented via X-ray radiography. Specimens were selected for residual tensile strength measurement and a laminate deply process at middle and late stages of T-C fatigue damage development to complement the damage data acquired by non-destructive means. Several T-T, C-C and mixed block loadings (different load ratios in sequential blocks of cycles) were performed for comparative purposes. A variety of negative load ratios from -0.3 to -1.0 were used to observe the effect of different amounts of compression (with the same peak tension) in the load cycle.

2.2.2 Mechanical Testing Apparatus

All mechanical tests but one were run on an MTS 50 kip (220 kN) electro-hydraulic servo controlled load frame in the load control mode of operation (Figure 4). This testing machine was fitted with hydraulic wedge grips that are designed for either tension or compression loads. One monotonic compression test that did not require grips was run on a 20 kip (89 kN) screw-driven Instron testing machine in displacement control. A 10 Hz sinusoidal load was chosen for the fatigue tests because of the existence of a substantial data base of related tests at that frequency.

Below 100 cycles, lower loading frequencies were used to eliminate the effects of start-up transients on the recorded damage history. To minimize grip-induced damage to the specimen surface during cyclic loading, 180-grit emery cloth was placed between the specimen and the grip surface, with the rough side toward the specimen. Alignment plates, as illustrated in Figure 5, were used for lateral alignment of the specimen within the grip housing and to prevent grip-induced "brooming" at the specimen ends. This arrangement allowed approximately 1.2 inches (30.5mm) of the specimen to be gripped at each end and eliminated the occurrence of the specimen slipping out of the grips during high tensile loads. Axial and torsional alignment of the grips were periodically checked to minimize undesirable loads on the specimen. The laboratory environment was air-conditioned, with approximately uniform temperature and humidity for all tests.

2.3 PRELIMINARY TESTING

Four specimens with unsupported lengths of 4.0, 3.0, 2.375 and 1.625 inches (101.6, 76.2, 60.3, 41.3 mm) were chosen for preliminary static compression testing. The unsupported length for the first three tests (and as it turns out, for all fatigue tests) is defined to be the length of specimen

ORIGINAL PAGE IS
OF POOR QUALITY

ORIGINAL ...
OF POOR ...

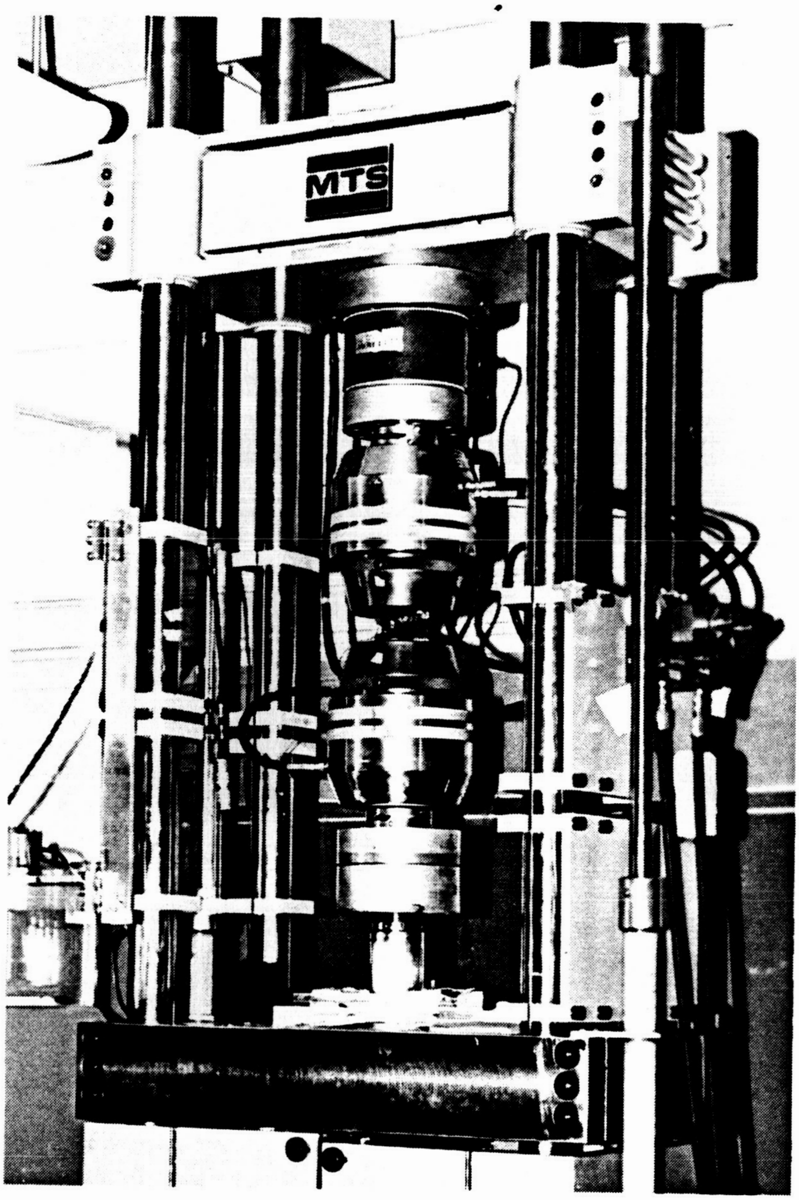

Figure 4: MTS Load Frame

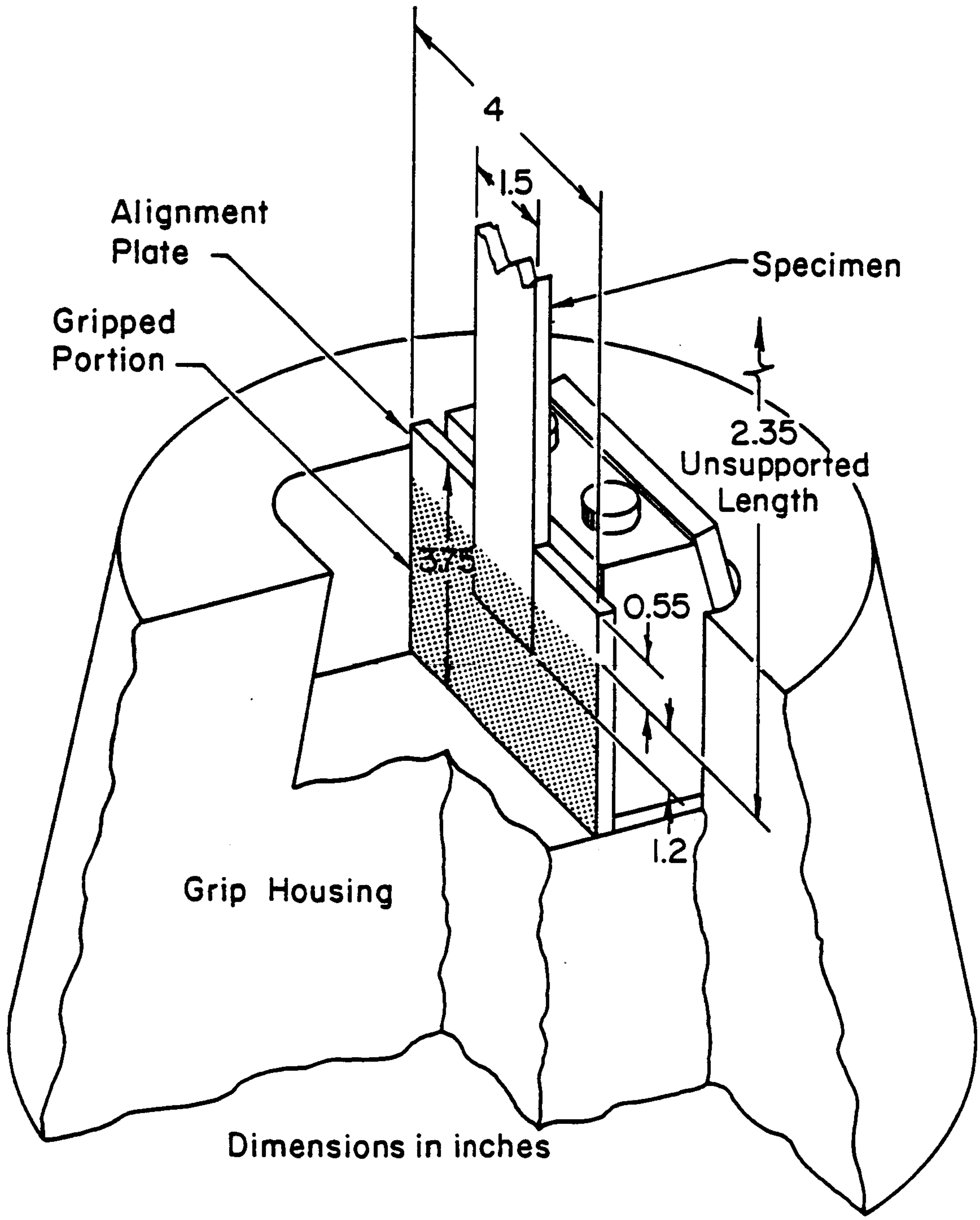

Figure 5: Test Specimen Gripping Configuration

not in contact with the grips of the testing machine. The fourth specimen was tested for compression strength using a side support fixture originally designed and optimized by Phillips [53] and refined by Harris [30] for notched laminates. This fixture provides a 1.625 X 1.625 in. (41.2 x 41.2 mm) "window" of unsupported specimen area centered on the notch. The remainder of the specimen is supported by rigid aluminum plates. Load is introduced to the specimen by direct bearing on both ends (Figure 6). This arrangement was deemed most desirable for observing unimpeded fatigue damage growth in 2 in. (50.8 mm) wide notched specimens. Since the specimens for this study are only 1.5 in. (38.1 mm) wide, the fixture effectively provided for a 1.625 in. (41.3 mm) UNSL, with no window effect. However, the stress distribution in the specimen will undoubtedly be different in this fixture compared to the other tests with rigidly gripped end-constraints.

Specimens for this phase of testing were instrumented with front and back longitudinal strain gages (Micro-Measurements EA-06-060LZ-120) at two locations around the hole (Figure 6). The outputs from front and back gages could be compared to determine the onset of instability. The 2.375 in. UNSL specimen was instrumented with an additional longitudinal strain gage (M-M EA-06-240LZ-120)

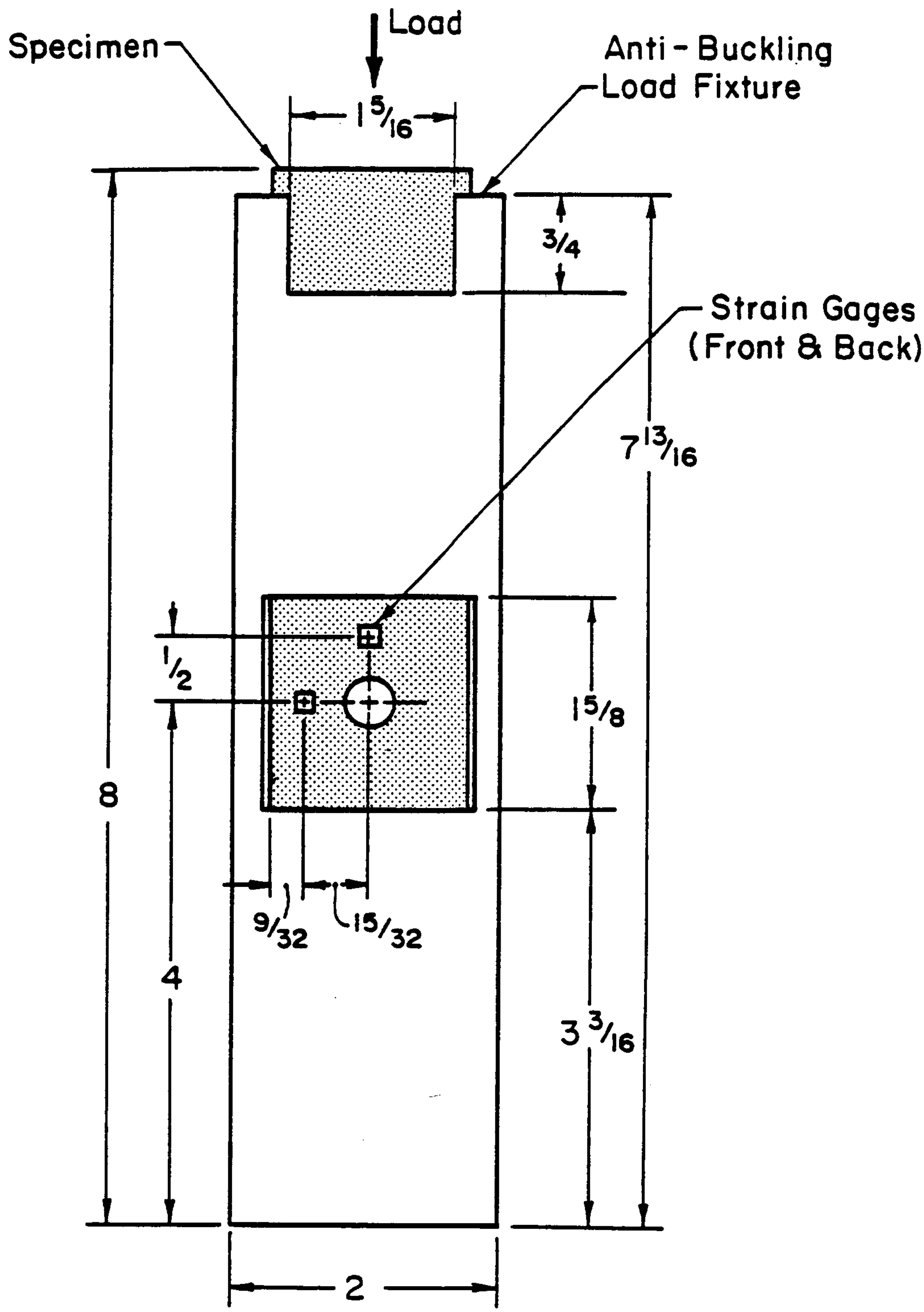

Figure 6: Anti-Buckling Support Fixture, Schematic

located on the center of the thin edge of the specimen and along the transverse centerline, where an out-of-plane deflection would not strongly influence the strain measurement (Figure 2). The strain gages at the notched section of the laminate were more sensitive to out-of-plane deflection than the ones situated on the longitudinal centerline. The edge gage indicated strains that were linear to failure.

Although this chapter does not deal with results, it is necessary to present some results of the preliminary tests at this time in order to justify the final specimen design. Load at static failure for each of the preliminary tests are summarized as:

UNSL (in/mm)	Failure Load (kip/kN)	Failure Stress* (ksi/MPa)
4.0 /102.	-7.0/-31.	-28./-200.
3.0 / 76.	-9.0/-40.	-37./-250.
2.375/ 60.	-10.0/-45.	-41./-280.
1.625/ 41.	-10.0/-45.	-41./-280.

* computed on unnotched area of .246 in^2 (159 mm^2)

As one would expect, the longer specimens failed at a lower load than the shorter specimens. For unsupported lengths less than or equal to 2.375 in. (60.3 mm), the failure load does not increase beyond 10kip (45 kN), suggesting that buckling effects have been minimized or eliminated. In a parallel study of identical laminates at NASA Langley Research Center, compression strengths of several UNSL's agreed well with the present data (Figure 7). In Figure 7, the NASA data includes the mean, range, and number of specimens tested at each UNSL. Each of the data points generated in the present investigation (VPI) represents a single test. Examination of the failed specimens revealed different modes of failure for each length. The longest specimen had a failure surface characterized by large delaminations over the entire gage length. Fiber fractures occurred over a large region, and were not necessarily directly associated with the hole, suggesting that failure may have resulted from buckling-induced bending. The shorter specimens had correspondingly less delamination at the failure surface, and fiber fractures were along a transverse section through the hole, giving the appearance of a crushing mode of failure (Figure 8).

Several fatigue tests on identical laminates were run at NASA Langley to determine the effects of UNSL on cyclic loading response when the load ratio (R), defined as minimum load/maximum load, equals -1. Figure 9 illustrates the NASA data, along with fatigue life data recorded in the present investigation for 2.375 in. (60.3 mm) UNSL. Lengths near

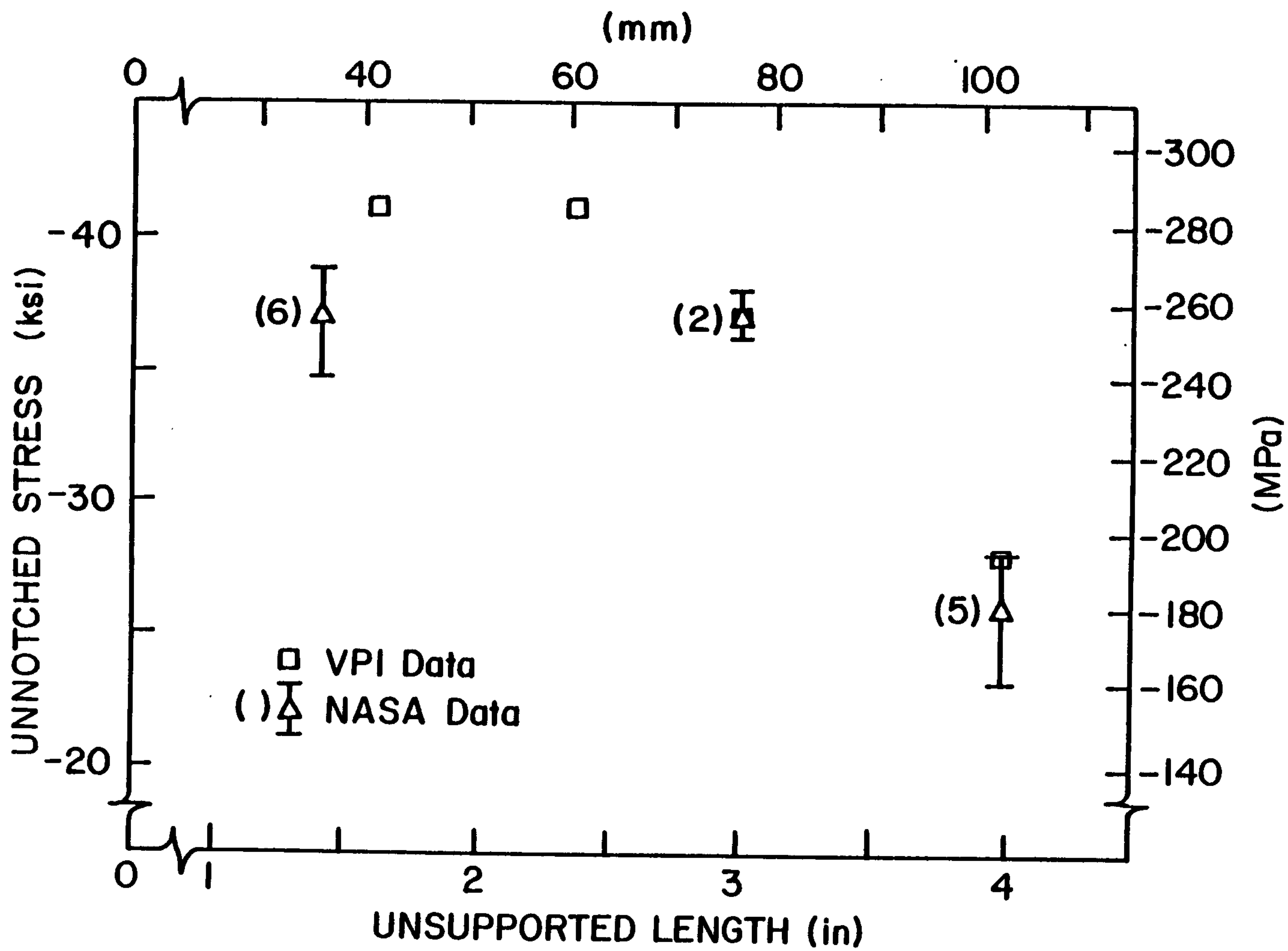

Figure 7: Compressive Strength for Various Specimen Lengths

a) Edge View

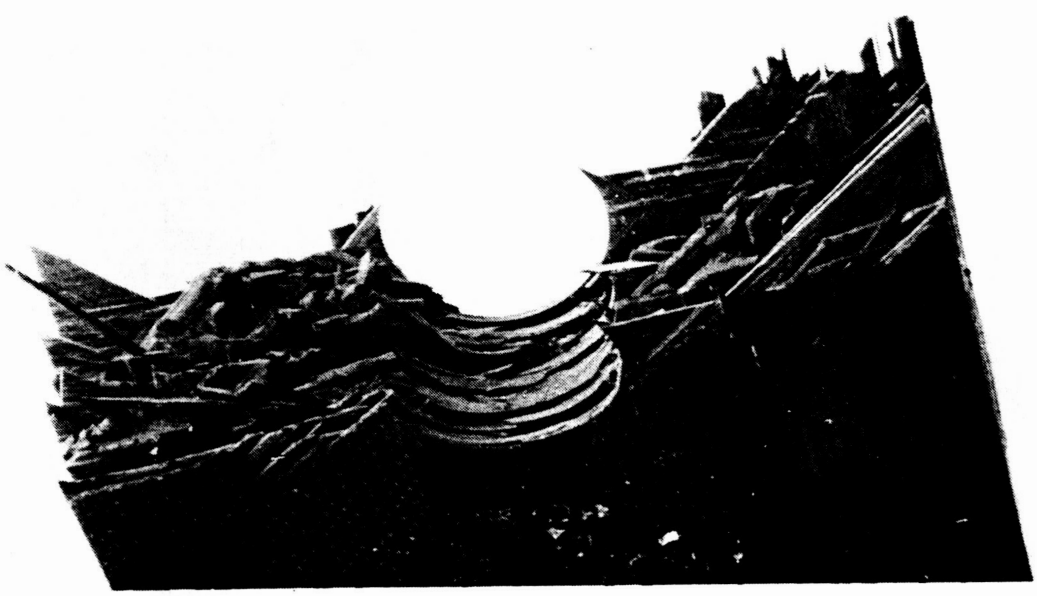

b) Front Face View

Figure 8: Static Compressive Failure Surface, 2.375 Inch UNSL

2.5 in. (76.2 mm) were found to be optimum for inducing sufficient damage initiation and growth before fatigue failures at 10^5 to 10^6 cycles. Therefore, 2.375 in. (60.3 mm) was chosen as the UNSL for the remainder of the tests. The two load levels resulting in these limits of fatigue life are ±4500 and ±5500 lb. (±20.0 and ±24.5 kN). Based on the .246 in^2 (159 mm^2) mean unnotched cross-sectional area of the test coupons, these loads correspond to stress levels of 18 and 22 ksi. (±130 and ±150 MPa.). For convenience, these load levels will simply be called "high" and "low". A more detailed description of compressive failure of the specimen chosen for the fatigue tests will be presented in Chapter III.

Load and strain data from the static tests were used to verify lamina elastic properties used in previous studies with this material [51,59]. This was accomplished with the aid a two-dimensional finite element computer code with a uniform displacement loading, linear isoparametric elements and isotropic, plane stress assumptions [65]. The lamina material properties will be used in subsequent analysis and are given in Chapter 4.

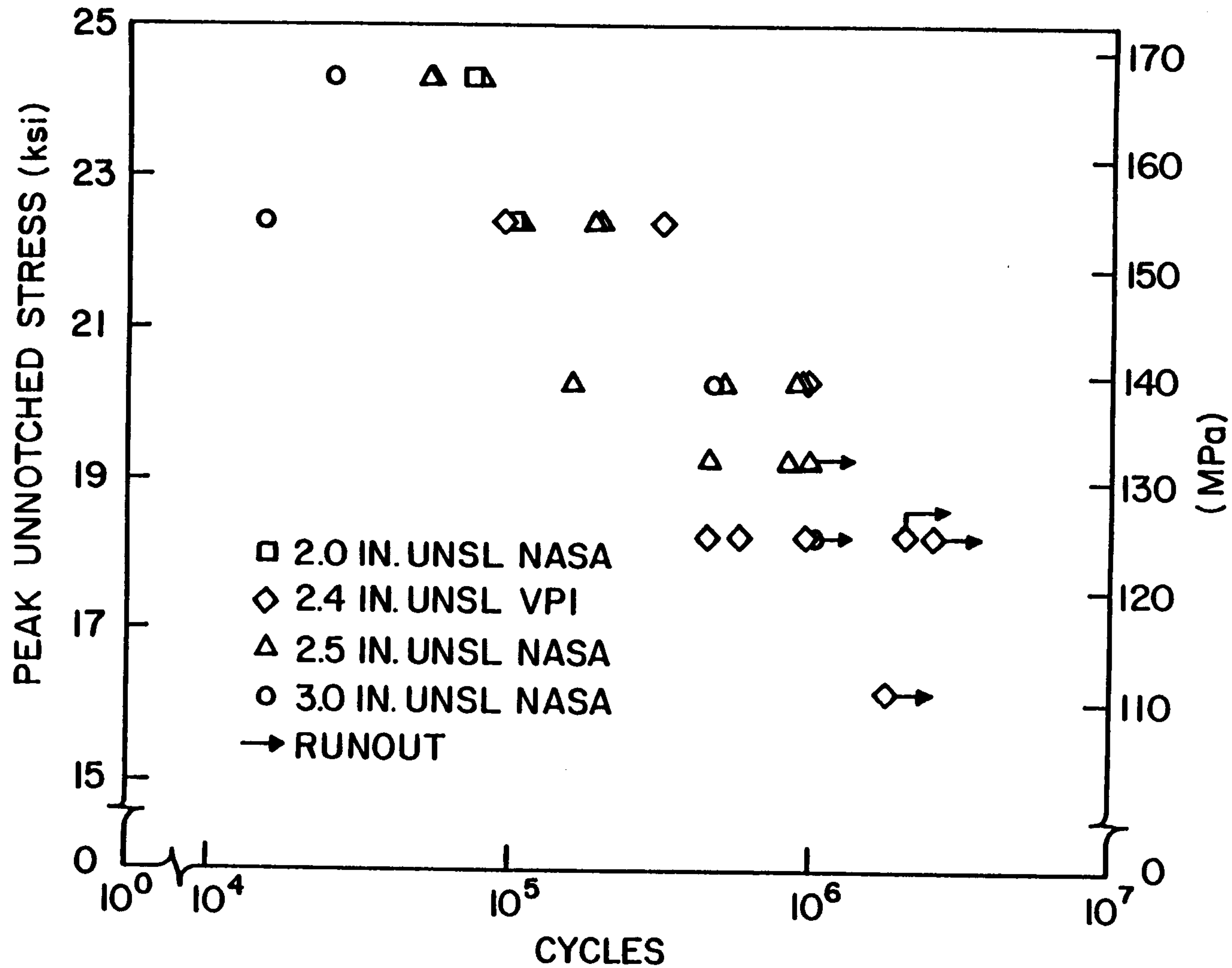

Figure 9: Stress - Life Relation for Various Specimen Lengths, R=-1

2.4 DAMAGE EVALUATION

Damage evaluation techniques are required in the experimental procedure to identify the actual modes of damage initiation, growth and interaction. These may be classified as either nondestructive or destructive evaluation.

2.4.1 Nondestructive Evaluation

For the purposes of this investigation, nondestructive evaluation (NDE) is defined as a means of interrogating the state of the material without affecting its life, stiffness or strength. Individual damage micro-events can thus be monitored as they grow and interact through the life of the specimen. The particular techniques used were stiffness change, penetrant-enhanced X-ray radiography and ultrasonic C-scan.

2.4.1.1 Stiffness Change

Stiffness change has been shown to correlate quite well with the development of damage, as mentioned in Section 1.3. Due to the short unsupported length of the specimens necessary to minimize out-of-plane deflection, there was not much area available on which to place stiffness monitoring devices. Strain gages are ideal for such situations, but they are not reliable for long term damage studies for two reasons. The first is that the gage adhesive does not have a sufficiently long fatigue life at the strain levels of interest. The second is that strain gages have been shown to be overly sensitive to matrix cracking if it occurs in the surface ply directly under the gage [66]. Extensometers, on the other hand, avoid both of these problems and are removable to permit inspections using other NDE techniques.

A one-inch gage length extensometer was chosen for this study as a compromise between the tight space restrictions and the need for a large gage length to minimize local effects. Using eight-ply, notched quasi-isotropic laminates, Kress [18] observed that stiffness loss measured over a length of the specimen including the hole was a function of the gage length. It was hypothesized (and supported with full-field displacement data via the Moire technique) that a shorter gage length will indicate earlier stiffness loss because the underlying material near the hole achieves a saturated damage state before that of a longer gage length. A notch was machined in the wedges on the front of the load frame grips to establish clearance for the extensometer (Figure 10a). This does not degrade grip effectiveness since this portion of the wedge is not active in gripping the specimen. To assure a firm and reasonably repeatable mounting for the extensometer, flat aluminum tabs with V-notches were bonded to the specimen surface using a compliant silicone adhesive (Figure 2). Rubber bands were used to hold the extensometer knife-edges in the V-notches (Figure 10b).

There are several sources of scatter in stiffness data recorded in the laboratory. One is the inexact placement and size of the extensometer mounting tabs. This can cause a variation of up to 10 percent in measured stiffness among specimens because of the large strain gradient in the vicinity of the notch, but it is not a problem for an individual specimen as long as the tabs are not moved during the test. To eliminate initial scatter of specimen stiffness, each stiffness vs. cycles plot in this investigation was normalized to the corresponding specimen's initial stiffness. Another opportunity for error arises when a specimen is initially gripped in the testing machine. An apparent stiffness gain or loss can occur during the first few cycles of full amplitude loading. This is hypothesized to be due to a "settling in" of all the interfaces in the load-to-extensometer path: bearings of the testing machine, hydraulic grip float, grip-specimen interface, and specimen-extensometer interface. Still another source of error is the placement of the extensometer

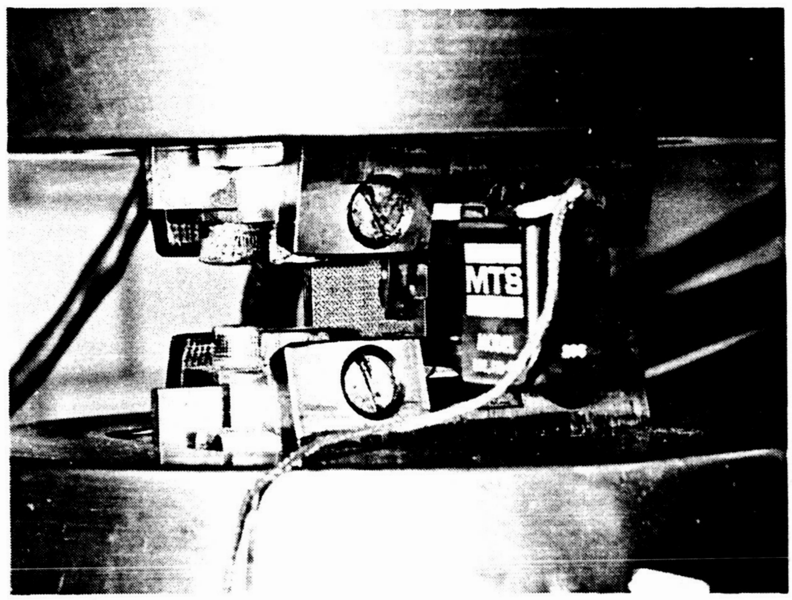

a) Specimen and Instrumentation in Testing Machine

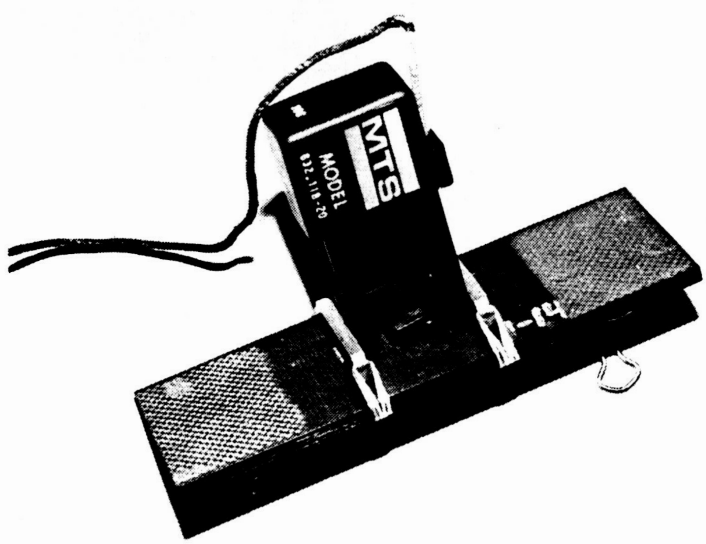

b) Extensometer Mounted on Specimen

Figure 10: Experimental Setup and Instrumentation

on the specimen. It is very probable that each time the extensometer is removed and replaced it will not be positioned exactly the same, thus indicating a different apparent stiffness.

For a particular specimen, stiffness errors are typically less than one percent for each test startup, but may become significant in certain types of tests. An example would be a test requiring frequent removal of the specimen for NDE. In such a test, absolute stiffness change for each continuous cycling segment was calculated as a percentage of the stiffness measured on cycle number one. A summation of these partial stiffness losses as a function of number of load cycles or percentage of cycles-to-failure is used as a graphical representation of damage accumulation in the test coupons.

Stiffness monitoring during fatigue tests was performed on a quasi-continuous basis. That is, actual measurements were taken statically at selected cyclic intervals such that a continuous plot of the stiffness could be made with insignificant interpolation error. Continuous monitoring of the dynamic strain amplitude using a peak detector enabled tests to be stopped for static measurement at a prescribed change in strain. Separate tension and compression stiffnesses were measured by slowly loading to the maximum and minimum fatigue load amplitudes and measuring the calibrated voltage output from the extensometer. Following this, the test was either resumed or the specimen was removed for damage evaluation. This type of stiffness is more accurately called a "secant" stiffness because it is based on the slope of a straight line drawn from the origin of the load-strain coordinates to the maximum point on the load curve. If there is significant nonlinearity in the curve, the secant stiffness will be noticeably different than the tangent stiffness measured at the beginning of the curve. Differences measured at the fatigue load levels were generally less than three or four percent, except in highly damaged specimens, where out-of-plane deflection could increase them to nearly ten percent in compression.

2.4.1.2 Ultrasonic C-Scan

The C-scan technique makes use of high-frequency (ultrasonic) sound waves to provide a qualitative estimate of the damage condition in materials. Irregularities (damage or other forms of inhomogeneity) in the material will reflect and scatter ultrasonic waves such that the resulting attenuation can be plotted as a function of position on the test subject. The technique is qualitative in the sense that one form of damage cannot, in general, be distinguished from another. The amount and nature of attenuation is difficult to quantify without complex signal processing, and must be calibrated against a specimen with a "known" state of damage. For these reasons, C-scanning was used as a quick interrogation of the damage state whenever minute details were not necessary. C-scanning as a principle investigative tool was limited to initial evaluation of test coupons before introducing damage so that embedded defects such as voids or excessive porosity could be detected. It was also used as a "second opinion" to verify the extent of damage indicated by X-ray radiography. Figure 11a illustrates a C-scan of a moderately damaged fatigue specimen. Three passes were made so that gradients of attenuation are visible. White represents regions of highest attenuation (damage), and black is the reference state of attenuation (undamaged). A limitation of the C-scanning device used in this investigation is that the mapping of attenuation is produced at a one-to-one scale, with only fair resolution of fine details.

There are advantages of C-scanning that make it a valuable NDE tool. It does not depend on the use of penetrants to highlight damage and can therefore detect damage that is inaccessable from the surface. The coupling medium between the transducer and the test subject is water, which can easily be driven off by evaporation before testing is resumed.

2.4.1.3 X-Ray Radiography

X-rays have been used in several fields of science to resolve images of regions in a medium with different absorptivities of this type of ionizing radiation. As such, X-ray radiography can be used to detect regions of discontinuity in composite materials, such as interply and intraply matrix cracking [67]. When using commercially available films to produce X-ray radiographs of damaged graphite-epoxy laminates, there is not a satisfactory contrast between the damaged and undamaged regions. Penetrants that are relatively opaque to X-rays (compared to the surrounding material) are commonly used to highlight damage with connectivity to the surface. Rummel, et. al. [68] have compared different penetrants and found that zinc iodide (ZnI_2) dissolved in a liquid carrier solution provides sufficient detail of damage with no observable effect on material properties. The best images of damage were obtained with long exposure times at a low accelerating voltage.

The particular penetrant solution used for this investigation was: zinc iodide (60 g), isopropyl alcohol

←Load Axis→

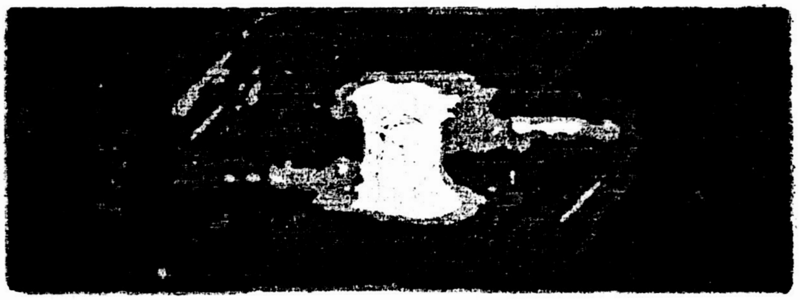

a) C-Scan

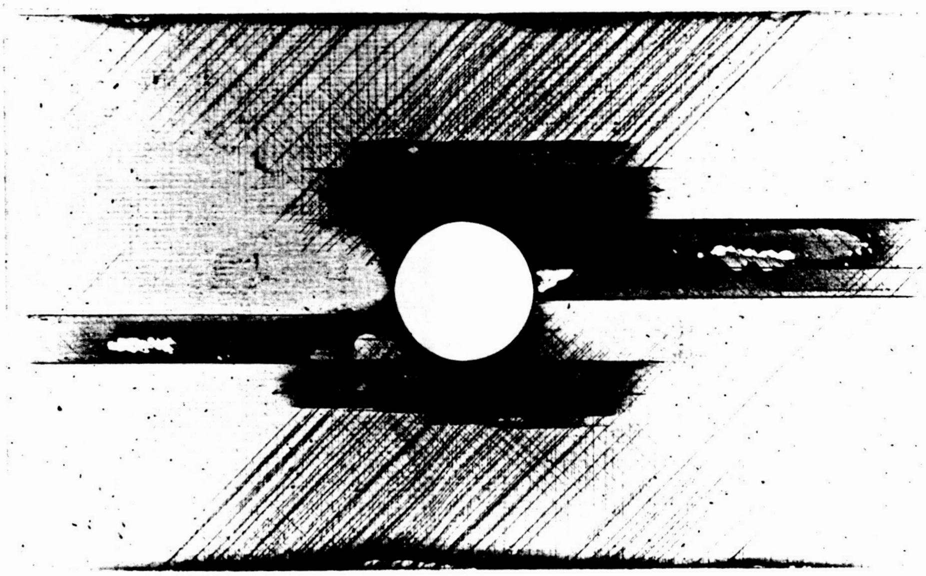

b) X-Ray

Figure 11: C-Scan and X-Ray Illustrations — Specimen 1-2, Low Level Fatigue Run-out

(10 ml), water (10 ml), and a wetting agent such as Kodak Photo-Flo 200 (10 ml). The procedure for taking an X-ray of a specimen at some point during a fatigue test was:

1. Stop cycling, remove instrumentation on the specimen and apply a nominal static load to open cracks.
2. Apply zinc iodide to all exposed edges and allow at least 10 minutes of penetration.
3. A relatively low level load cycling may help penetration without affecting results when the damage state is not rapidly changing.
4. Remove the specimen from load frame and lightly clean surface with acetone or water to remove excess penetrant. Cleaning too vigorously can dilute the penetrant in large flaws near the surface.
5. Place X-ray film (Kodak Industrex R, Single Emulsion or equivalent) under the specimen and expose to X-rays (Hewlett Packard 43805N Faxitron Series X-Ray System or equivalent).
6. Replace instrumentation on the specimen and put the assembly back into the load frame for further cycling.

To reduce the possibility of data biasing due to moisture, a moderate heating cycle (130°F or 54°C for several hours) was used in later tests to drive off the liquid carrier of the zinc iodide particles.

Up to three views of a specimen were needed to resolve the spatial distribution of damage throughout the material. The most commonly used was the face view (0 deg.), which projects transverse matrix cracks and delaminations through the thickness onto a two-dimensional image. An equally important view was from the thin edge (90 deg.), which enabled the extent of damage through the thickness to be determined by passing X-rays through the width of the specimen. Transverse cracks in the 90 deg. plies and delaminations were visible in this view. Only cracked 90 deg. plies and wide delaminations filled with penetrant provided enough opacity to block the passage of very high-energy X-rays passing through the width of the coupon. Occasionally, a third intermediate view was needed to pinpoint damage that could not be resolved with the other views. This is the angle view, named as such because it was taken at an intermediate angle (15 deg.) from the face view. Conventional stereo imaging was not utilized because of the overwhelming amount of information to be resolved through the thickness of 32-ply laminates.

The exposure settings for 0 and 15 deg. views were nominally three minutes at 25 thousand volts with approximately 21 in. (53 cm) between the source and specimen. For the 90 deg. views, a setting of four minutes at 85 thousand volts with a source distance of approximately 45 in. (114 cm) was deemed optimum. Tube current was approximately 2.5 milliamps. A longer distance between the X-ray source and the specimen ensures a sharper focus of minute damage details, particularly for the edge views.

A peculiarity of thick laminates is that certain types of damage are not highlighted as well as they would be in a thinner laminate. This is due to the integrating nature of radiography. For example, if there is a single delamination filled with zinc iodide in both a thick and thin laminate, it will not be as well contrasted in the thick. The X-rays must have a much higher energy level to pass through a thicker laminate, and are therefore less sensitive to an equal thickness of zinc iodide. This effect is proportional to thickness of the target, and is therefore more evident in the edge view radiograph than the face view.

A disadvantage of penetrant-enhanced radiography is that it is most effective when there is a direct path between the damage and the surface area on which penetrant is applied. However, Jamison [41] observed that even regions with no apparent connectivity to the surface had been infiltrated by zinc iodide after a long period of time had passed, which suggests that a diffusion process had occurred through an undamaged region of the laminate. It is therefore imperative that sufficient time be allowed for the penetrant to reach remote regions of damage in the interior of the laminate.

X-ray radiography was used extensively in this investigation to acquire the most complete estimate of the damage state. An example of an X-ray image of the same specimen C-scanned in Figure 11a is shown in Figure 11b. There is good overall agreement between the indicated regions of damage. Only the radiograph, however, distinguishes the actual damage modes. Transverse matrix cracks appear as sharp, thin lines parallel to the various ply orientations. Delaminations appear as broad, darkened regions. Frequently, when the gap between delaminated plies becomes too large to hold a significant amount of penetrant liquid, the delamination is indicated only along its frontier in the X-ray images. This may give the false impression of delaminations that disappear in areas where they were once indicated. In numerous X-ray radiographs presented later, the aluminum extensometer tabs that appear as black rectangles just above and below the notch should not be confused with damage.

Two specimens were cycled to failure with R=-1 at the high and low load levels mentioned earlier for the purpose of correlating the change of stiffness with the damage state as estimated with X-ray radiography. This enabled the recording of a complete damage history to failure that could be used to plan additional tests with different min/max load ratios.

2.4.2 Destructive Evaluation

An unfortunate consequence of two additional damage evaluation techniques utilized in this investigation is that the specimen is destroyed. These techniques are: residual strength measurement; and laminate deply. Destructive evaluations cannot be used to continuously monitor the change of a material property in the same laminate, but they do provide information that cannot as yet be obtained nondestructively. Eight specimens were cycled in pairs to similar amounts of damage, as determined by NDE methods, and subjected to destructive evaluation. These pairs were: low load level to middle and late states of damage; and high load level to the same states of damage. One of each pair was subjected to a measurement of tensile residual strength and the other was deplied.

2.4.2.1 Residual Strength

Residual strength is a topic of major concern to designers who are concerned with long-term durability of structural components. It is also important to scientists and engineers striving to understand the mechanisms of damage development and how they affect laminate life. This investigation addresses the residual tensile strength properties in particular. Residual compressive strength of the laminate (defined by the onset of compressive instability) is also considered in the context of its affect on fatigue life.

Several test coupons were monotonically loaded to tensile failure at various stages of damage development. Load-strain curves were recorded using strain from a one inch (25.4 mm) extensometer centered over the hole and a strain gage centered on the thin edge. Strength and strain data are compared to those of undamaged specimens.

2.4.2.2 Laminate Deply

The deply technique facilitates the location and identification of damage at the ply interfaces of a laminate [69,70] by enabling the separation of individual laminae. Fiber fractures, delaminations and transverse matrix cracks are among the principle forms of damage that can be resolved with this technique. In this investigation, deply was used primarily to determine the extent of matrix-related damage through the thickness of the laminate. An abbreviated procedure for the technique is provided in the sequel.

A marking agent (gold chloride) is dispersed in a low-viscosity, low-surface-tension liquid carrier and applied to the edges of the damaged laminate in a manner similar to zinc iodide in X-ray radiography. When allowed sufficient time to penetrate (at least 30 minutes), the gold particles will mark all interior damage areas accessible from the surface so that they may be viewed upon separation of the laminae.

The marking solution consists of 9.2 to 9.6 percent by weight AuCl, with the remainder being diethyl ether or isopropyl alcohol. A few drops of wetting agent, such as Kodak Photo-Flo 200, are added to improve penetration into small cracks. After the AuCl solution has been introduced to the regions of damage, a low temperature heating cycle is applied to the laminate to drive off the liquid carrier (this prevents gas bubble formation during the higher temperature heating cycle). Next, the laminate is heated in an oven at 785 degrees Fahrenheit (418 degrees Celsius) for two hours so that the epoxy matrix becomes pyrolized. This must be done in an externally ventilated and inert (argon gas) environment to avoid the inhaling of noxious fumes released during the process, and to prevent oxidation of the laminate. Plies of different orientations can then be separated using a sharp, thin blade to free any local spots that are not completely pyrolized.

Matrix cracks are indirectly visible by their fine gold tracings on adjacent plies. Some large regions marked by the AuCl, such as well-developed delaminations, are visible with the naked eye, but magnification of 7X to 140X is needed to distinguish fine details such as matrix crack tracings and small delaminations. When a high-intensity light is aligned such that the beam is at a shallow angle to the lamina and parallel to the fibers, optimum contrast is obtained for viewing forms of matrix damage with optical microscopy. Optical microscopes are not acceptable for magnifications exceeding 140X because their depth-of-field is exceeded by surface irregularities. Very small forms of damage, such as fiber fracture are best viewed with a scanning electron microscope at magnifications of 200 to 300X. Images of gold tracings on a black lamina are difficult to distinguish from artifacts of the deply process resulting from incomplete pyrolysis since they both appear as grey regions in a black and white photograph (Figure 12). Improved recording of observations could be realized by tracing the marked regions onto clear acetate film with a marking pen.

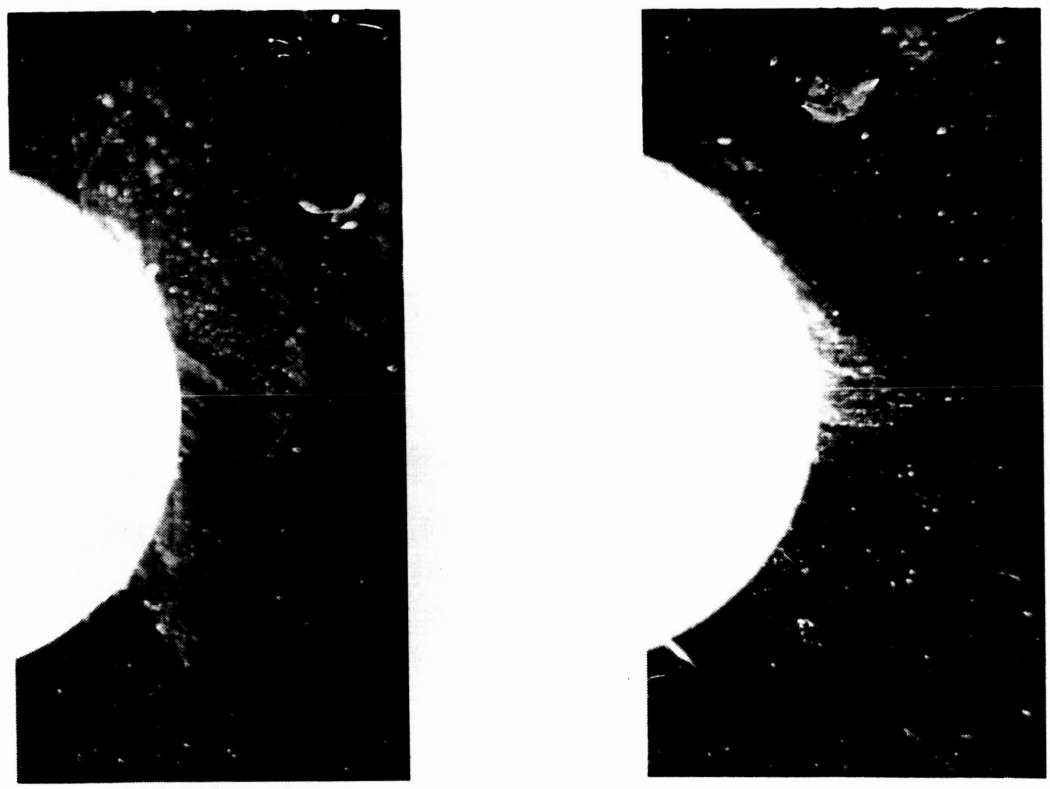

(a) 0/45 Interface (b) 45/90 Interface

Figure 12: Photographs of Deplied Laminae Near the Notch (Rear View)

2.5 DATA REDUCTION

In experimental studies of composite materials, there is frequently a large variation in the mechanical response of different test specimens. For example, in this investigation, initial stiffness measurements of undamaged specimens varied by as much as ten percent. A large data base with a statistical analysis to account for such variation was not possible within the scope of this investigation. Therefore, conclusions regarding stiffness behavior had to be based on mostly qualitative information. To achieve this, special data reduction techniques were employed to interpret scattered data. Stiffness change during fatigue cycling of different coupons could be compared by normalizing each to its initial, undamaged stiffness. Large variations in the life of different coupons tested at the same load level sometimes make it useful to express the "age" of the specimen as a fraction of its life (which was only possible in the several tests run until failure). This normalization technique simplifies the characterization of stiffness behavior so that a valid and consistent correlation between stiffness and damage can be realized in any test. Two or more specimens at approximately the same damage state can then be compared via destructive or nondestructive damage evaluation techniques.

The choice of a parameter on which to base comparisons is of course arbitrary, but the correlation of damage with stiffness was seen to be better than with a simple cycle count.

Chapter III

RESULTS AND DISCUSSION

3.1 STATIC MATERIAL PROPERTIES

Based on all tests performed, the mean undamaged tensile and compressive stiffnesses (unnotched area stress divided by strain measured by the one inch extensometer centered on the hole) were 5.2 and 4.9 Msi (35 and 34 GPa), respectively. The standard deviation was three percent in each case. Compressive strength, as reported in Section 2.3, was -10 kip (-45 kN), or -41 ksi (-280 MPa) on the unnotched area (Table 1). Ultimate compressive strains at the hole and at the straight edge were -7900 and -5000 $\mu\varepsilon$, respectively. For comparative purposes, compression tests on different graphite-epoxy material systems of similar stacking sequence, but different structural geometry (such as hole dia./width ratio, length, thickness, constraint) in [22] and [57] indicated strengths of -45 ksi (-310 MPa) for 16-ply laminates, and -59 ksi (-410 MPa) for 48-ply laminates, respectively. Visual examination of the compression fracture surface indicated a crushing mode of failure along a section transverse to the load axis and passing through the hole (Figure 8). Fracture of the surface 0 deg. plies followed the underlying +45 deg. plies a short distance away from the hole. Major delaminations were adjacent to the 0 deg. plies through the thickness. Many of the details of the fracture surface were lost due to the crushing of the specimen after failure.

Mean ultimate load in tension for seven specimens was 9400 lb. (42 kN), or 38 ksi (260 MPa) on the unnotched area. Mean tensile strains for two specimens across the hole and on the edge were 7300 and 4600 $\mu\varepsilon$, respectively. In comparison, the static tensile strength of somewhat similar laminates in [22] and [57] were 41 ksi (280 MPa) and 44 ksi (300 MPa), respectively. Visual observation of the tensile fracture surface revealed that few -45 deg. plies through the thickness had broken fibers. That is, most of these double-thick plies sheared out of the surrounding 90 deg. plies, creating a large delaminated surface in the process (Figure 13). Fibers in the surface +45 deg. plies remained intact close to the hole. Further in the interior of the laminate and away from the hole, fibers in these plies broke along a transverse section to the load axis. Practically all 90 deg. plies exhibited a matrix-mode of failure through the hole center. There were broken fibers in the zero deg. plies along the underlying +45 deg. matrix fracture line near the hole. Further away from the hole, the 0 deg. plies usually fractured more uniformly

TABLE 1

Static and Residual Properties‡

Fatigue Data					Static and Residual Data			
Specimen I.D.	Load History, min load/max load (lb)	to cycles (K)	Extensometer Stiffness** T	C	Hole Strain, ϵ_1 ($\mu\epsilon$)	Edge Strain, ϵ_2 ($\mu\epsilon$)	$\frac{\epsilon_1}{\epsilon_2}$	Load (lb)
5-14	Static Tension	--	--	--	7300## [1.0]	4600## [1.0]	1.6## [1.0]	9400* [1.0]
6-11	Static Compression	--	--	--	-7900	-5000	1.6	-10000
3-11	Quasi-Static Tension	--	--	--	7300 [1.0]	4300 [.93]	1.7 [1.1]	9300 [.99]
2-8	-4500/+4500 (Early Stage II)	300	[.92]	[.91]	8800 [1.2]	5000 [1.1]	1.8 [1.1]	10200 [1.1]
2-11	-4500/+4500 (Late Stage II)	500	[.86]	[.83]	12000 [1.6]	6200 [1.3]	1.9 [1.2]	13100 [1.4]
1-8	-5000/+5000 (Late Stage III)	961	[.84]	[.87]***	10300 [1.4]	5300 [1.2]	1.9 [1.2]	11200 [1.2]
2-14	-5500/+5500 (Early Stage II)	25	[.90]	[.90]	10300 [1.4]	5800 [1.3]	1.8 [1.1]	12000 [1.3]
2-5	-5500/+5500 (Late Stage II)	250	[.86]	[.79]	10800 [1.5]	5500 [1.2]	2.0 [1.3]	11900 [1.3]
1-11	-5500/+5500 (Late Stage III)	315	[.80]	[.73]	11300 [1.5]	5200 [1.1]	2.2 [1.4]	11500 [1.2]
5-8	-4500/+4500 -4500/+7500 (Late Stage III)	200 245	[.71]	[.70]	11900 [1.6]	5100 [1.1]	2.3 [1.4]	11600 [1.2]
3-8	-4500/+4500 -2200/+7500 (Late Stage III)	200 361	[.61]	[.64]	11500 [1.6]	5100 [1.1]	2.3 [1.4]	12400 [1.3]
3-14	-4500/+4500 + 750/+7500 (Run-out)	200 1000	[.88]	[.88]	9900 [1.4]	5700 [1.2]	1.7 [1.1]	12100 [1.3]

Unit Conversion Factors: 4.45N=1 lb; 6.90 MPa=1 ksi.

‡ Numbers in square brackets are normalized to initial, undamaged values.

** T=tension, C=compression.

Mean of two tests.

* Mean of seven tests.

*** Increasing, due to out-of-plane deformation.

perpendicular to the load axis. Occasionally, the fracture line in the outermost 0 deg. plies travelled along an underlying +45 transverse crack the entire distance from the hole to the straight edge. These results suggest an interaction between the fracture locus of zero deg. fibers and early-forming matrix cracks in an adjacent ply. There was a certain amount of variability in the appearance of static tensile fracture surfaces, with some not displaying any shearout of double -45 deg. plies.

The ratio of strain at the hole to strain at the straight edge was computed for the undamaged specimens so that a comparison could be made with specimens damaged by fatigue loading. The ratios for compression and tension static failure were 1.58 and 1.59, respectively. Mean ultimate strains from two tests and mean ultimate loads from seven tests were used as a normalization factor for tensile tests to be performed on fatigue-damaged specimens. Table 1 contains the absolute and normalized values of ultimate load and strain measured with a one inch extensometer across the hole and with a strain gage on the thin edge of the laminate (Figure 2).

a) Edge View

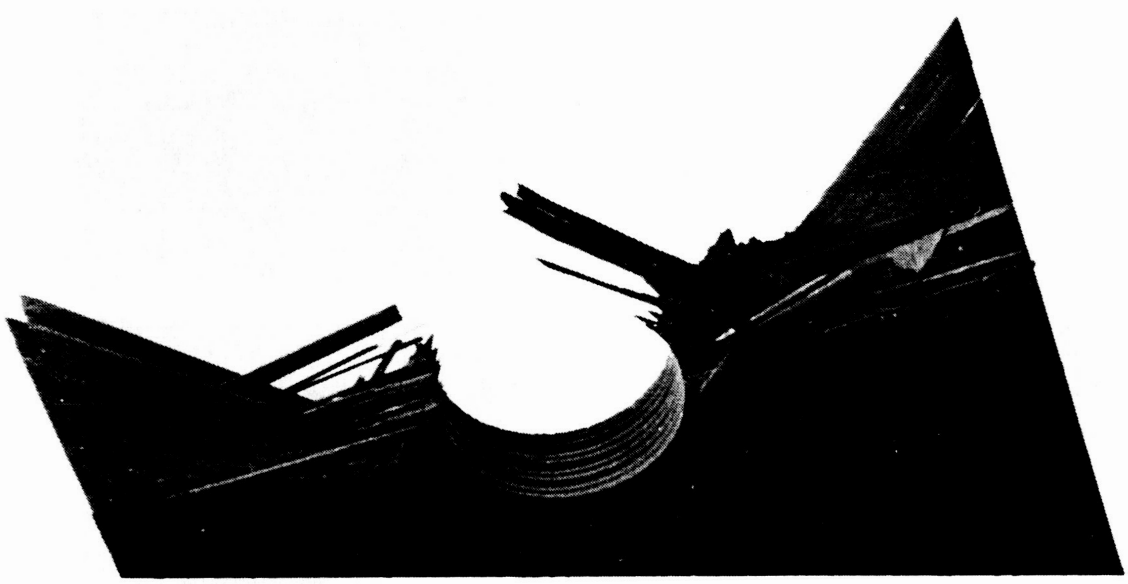

b) Front Face View

Figure 13: Static Tensile Fracture Surface

3.2 T-C FATIGUE LIFE DATA

Specimens cycled at the low load level (R=-1) experienced lives of 451K cycles to run-outs at 2.6M cycles. At the high load level, lives were on the order of 100K cycles. Unnotched area stress is plotted versus cycles to failure for the tests run at R=-1 in Figure 14. Life data from previous T-C fatigue studies of similar laminates (same stacking sequence, nearly same material, but different geometry and constraint) [22,57] are included in this figure for comparison, and agree reasonably well with the present data. The limited life information from several tests run at load ratios other than -1 will be discussed under separate headings for each particular test.

3.3 STIFFNESS RESPONSE TO T-C FATIGUE

Three regions can be distinguished in a plot of normalized tension and compression secant stiffnesses (E_T and E_C) versus cycles for high and low level fatigue tests at R=-1, as shown in Figure 15. Analogous stiffness behavior has been reported previously in the literature for various notched and unnotched laminates [36]. The first region, called stage I, is distinguished by a rapid, but slowing loss of stiffness. The compression stiffness decreases faster than tension stiffness during this stage. During

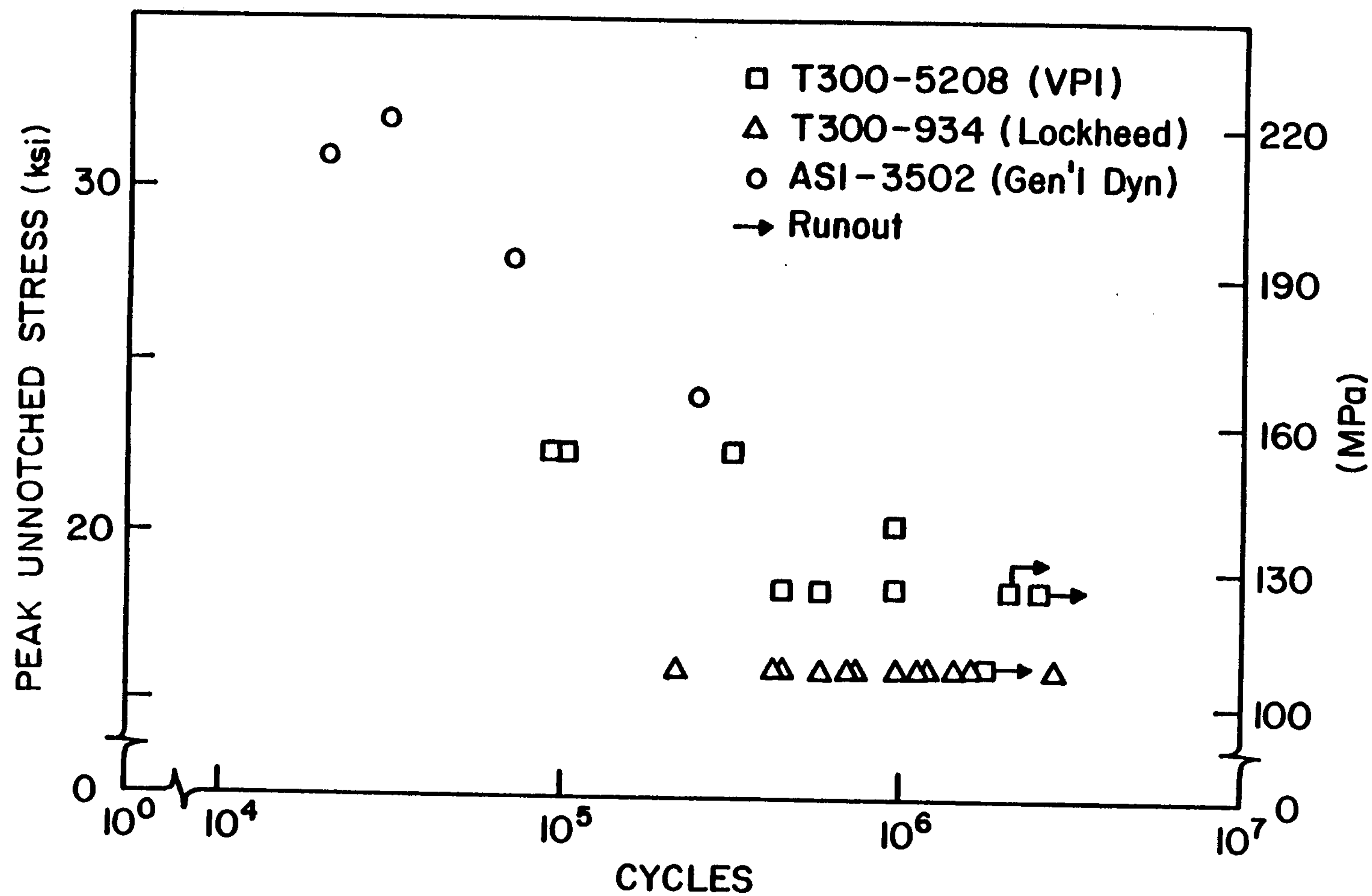

Figure 14: Stress - Life Relation for Different Material and Geometry, R=-1, $[(0/45/90/-45)_s]_4$

stage II, stiffness loss is the slowest of any time in the fatigue life of the specimen, and is roughly linear with respect to cycles. Compression and tension stiffnesses decrease at about the same rate. Stage III is a period of relatively rapid stiffness change that accelerates immediately preceding failure. During the last stage, apparent compression stiffness may decrease, increase or undergo some combination thereof, depending on the out-of-plane deflection of the coupon relative to the strain measuring device. Tension stiffness will decrease if stage III is long enough to permit this. Often, the laminate's buckling resistance decreases too rapidly near the end of life to observe a change in tensile stiffness using quasi-continuous stiffness monitoring. These three stages will be referred to throughout the detailed discussion of damage accumulation for each load level at R=-1. The stiffness response of laminates under load ratios different than -1 will be discussed separately in their respective sections.

A comparison of fundamental stiffness behavior at the two loads is facilitated by using a normalized life axis in place of the cycles axis. Figure 15 contains such scales to compare the typical location of stiffness transitions as a percentage of fatigue life. The transition between stages I

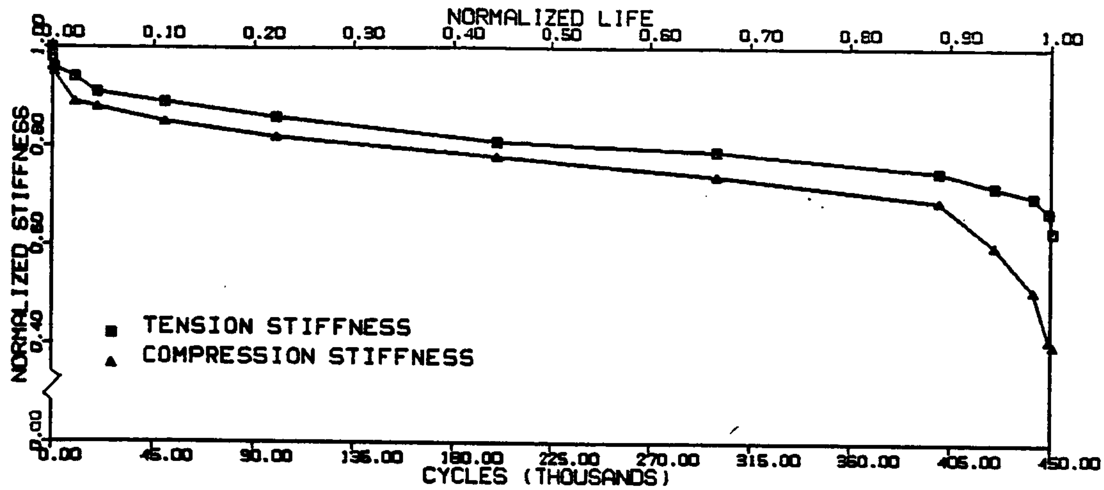

a) Low Load Level (±4500 lb., Specimen 6-2)

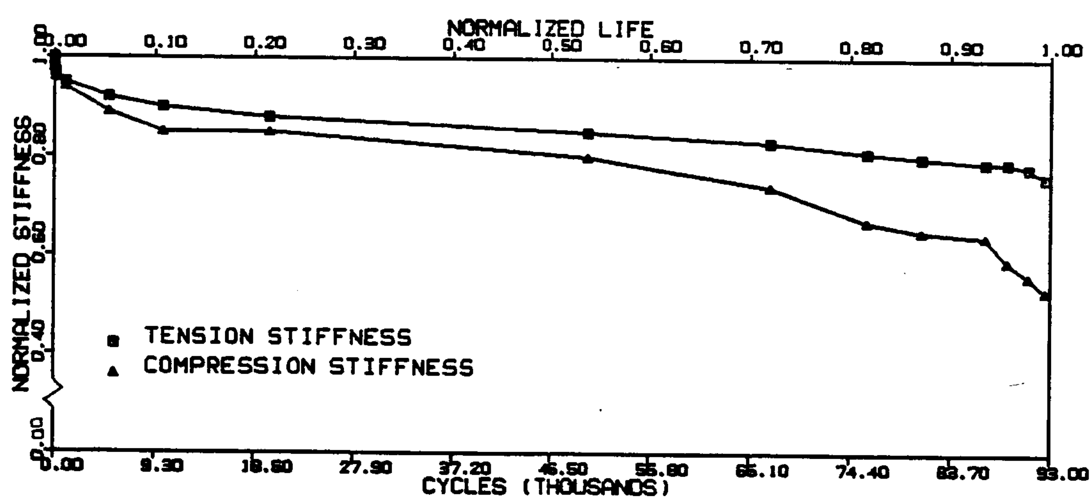

b) High Load Level (±5500 lb., Specimen 1-5)

Figure 15: Secant Stiffness Degradation to Failure, R=-1

and II occurs at about 10 percent of life at both load levels. The transition between stages II and III occurs at about 90 percent of life for the low load level and 95 percent for the high load level. A more direct comparison of tensile and compressive stiffness behavior is illustrated in Figure 16a, where the tensile stiffnesses of high and low level tests have been superimposed, and Figure 16b, where the same has been done for compressive stiffnesses. The utility of stiffness degradation as an indicator of "age" in different specimens at various load levels is apparent. To compare high and low load level stiffness behavior on a "real time" basis, the same stiffness data have been replotted on a linear cycles axis in Figure 17.

As a check on the possibility of stiffness bias caused by the use of the secant measurement technique (at peak fatigue load), several sets of strain measurements were acquired at ±1000 lb. (±4.45 kN) as a representation of the tangent tension and compression stiffnesses. Results of one such data set recorded during a high load level test are shown in Figure 18, along with the usual secant stiffness measured at the peak fatigue load amplitude. The conclusion drawn from several such comparisons is that there is no significant difference between secant and tangent stiffness behavior at the load levels used in this investigation, particularly when the stiffnesses are normalized to their initial values.

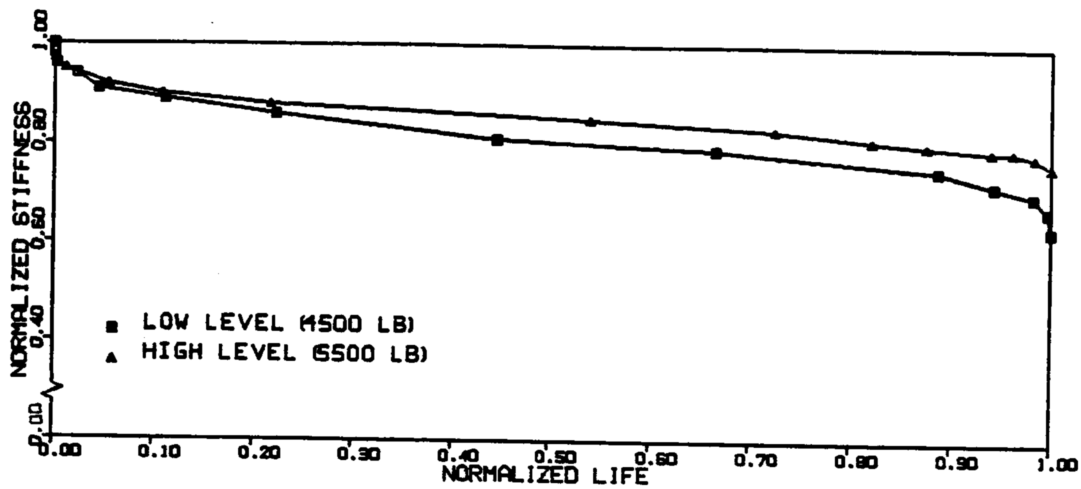

a) Tension Stiffness

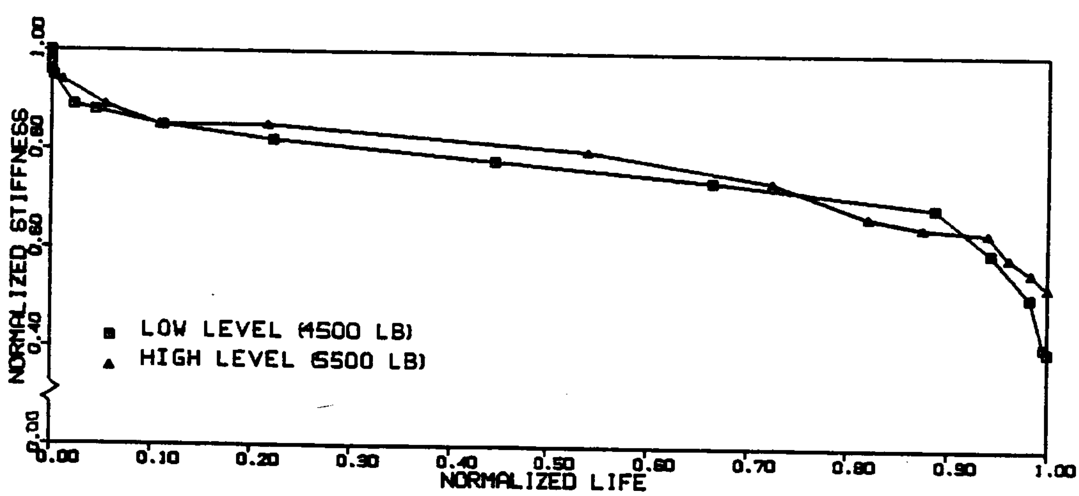

b) Compression Stiffness

Figure 16: Secant Stiffness - Normalized Life Relation to Failure, R=-1

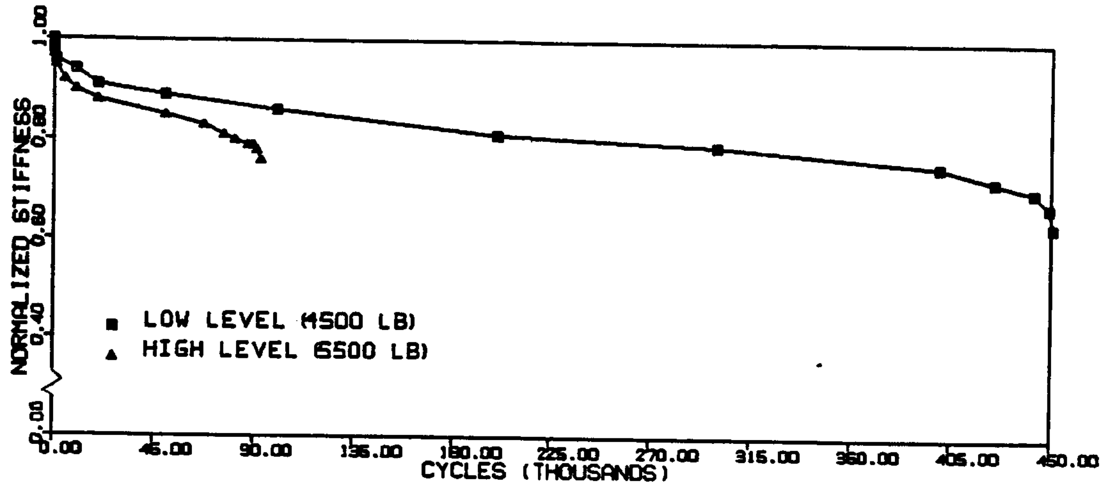

a) Tension Stiffness

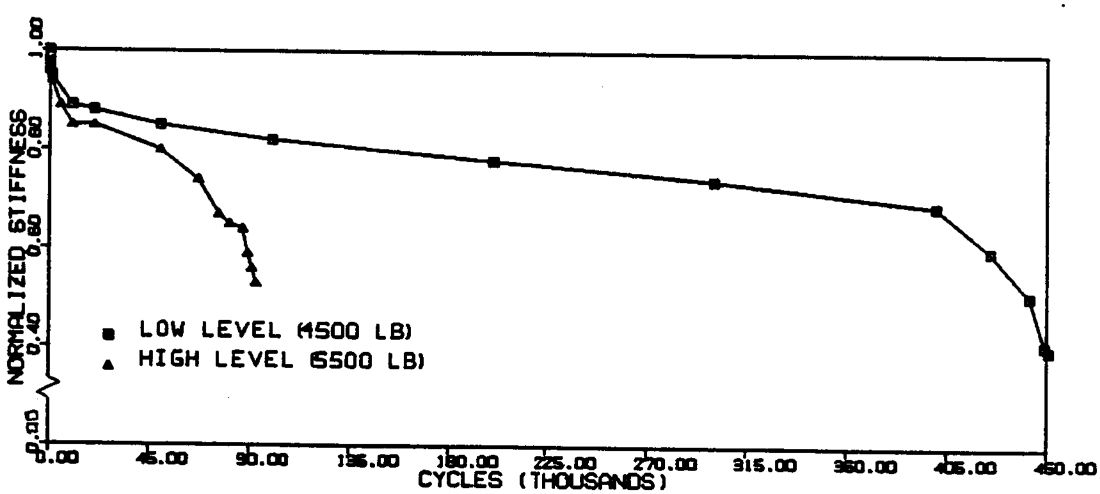

b) Compression Stiffness

Figure 17: Real-Time Secant Stiffness - Life Relation to Failure, R=-1

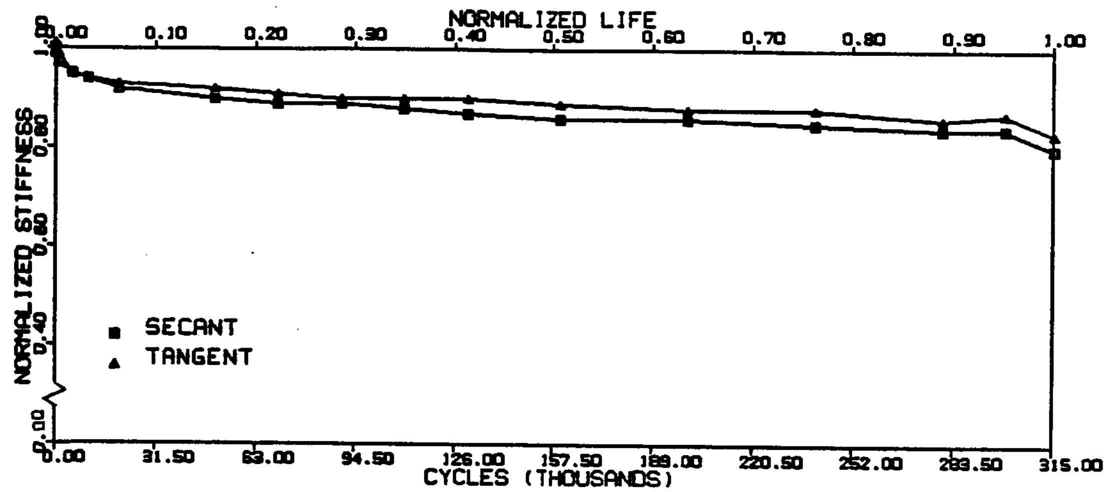

a) Tension Stiffness

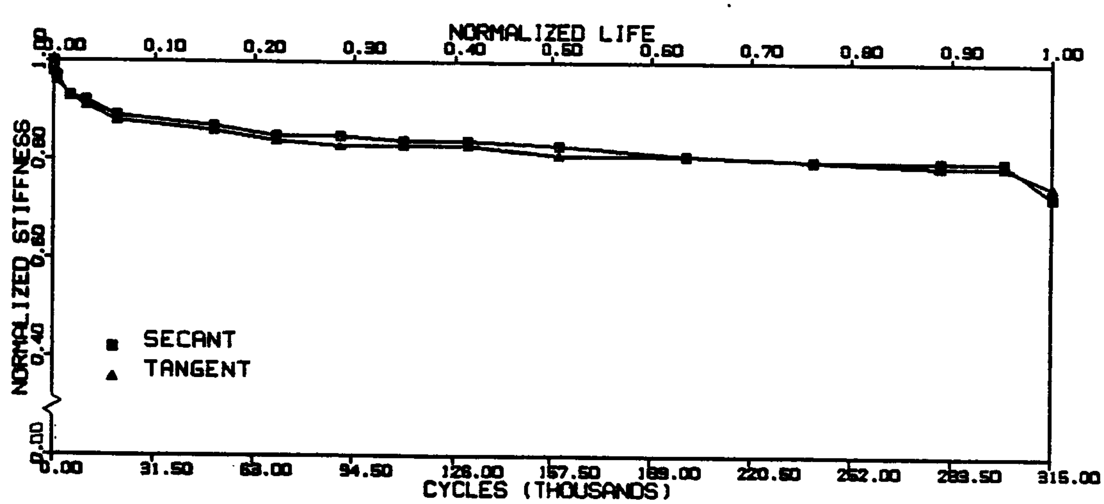

b) Compression Stiffness

Figure 18: Secant and Tangent Stiffness, High Level Fatigue to Failure (±5500 lb.), Specimen 1-11

3.4 FATIGUE DAMAGE MECHANISMS

The significance of characteristic stiffness behavior in the context of damage development will be discussed in the sequel for each of the load levels addressed. Under several different load amplitudes and negative load ratios, the laminate used in this investigation displayed fundamentally similar mechanisms of damage development. X-ray radiographs of several specimens may be used to illustrate damage development during a particular load case. This should not present any problem since damage development in different specimens at the same load level and ratio was nearly the same up to stage III. The last few damage events observed prior to failure are peculiar to each specimen, but actually represent the same mode of damage for this particular laminate. Information regarding the material's response is presented in chronological order. For brevity, transverse matrix cracks (parallel to fibers) are often called simply "cracks." "Delaminations" are also forms of matrix cracks, but are called by their own name.

3.4.1 Low Load Level Damage Development, R=-1

Three specimens cycled at the low load level (±4500 lb, ±20.0 kN) failed at 451K, 584K, and 970K cycles. Two additional tests were halted at 2.1M and 2.6M cycles with no sign of imminent failure, and were classified as run-outs. A photograph of a specimen that failed in low level fatigue is shown in Figure 19. Note the highly dispersed fracture surface, which is characteristic of highly damaged specimens. Laminate failure was caused by the buckling of delaminated groups of laminae and the resulting loss of compressive stiffness.

3.4.1.1 Stage I

As a reference radiograph, the initial state of damage caused by machining in specimen 3-8 is shown in Figure 20a. Within 10 load cycles, 0 deg. cracks tangent to the hole appear. At this early stage of life, any delaminations under the surface plies resulting from the drilling process grow slowly away from the hole boundary. Cracks in all other off-axis plies form along the hole boundary by 100 cycles. Cracking is concentrated along the 0 deg. cracks tangent to the hole. The 90 deg. cracks are most dense where there are ±45 deg. cracks, and appear to initiate and grow along the double-thickness -45 deg. cracks. Cracks in

a) Edge View

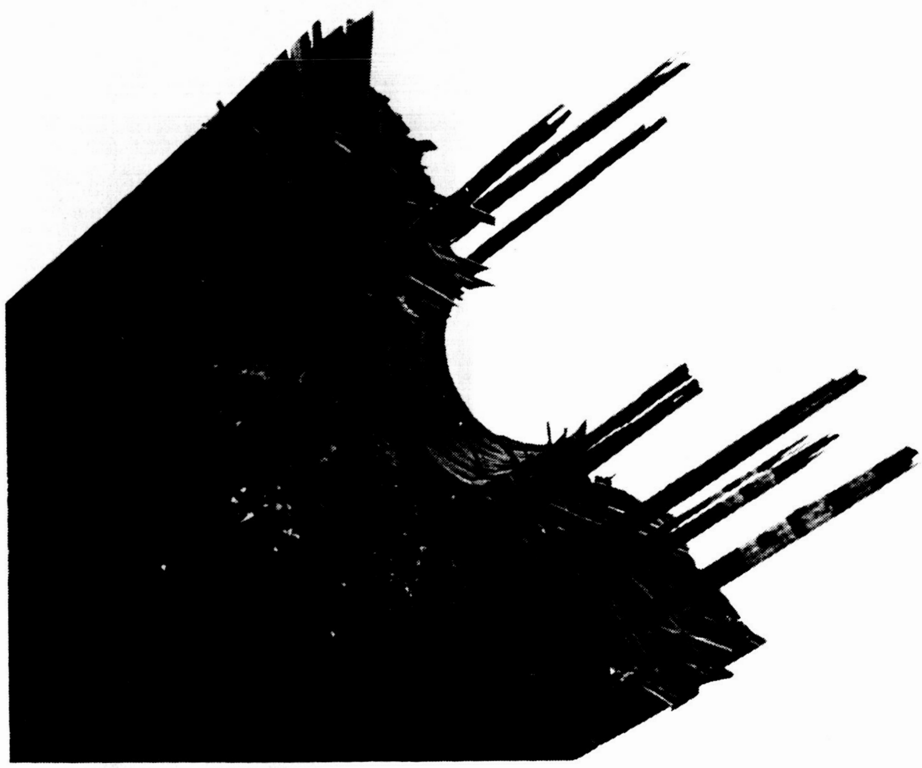

b) Front Face View

Figure 19: Low Level Fatigue Fracture Surface

the +45 deg. plies are much denser, but not as long as the -45 deg. cracks. All matrix cracking initiates randomly through the thickness and within a thousand cycles is distributed rather uniformly in this respect (Figure 20b, specimen 3-8). Tension and compression stiffnesses at this time are about 96 to 98 percent of initial values, with compression generally being the lesser of the two.

At one to five thousand cycles, interlaminar cracking begins to take place on the 45/90 interfaces closest to both surfaces, followed closely by 90/-45 interfaces. Thus, at the point where a 90 deg. matrix crack meets the neighboring ±45 deg. ply, the crack makes a turn and follows that interface. This occurs at the 90 deg. and 270 deg. angular positions on the hole boundary and represents delamination initiation. The direction of growth is very consistent in that the delaminations on opposite sides of the 90 deg. crack travel in opposite directions (Figure 21). Perhaps more than coincidentally, the +45 and -45 deg. tangent cracks closest to the surface have crossed the 90 deg. crack at the 90 deg. and 270 deg. angular positions on the hole boundary in this same interval of cycles, suggesting a connection of these events.

There are other delamination initiation processes occurring along the hole at the same time as those at the

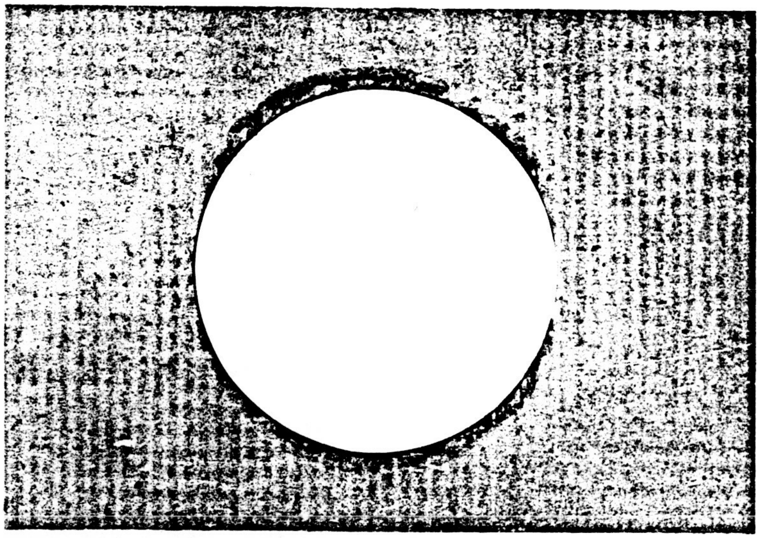

a) Zero Cycles

↑ Load Axis ↓

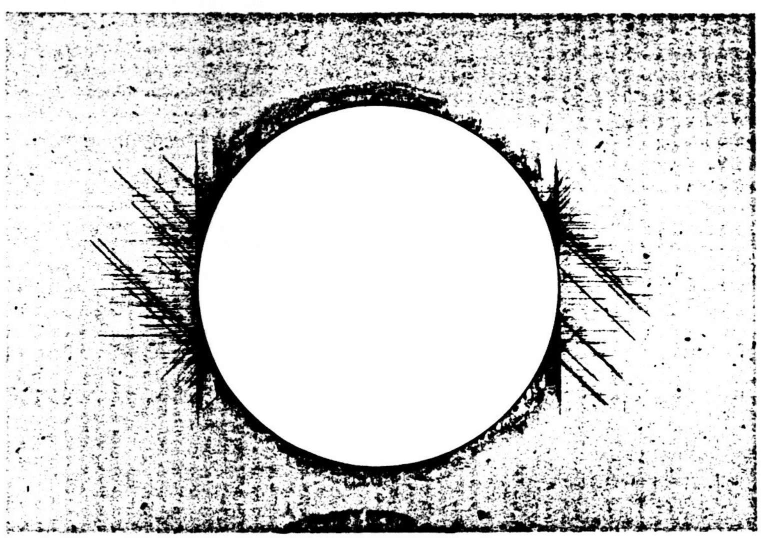

b) 1K Cycles

Figure 20: Radiographs, Early Stage I, Low Level

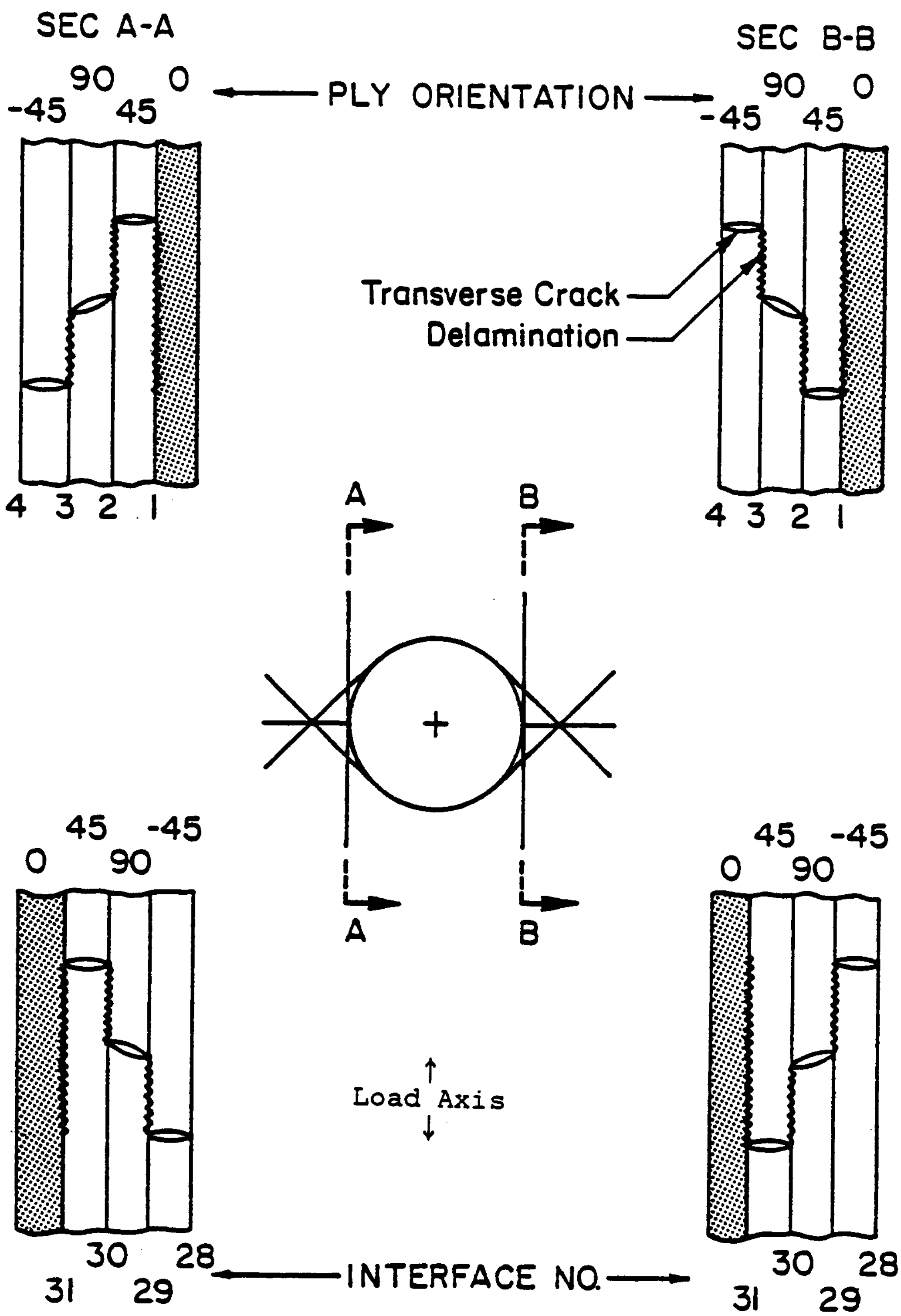

Figure 21: Delamination Initiation Schematic

45/90 and 90/-45 interfaces. At the first 0/45 interfaces under both surfaces (provided there was no drill breakout damage there initially), eight individual delaminations initiate in the densely cracked regions bounded by 0 and ±45 deg. tangent cracks. Often, delamination at this interface occurs earlier in the second and fourth quadrants around the hole, where the 0 and +45 deg. cracks overlap each other in adjacent plies. These surface delaminations grow away from the hole, but are arrested in lateral growth by the presence of the 0 deg. tangent cracks. Within a few thousand cycles, the edge-view X-ray indicates delamination formation at each 0/45 interface through the thickness in the region bounded by 0 deg. tangent cracks and the hole boundary. Figure 22 illustrates the face and edge view radiographs of specimen 3-8 at 5K cycles. Some of the delamination locations just described may not yet be clear in the edge view, since some fidelity is lost in the printing process. Stiffnesses measured with the extensometer during this delamination initiation period are 94 to 96 percent of initial values.

Between 5K and 10K cycles, the second set of 45/90 and 90/-45 interfaces beneath the surface delaminate in an identical manner as the first, while all transverse matrix cracks extend in length. New delaminations initiate on the

←Load Axis→

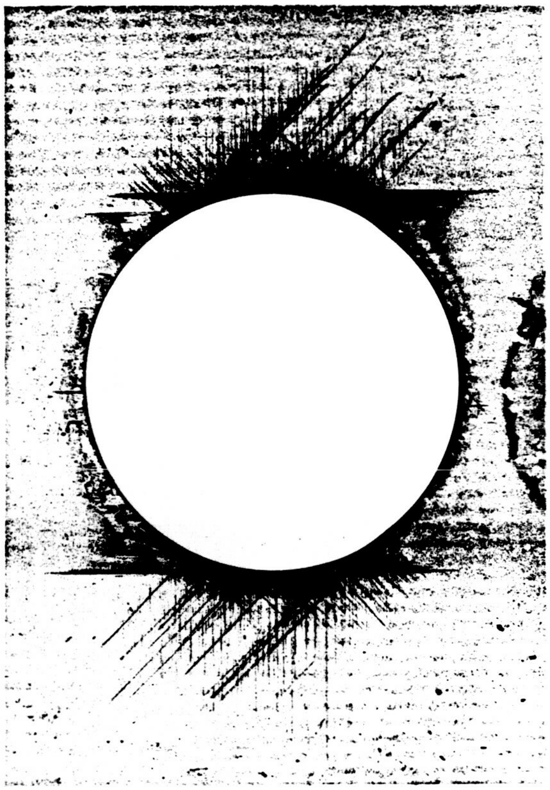

Front Face View

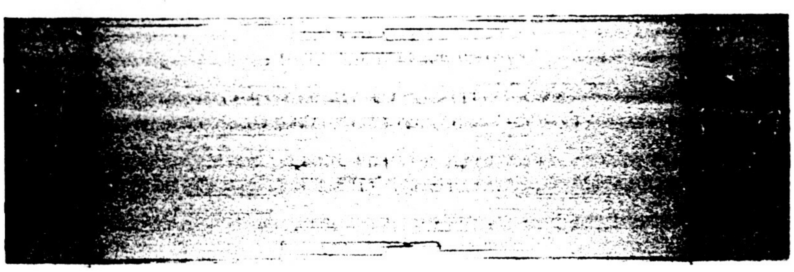

Left Edge View

Figure 22: Radiographs at Stage I (5K), Low Level

outside of the 0 deg. tangents under the surface plies. This event can be sudden, and results in a narrow strip of 0 deg. fibers buckling away from the remainder of the laminate within a few cycles. "Second generation" cracks occur as ±45 deg. cracks initiate along the length of the existing 0 deg. tangents. Delaminations on the 0/45 interfaces through the thickness extend with the 0 deg. cracks tangent to the hole. The length of these tangent cracks and delaminations are a function of distance from the surface, with those at the surface being longest. Stiffnesses by 10K cycles are between 91 and 93 percent of the initial values.

Up to this point, there has been rapid damage development and stiffness loss. Most unique modes of damage have appeared near the surface of the laminate, but not necessarily in the interior. Between 10K cycles and 40K cycles, the damage development process begins to gradually slow as all like interfaces through the thickness delaminate in a similar manner (Figure 23, specimen 3-8 at 40K cycles). "Third generation" cracks appear in the region between the 0 deg. tangents when 90 deg. cracks initiate along the 45 deg. cracks, which in turn initiated from the 0 deg. cracks. Assuming that this phenomenon is not caused by a delayed infusion of zinc iodide into cracks formed earlier in the fatigue life (which cannot be determined), the implication here is that the region above and below the hole must still bear significant load, even though it is somewhat isolated by 0 deg. cracks. The -45 deg. cracks extend approximately half the distance to the straight edge of the test coupon. At the straight edge, there may be some edge-initiated matrix cracking in off-axis plies. This typically begins with 90 deg. cracks, followed by a -45 deg. crack that crosses the first at a small distance from the edge. Cracks in the +45 deg. plies later initiate in the same vicinity, which would eventually complete the formation of the "characteristic damage state" on the free edge if a uniform state of stress were present.

Stage I of damage development is usually completed by 40K to 60K cycles. Delaminations at this time are present at all like interfaces through the thickness of the laminate. The 0 deg. cracks closer to the surface, and the 0/45 delaminations that follow them, are still of larger extent than their counterparts in the laminate interior. Lateral growth of the outermost 0/45 delaminations consists of narrow strips of 0 deg. fibers buckling away from the remainder of the laminate. This process usually initiates at the underlying +45 deg. crack that is tangent to the hole and quickly spreads longitudinally in both directions. Edge radiographs indicate that the delaminations on either side

←Load Axis→

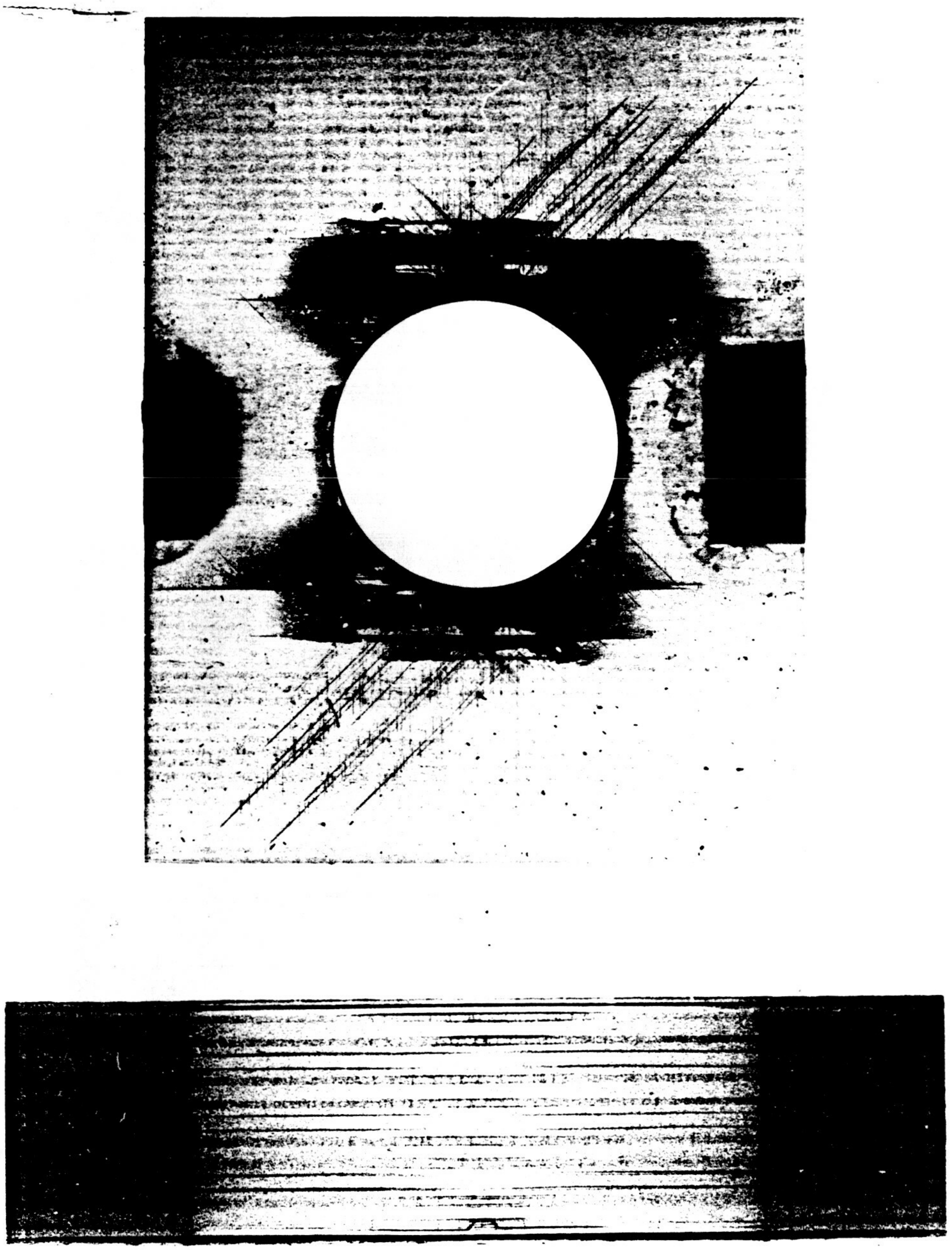

Figure 23: Radiographs Near the End of Stage I, Low Level

of the 90 deg. plies are of equal extent and that these particular delaminations remain confined to the triangular region formed by the ±45 deg. tangent cracks and the hole boundary. For specimens with finite fatigue life at this load level, stage I comprises roughly 10 percent of life. Stiffnesses are between 85 and 91 percent of their initial values, where E_C is about five percent less than E_T.

3.4.1.2 Stage II

Stage II of stiffness degradation and damage development is characterized by a relatively slow growth of matrix cracking and delamination during roughly 80 percent of finite fatigue life. In the first half of stage II, matrix cracks become denser and longer throughout the laminate, with most new crack initiation and growth occurring away from the hole. Matrix cracks in the -45 deg. plies, along with their secondary 90 deg. cracks, extend continuously from the hole to the straight edge in the early part of stage II. Figure 24a is a magnification of +45 deg. cracks initiating along 90 deg. cracks in an area far from the hole (specimen 2-2 at 100K cycles). Hole-related delaminations in the outermost 0/45 interfaces continue to slowly grow laterally and longitudinally away from the hole. The 45/90 and 90/-45 interfaces do not grow longitudinally, but become bolder in

c-2

the edge view radiograph, which suggests that they are growing laterally (Figure 24b). Stiffnesses at this time are degrading roughly linearly with cycles, and are about 78 to 90 percent of their initial values (tension approximately 5 percent greater than compression).

During the second half of stage II, straight edge delamination growth occurs in regions of dense transverse cracks, as shown in Figure 25a for specimen 6-2 at 90 percent of life. This type of delamination tends to grow along one of the prominent ±45 deg. transverse matrix cracks that originates tangent to the hole, and is frequently on more than one interface near the laminate's surface that contains a +45 or -45 deg. ply (interfaces 1 through 11 and 19 through 31 in Figure 1). Edge view radiographs at this time still indicate that the 0 deg. tangent cracks and 0/45 delaminations favor the surface in a somewhat exponential manner. That is, there is an asymptotic decrease in delamination and crack size as the distance from the surface increases (especially in the second and fourth quadrants around the hole). In the region between the 0 deg. tangents above and below the hole, splits occur in the surface 0 deg. ply, allowing the underlying 0/45 delamination to rapidly grow longitudinally. At the low load level, these particular delaminations have a width of approximately one

←Load Axis→

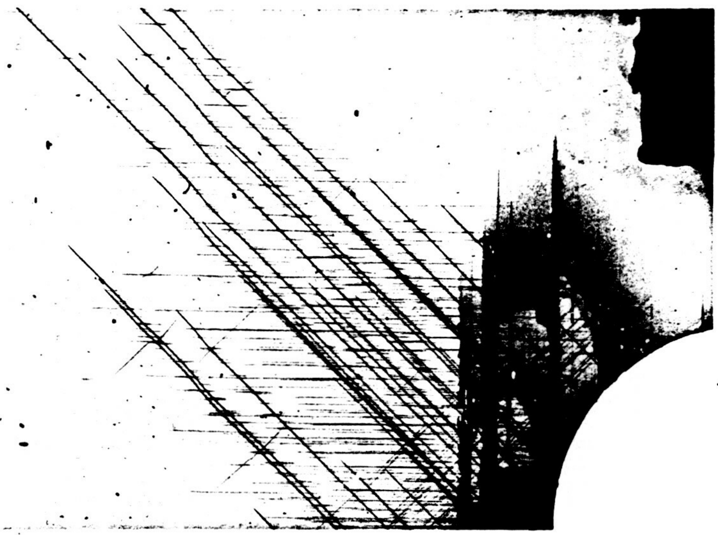

a) Specimen 2-2 At 100K, Fourth Quadrant

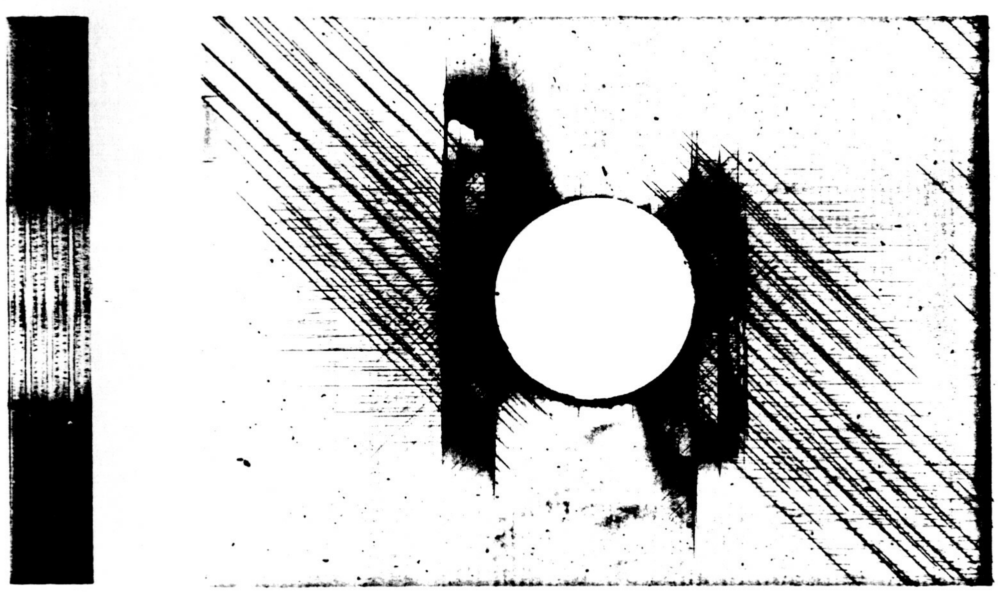

b) Specimen 4-11 at 300K

Figure 24: Radiographs, Stage II, Low Level

hole radius, and they are situated anti-symmetrically with respect to the hole center (Figure 25a). If late-forming damage disrupts the in-plane elastic symmetry of the laminate, compressive instability results and stage III begins. At the end of stage II, normalized stiffnesses are typically 75 to 80 percent, with compression being 5 to 10 percent lower than tension.

Residual strength and deply data were obtained for test specimens at approximately 30 and 70 percent of life. One pair of specimens was matched in stiffness degradation for each of the two selected states of damage. Mean normalized stiffnesses of the first pair were about 90 percent, while those of the second pair were about 88 percent in tension and 81 percent in compression. One of each pair was deplied and the other monotonically loaded in tension to failure. Previous non-destructive inspection of these specimens with C-scanning and X-ray radiography supported the contention that a similar state of damage had been induced in each of the matched pairs.

Photographs of gold-chloride-enhanced indications of matrix cracks and delaminations in the early stage II, low level fatigue specimen (no. 4-11) are shown in Figures 12a and b. Because of the low resolution of these photos, schematic reproductions of the first half of the deplied

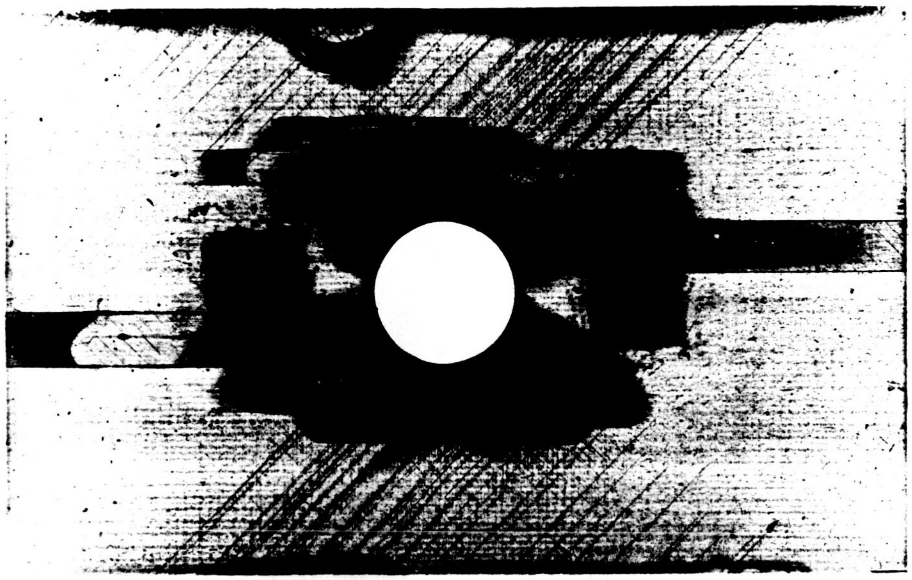

a) Specimen 6-2 at Late Stage II

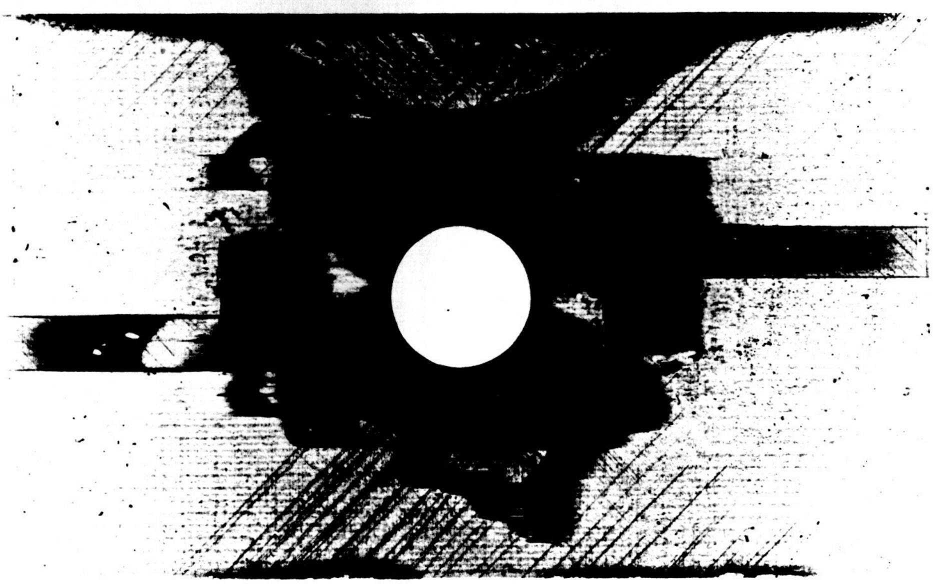

b) Specimen 6-2 at Early Stage III

Figure 25: Radiographs, Stages II and III, Low Level

mid-stage II laminate were drawn in Figure 26. Each diagram in this figure depicts the gold-chloride tracings at the interface of two plies of different orientations. The two crossed lines in the upper right corner of a diagram represent the orientations of the adjacent plies at the interface illustrated, and the numbers in the upper left corner are the interface-numbers from Figure 1. Interfaces located between double-thick 0 and -45 deg. plies are not included in this figure since these plies could not be separated. Interfaces through the second half of the laminate were not drawn, but indicated a damage distribution that was symmetric about the laminate midplane. Fine details of damage progression are too small to reproduce accurately with a schematic. Therefore, instead of attempting to reproduce every matrix crack indication and micro-delamination, just a few of these were drawn in the region where they occur. Large black areas indicate large scale delamination, whereas thin black lines represent transverse matrix crack tracings from cracks common to that interface.

The effect of thickness on delamination is made evident by noticing the much larger extent of the first interface delamination compared to the remainder in the interior. Differences among delaminations farther in the interior are

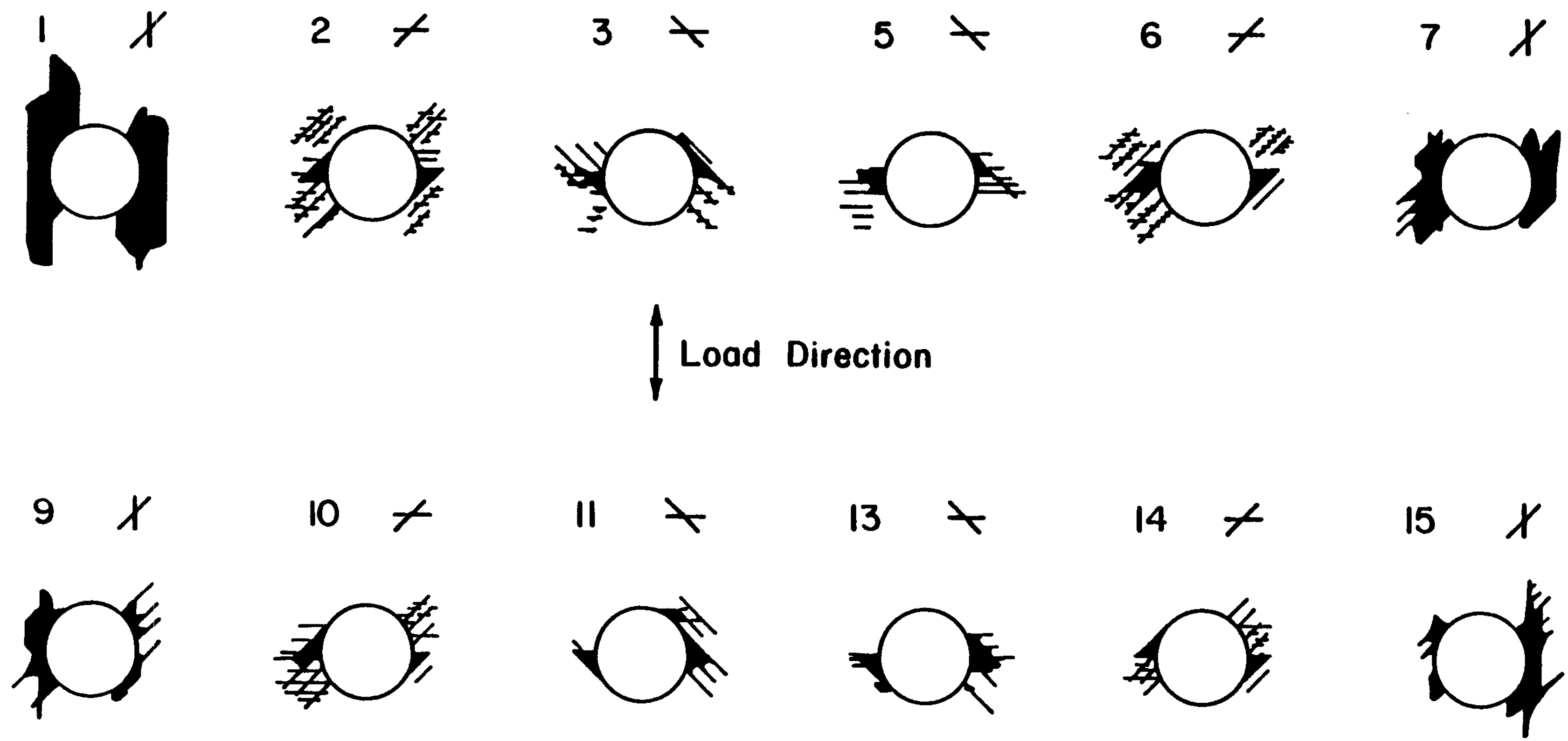

Figure 26: Schematic of Delamination Indications from a Deplied Laminate

less pronounced. At interior 0/45 interfaces, 0 deg. tangent cracks act as a border between two regions of different delamination growth modes. Both types of delamination follow the 0 deg. crack in path. In the region outside of the 0 deg. tangents, delaminations grow normal to the 0 and longer +45 deg. cracks extending from the hole (beginning near the hole boundary). In the region between the 0 deg. tangents, delaminations initiate in the "web" formed by these cracks and the hole boundary. Delamination initiation at 0/45 interfaces seems to occur immediately above and below the 90 and 270 deg. positions on the hole boundary, inside of the 0 deg. tangents. The ±45 deg. cracks tangent to the hole form a well-defined boundary containing delamination growth along 90 deg. plies. Dense cracks in any two adjoining plies often act as micro-delamination initiation sites. The micro-delaminations are not very visible in Figs. 12a and b, but they initiate in the acute angles formed by the crack crossings (see schematics in Figure 27). This phenomenon occurred most often along 90 deg. plies, and to a lesser extent along the 0 deg. plies. A delamination's growth is suspected to be influenced by micro-delamination coalescence along its frontier. However, as seen in the series of delamination schematics, large transverse cracks could arrest delamination growth for a certain amount of time. It should be kept in mind that the delamination growth sequence cannot be stated positively due to the non-continuous nature of damage monitoring with the deply technique.

The influence of transverse matrix cracking on delamination growth is perhaps the most important information on damage development revealed by the deply technique. For this particular laminate and loading, it appears that delaminations may initiate and grow at locations not immediately adjacent to an edge. This behavior has been observed before by Jamison with unnotched $[0/90n]_s$ laminates subject to T-T fatigue loading [41]. Many delaminations (particularly closer to the surface) had very straight boundaries formed by a single matrix crack, while others had more ragged boundaries formed by dense matrix cracks and microdelaminations.

As stage II progresses, deply data indicates that most new delamination growth occurs at the first 0/45 interface beneath the surface. The 0/45 delaminations deeper in the interior of the laminate grow at a much slower rate, and the 45/90 and 90/-45 delaminations grow little if at all. Large matrix cracks in +45, -45 and 90 deg. plies effectively arrest delamination growth at their associated interfaces throughout this stage of damage development.

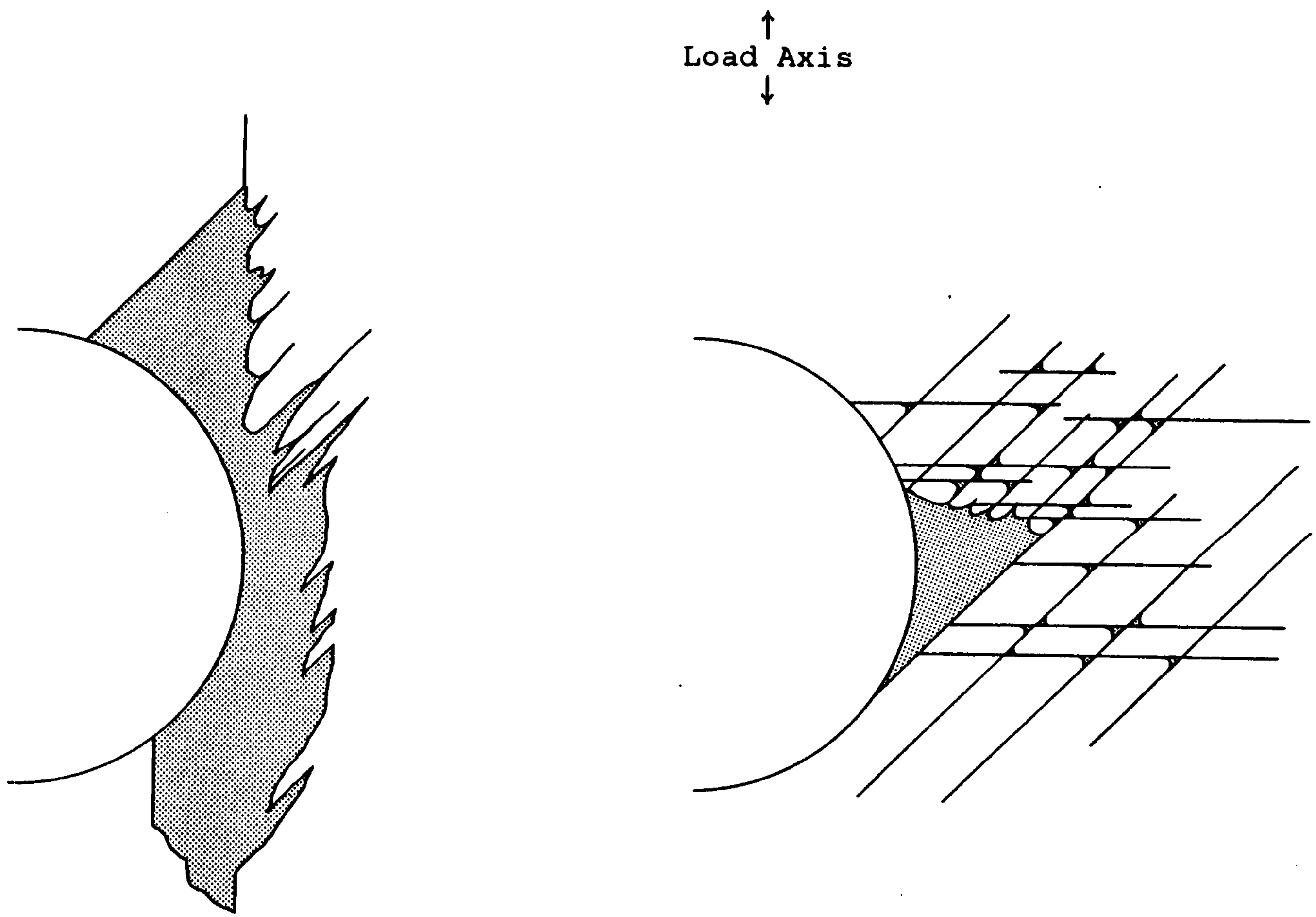

a) 0/45 Interface

b) 45/90 Interface

Figure 27: Schematic of Delamination at Matrix Crack Crossings

There is good overall agreement between the deply data and the extent of damage suggested by X-rays of the same specimen in Figure 24b. Delamination information from the edge view X-ray radiographs support the deply data, but it is not practical to combine different radiography views to provide an exact mapping of delaminations. The deply technique is superior to X-ray radiography for distinguishing delaminations at each interface through the thickness, but it is not very good for mapping transverse matrix cracks. A relative scarcity of transverse crack indications is thought to be caused by insufficient penetration of the gold-chloride particles. Application of a load to the specimen while applying the marking solution and/or increasing the wetting ability of the marking solution should alleviate this problem.

The tensile test data for the deply-strength pairs in stage II are listed in Table 1, and shown on normalized strength versus normalized life axes in Figure 28. The tensile strength increased to roughly 110 percent of mean initial strength in the first half of stage II (within scatter-band of initial), and 140 percent in the second half. Therefore, stage II is a period of tensile strength increase. At early stage II, the ultimate strains at the hole and edge were 120 and 110 percent of the mean initial values, respectively. The ratio of strain over the hole to that on the edge was 1.8, or 10 percent above the initial value. At late stage II, the strains at the hole and edge had increased to 160 and 130 percent, respectively. The ratio of strains had increased to 1.9, or 120 percent of the initial value. Post-failure examination of the specimens (Figure 29, specimen 2-11) reveals fracture surfaces that are more like a monotonic tensile failure than a fatigue failure. The fracture surface area increases with increasing damage, which may support the hypothesis that it is indeed a stress redistribution (over a larger area) that causes notched laminates to undergo a residual strength increase. The double -45 deg. plies through the thickness still show little sign of fiber fractures. Surface 0 deg. fibers tangent to the hole fracture at the point where they are not delaminated from the underlying ply, which may be far from the hole. Fibers in the +45 deg. plies do not break near the hole. Further from the hole in these plies, fibers do break transverse to the load axis. Aside from the surface 0 deg. plies, there is no significant difference in the appearance of fractured plies of similar orientation through the thickness.

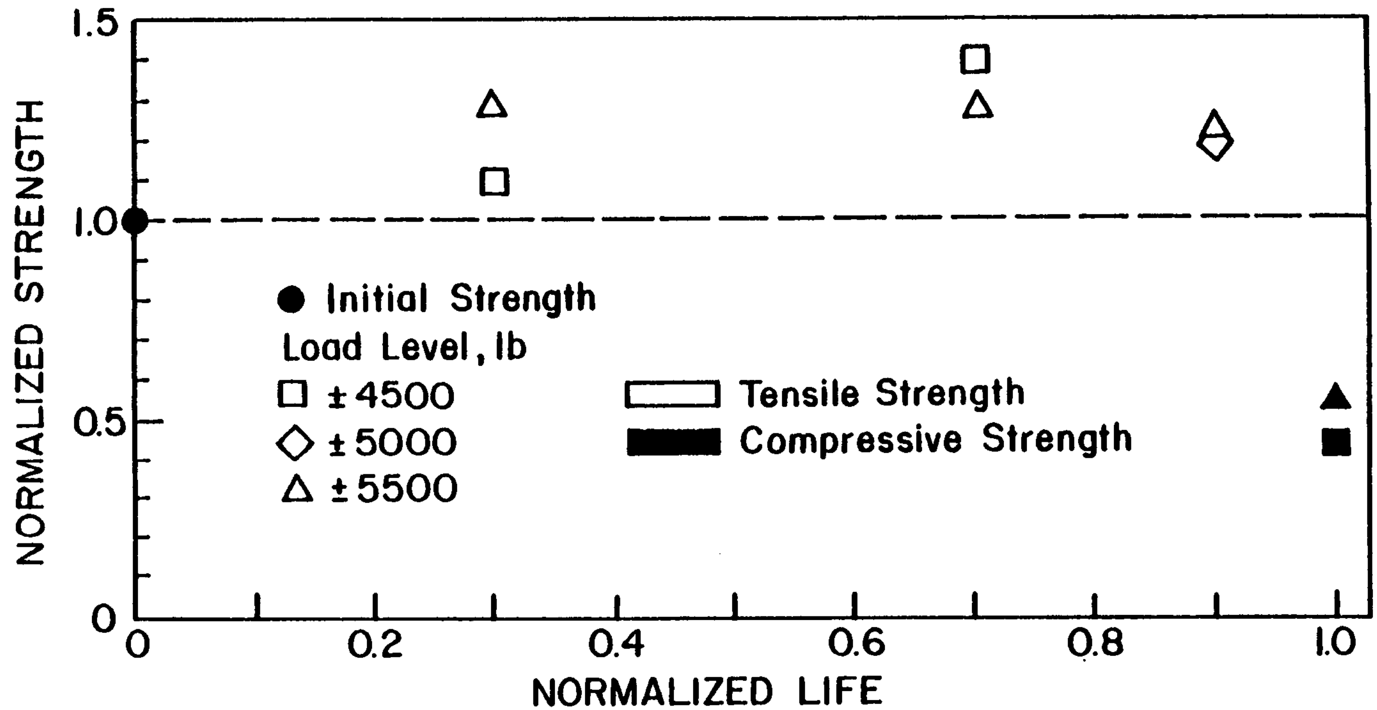

Figure 28: Residual Tensile and Compressive Strength During Fully Reversed Fatigue

a) Edge View

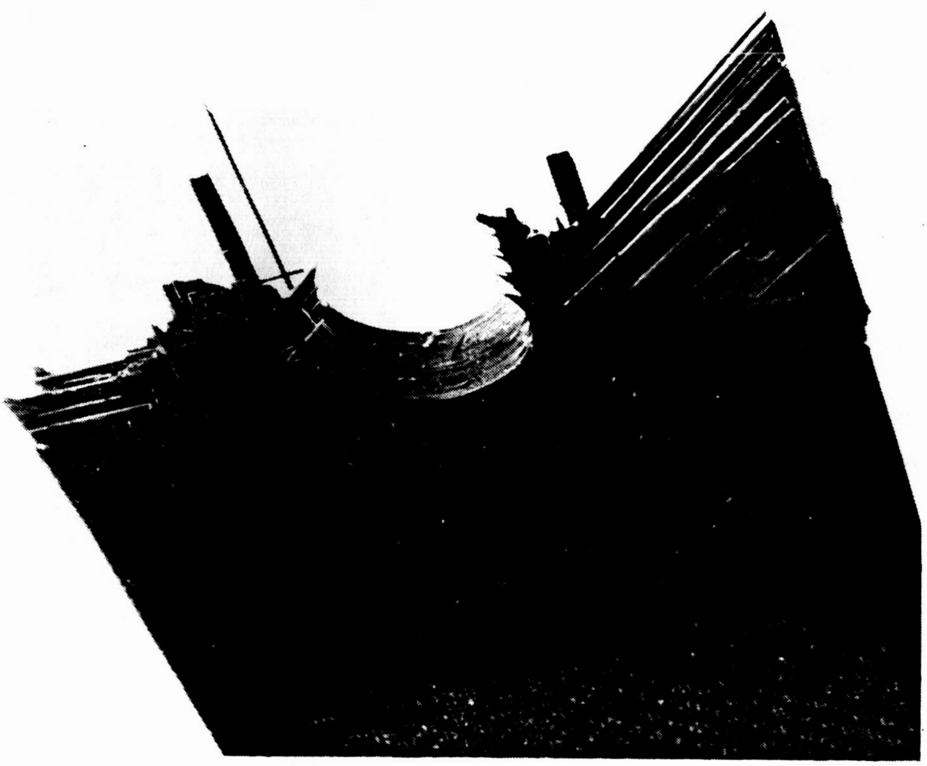

b) Rear Face View

Figure 29: Tensile Fracture, Stage II, Low Level

3.4.1.3 Stage III

Stage III comprises approximately the last 10 percent of finite fatigue life, but never occurs in run-out fatigue tests. Tension stiffness reduces about 10 percent of the initial stiffness, for a cumulative stiffness reduction of 30 to 40 percent of the initial value. Compression stiffness may change up to 30 percent of the initial value. Since significant out-of-plane deflection often occurs during stage III, the final value of compression stiffness varies widely. During stage III, the compression stiffness may show one or more "kinks" as separate delaminations initiate and grow irregularly. A slight amount of nonlinearity may appear in load-strain plots near the end of life. The difference between secant and tangent tensile stiffness may be up to four percent, with a higher apparent stiffness at the higher load. Compression stiffness may vary up to ±10 percent.

In the early part of stage III, all delaminations in the laminate begin to spread rapidly (Figure 25b). Just prior to the final failure event, one or more delaminations in any of the first few interfaces below the surface may extend continuously from the hole to the straight edge (Figure 30). The edge view X-ray shows that most of the delaminations on either side of ±45 deg. plies and bounding the hole have grown in length along the longitudinal axis such that they exceed the hole diameter. Transverse matrix cracks do not increase noticeably in density or extent during this stage. Visual observation of a specimen at the end of life indicates localized buckling of sublaminates near the surface of the laminate during the compressive portion of the loading.

An attempt was made to cycle a specimen at the low load level of ±4500 lb. (±20.0 KN) until late stage III behavior was noted so that the tensile strength could be measured. Two successive run-outs were achieved in this endeavor, so it was decided to raise the load level to ±5000 lb. (±22.3 KN), which is halfway between the usual low and high load levels. This specimen showed signs of impending failure at 961K cycles and thus could be considered along with the other low load level tests that displayed a similar state of damage at over a half million cycles. An X-ray radiograph just prior to the residual strength measurement resembles that shown in 30. Tension and compression stiffnesses were 84 and 87 (increasing due to out-of-plane deflection) percent, respectively (Table 1). Residual tensile strength was about 120 percent of the initial value, meaning that even at imminent failure, the tensile strength does not decrease significantly, or enough to cause a tensile mode of

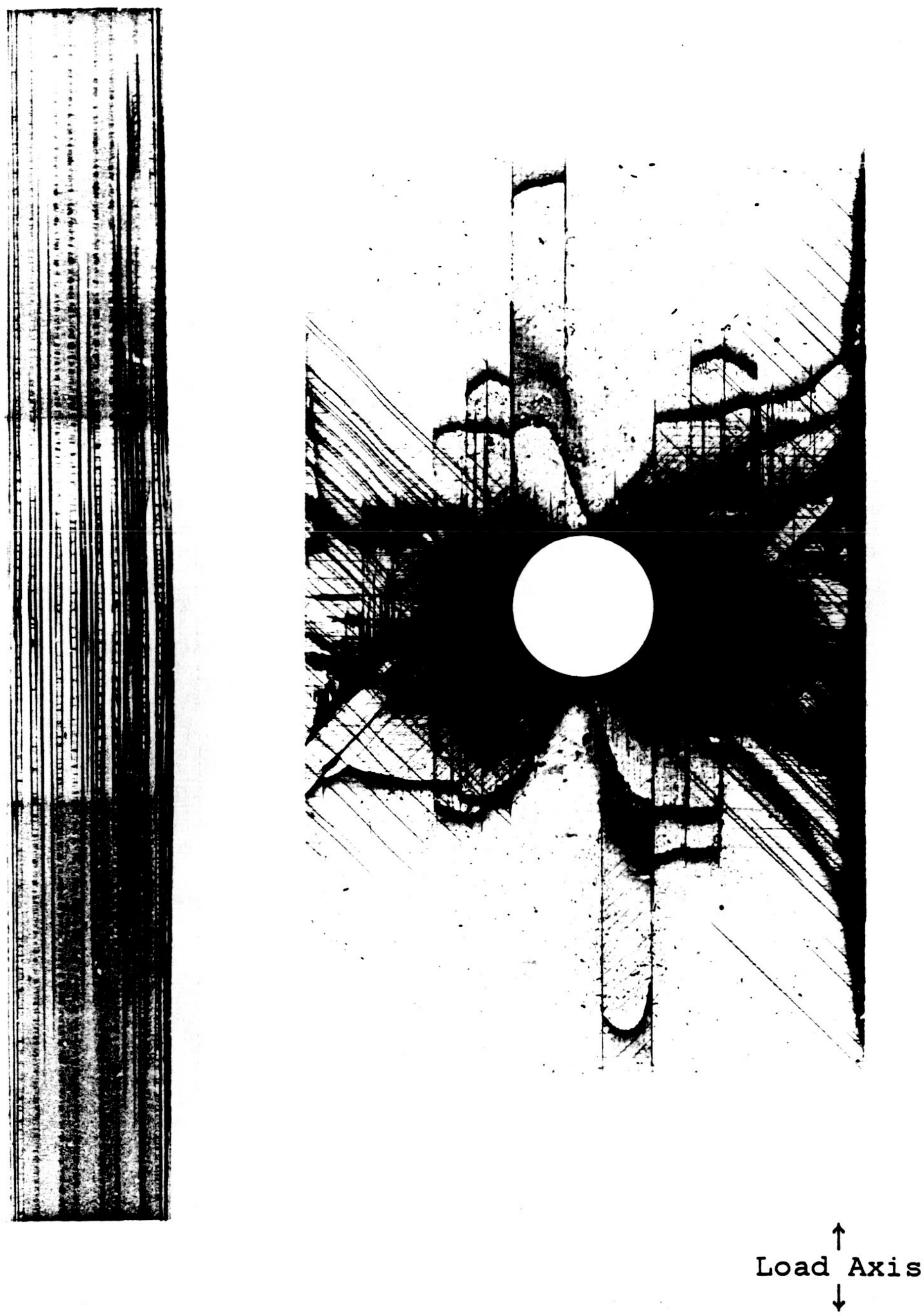

Figure 30: Radiographs at End of Life, Low Level

failure (Figure 28). The ultimate strains at the hole and edge had increased to 140 and 120 percent of initial values, respectively. The ratio of strain at hole to edge increased 20 percent to a value of 1.9. This information on ultimate load and strain change during progressive fatigue damage in a notched laminate suggests that the damage "softens" the material in the vicinity of the notch in a manner such that ultimate tensile strength is increased, but the compressive strength (or point of instability) is decreased. A photograph of the fractured specimen is shown in Figure 31. The large failure surface involves many of the large delaminations visible in the radiograph. The 0 deg. surface fibers tangent to the hole fracture farther away from the hole, and the first +45 deg. plies under the surface may not have any fiber fractures (similar to many -45 deg. plies throughout the thickness). It is therefore concluded that some surface effect begins to change the appearance of the tensile fracture surface toward the end of life for this load history.

3.4.1.4 Low Level Run-outs

Two specimens did not experience stage III and failure. Delamination growth was extensive, but very slow. In specimen 5-2, straight edge delamination appeared only on

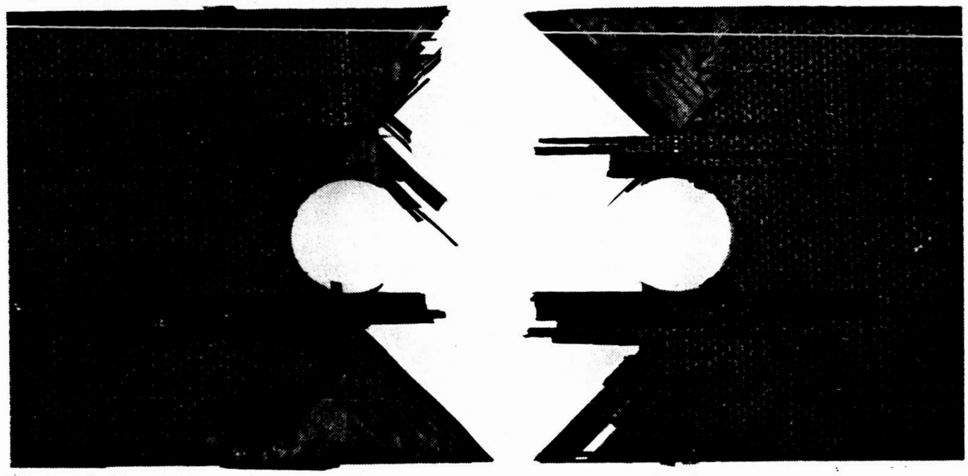

a) Rear Face View

b) Front Angle View

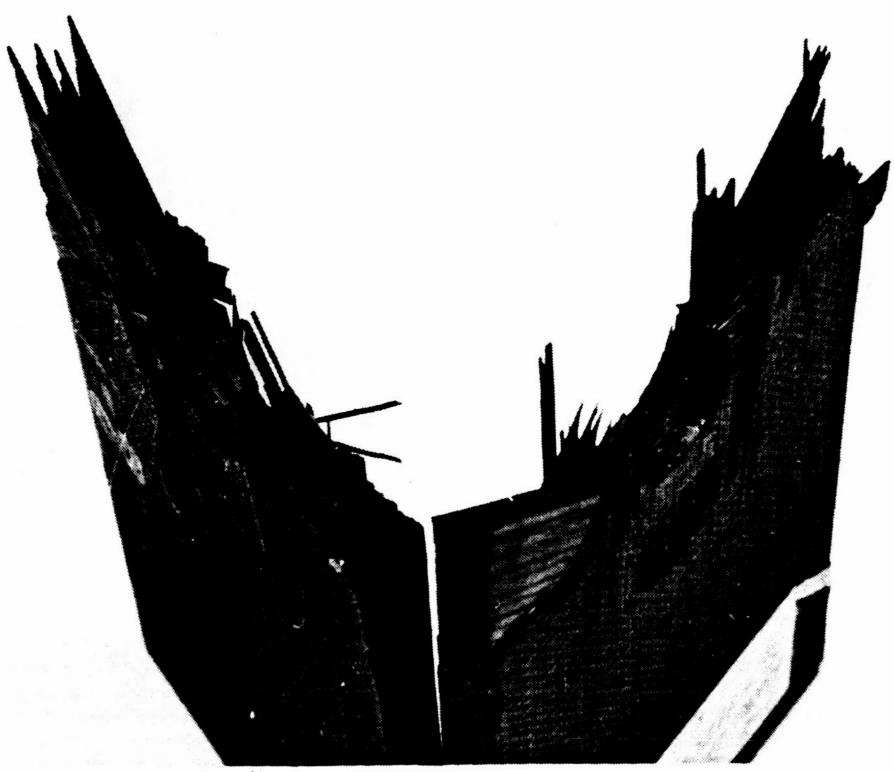

Figure 31: Tensile Fracture, Late Stage III, Low Level

the right side. These were adjacent to ±45 deg. plies that were situated closest to the surface of the laminate. Radiographs of these situations resembled those of specimens between stages II and III shown in this chapter.

Figure 32 illustrates a comparison of stiffness behavior of run-out specimens 5-2 and 1-2 and finite life specimen 6-2 on a regular cycles axis. It is suspected that infrequent interruptions of the test for nondestructive evaluation may be a factor in the resistance of these two specimens to degradation of stiffness and compressive strength. This thought is based on only a few tests and should be studied more extensively before firm conclusions are made.

3.4.2 High Load Level Damage Development, R=-1

Two specimens were cycled at the high load level (±5500 lb., ±24.5 kN) until fracture so that a complete history of stiffness and damage development could be recorded. These failed at 93K and 106K cycles. Another specimen, cycled for residual tensile strength measurement, indicated imminent failure at 315 cycles. Tensile and compressive stiffnesses for the three high level test specimens behaved similarly until approximately 50 percent of life, when the compressive stiffnesses diverged relative to each other. This should be

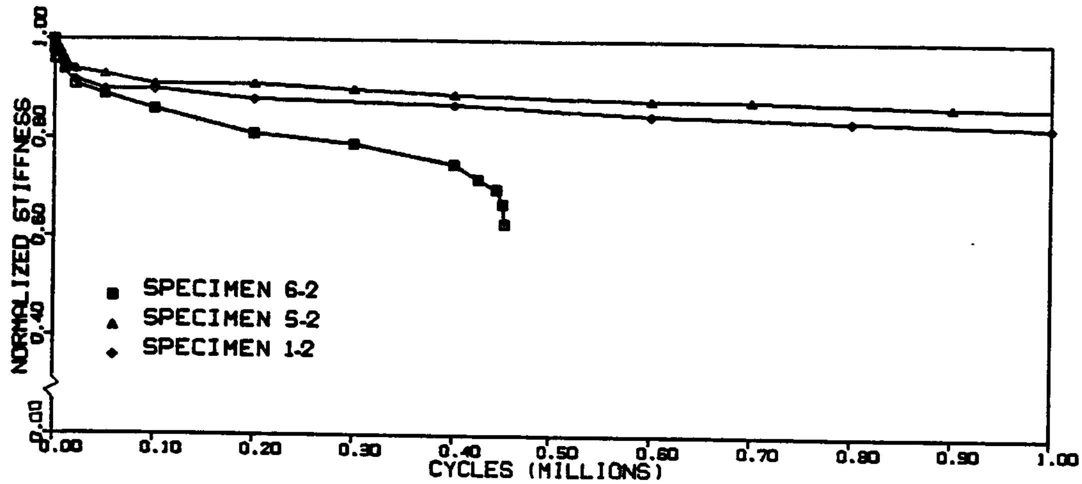

a) Tension Stiffness

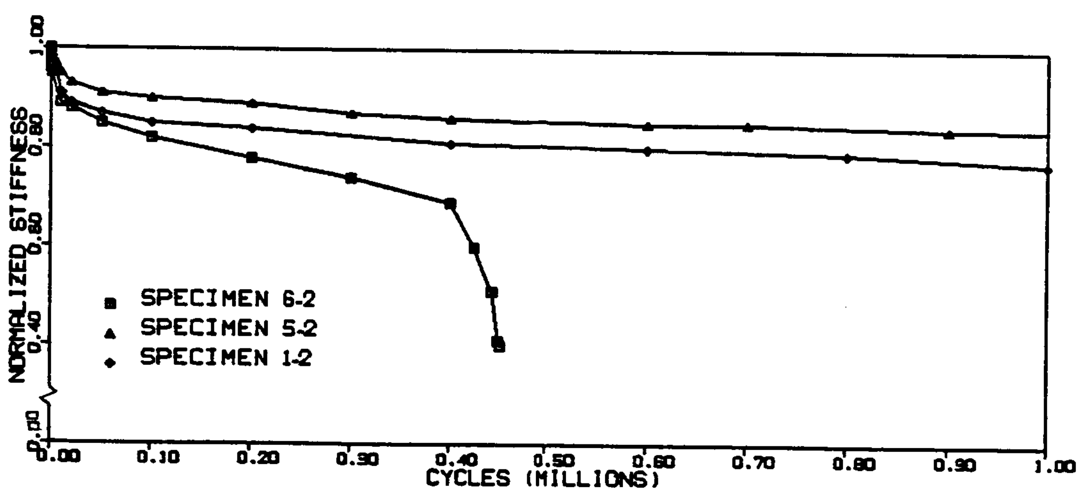

b) Compression Stiffness

Figure 32: Secant Stiffness Degradation of Run-outs, Low Level (±4500 lb.)

expected because of the sensitivity of compression stiffness to the randomly located damage sites. Damage development was similar in form to that at the low level, but it occured at a higher rate. Because of this similarity, some of the details are be omitted from the following summary of observations.

3.4.2.1 Stage I

Figure 33a illustrates the initial state of damage caused by fabrication in specimen no. 1-5. Within the first five cycles, transverse matrix cracks appear in all off-axis plies through the thickness of the laminate in the region to the left and right of the hole (Figure 33b). In the 0 deg. plies, the most prominent cracks are tangent to the hole, but small splits also appear near drill-induced damage on one surface of the specimen. These splits grow only during the first few cycles. If drill-induced delaminations at the last interface through the thickness are present, they will begin to grow away from the hole boundary. At ten cycles, delamination initiates at both the first and last 0/45 interfaces in the web-shaped region bounded by the 0 deg. tangent cracks and the hole boundary in the second and fourth quadrants. Tension and compression stiffnesses at this time are between 96 and 99 percent of the initial measured value. Compression stiffness, as in the low load level, is generally lower than the tension stiffness on both an absolute and normalized scale.

At 1000 cycles, transverse matrix cracks continue to grow in density and length in all plies except the 0 deg. ply, where only the tangent cracks grow in length. Surface delaminations begin to appear suddenly outside of the 0 deg. tangents, and the two outermost 45/90 interfaces delaminate at the densely cracked 90 deg. and 270 deg. positions (Figure 33c). Delaminations occur in all 0/45 interfaces through the thickness, and grow along the 0 deg. tangent cracks in the second and fourth quadrants in the web region defined earlier, favoring neither surface. No interior 0/45 delaminations have yet extended laterally beyond the 0 deg. tangents. As in the low load level, second-generation cracks appear in the form of 45 deg. cracks growing from the 0 deg. tangents, and 90 deg. cracks growing from the cracks in the -45 deg. plies.

At 5 to 10 thousand cycles, the 0/45 surface delaminations occupy all four quadrants between the 0 deg. tangents and are also at all four locations immediately outside of the 0 deg. tangents (Figure 33d). Transverse cracks in the 90 deg. plies initiate at the straight edge, which are soon crossed by -45 deg. cracks and eventually +45

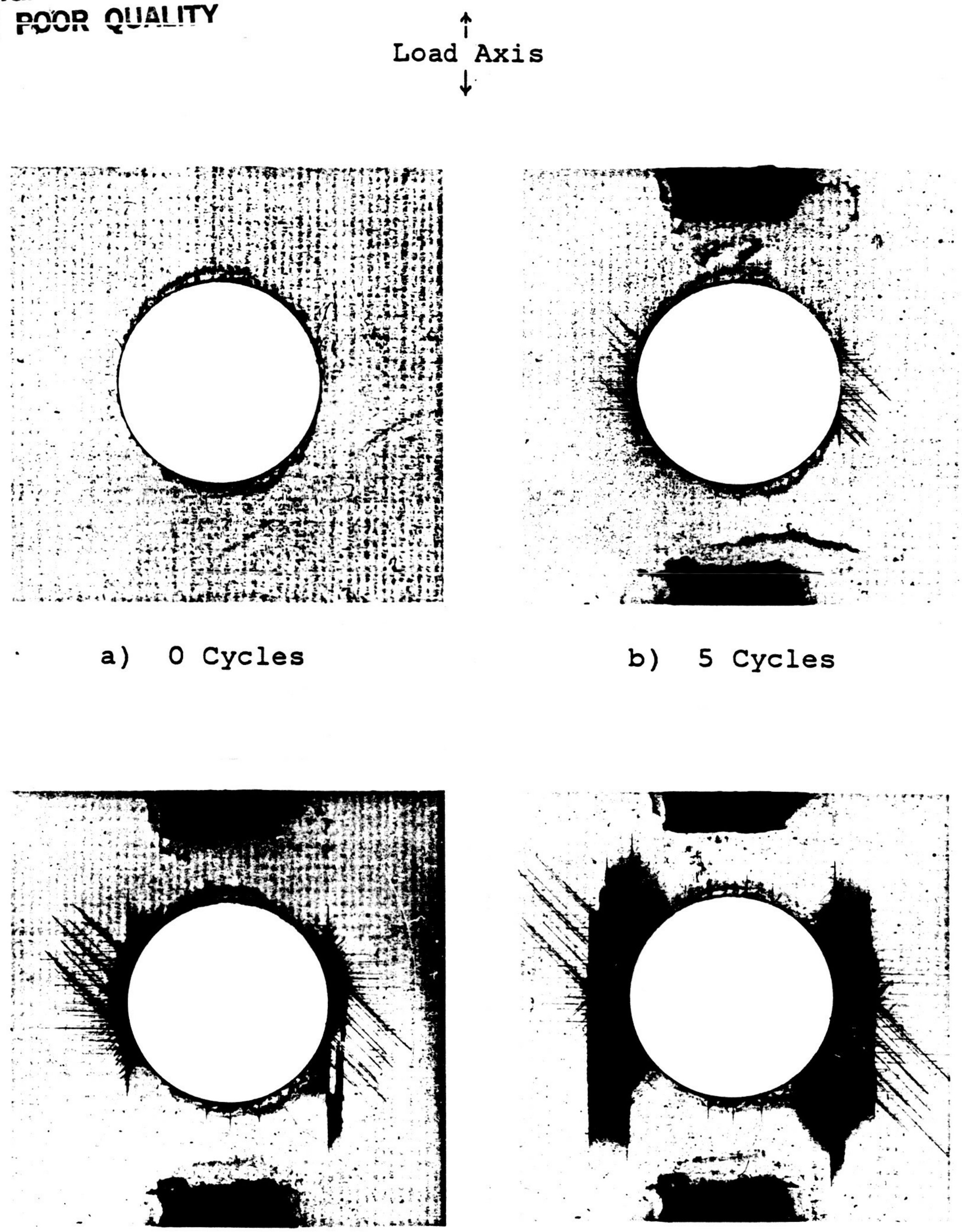

a) 0 Cycles

b) 5 Cycles

c) 1K Cycles

d) 5K Cycles

Figure 33: Radiographs at Early Life, High Level

deg. cracks in a characteristic pattern as was seen in the low level test. Delaminations initiate at the 90 deg. and 270 deg. positions at every interface through the thickness that involves a 90 deg. ply. These are quite even in length along the longitudinal axis, and seem to be confined to the triangular region formed by the ±45 deg. tangent cracks and the hole boundary, as in the low level tests. The 0/45 delaminations are slightly larger at interfaces closer to the surfaces. Stiffness behavior at this time indicates that stage I has ended. Tension stiffness retention is between 90 and 95 percent, and compression stiffness retention is between 87 and 93 percent. As in the low level, the end of stage I coincides with the completion of delamination at all similar interfaces through the thickness.

3.4.2.2 Stage II

Corresponding with the relatively slow change of stiffness during stage II, damage growth proceeds at a much slower rate. Figure 34 illustrates the damage condition at middle stage II (specimen no. 1-5, 50K cycles). Straight edge delamination has initiated in the region where dense -45 deg. cracks intersect the straight edge at interfaces involving these same plies. Notch-related delaminations between the 0 and 45 degree plies through the thickness have grown outside of the 0 deg. tangents, and those closer to the surface are slightly larger. Residual tensile strength measured during the first half of stage II (both E_T and E_C near 90 percent of initial value) was about 130 percent of the initial value (Figure 28). Strain at the hole was 140 percent of initial, and strain at the edge was 130 percent of initial. The ratio of hole strain to edge strain was 1.8, or 10 percent higher than the initial tensile value (Table 1). As in the low load level, the fracture surface after the introduction of fatigue damage was more irregular than that of a virgin coupon. This is typical for all tensile residual strength tests at the high load level. Delaminated surface 0 deg. fibers tangent to the hole fracture along the limits of the underlying delamination, which may be near the gripped region of the laminate. Outside of the delaminated region, 0 deg. plies fail at first along the underlying +45 deg. matrix failure, then revert back to a path perpendicular to the loading direction. The first +45 deg. plies beneath the surface also revert back to breaking fibers at some distance away from the hole.

Information gathered from the deply process of another laminate at the same stage of life indicated damage patterns

←Load Axis→

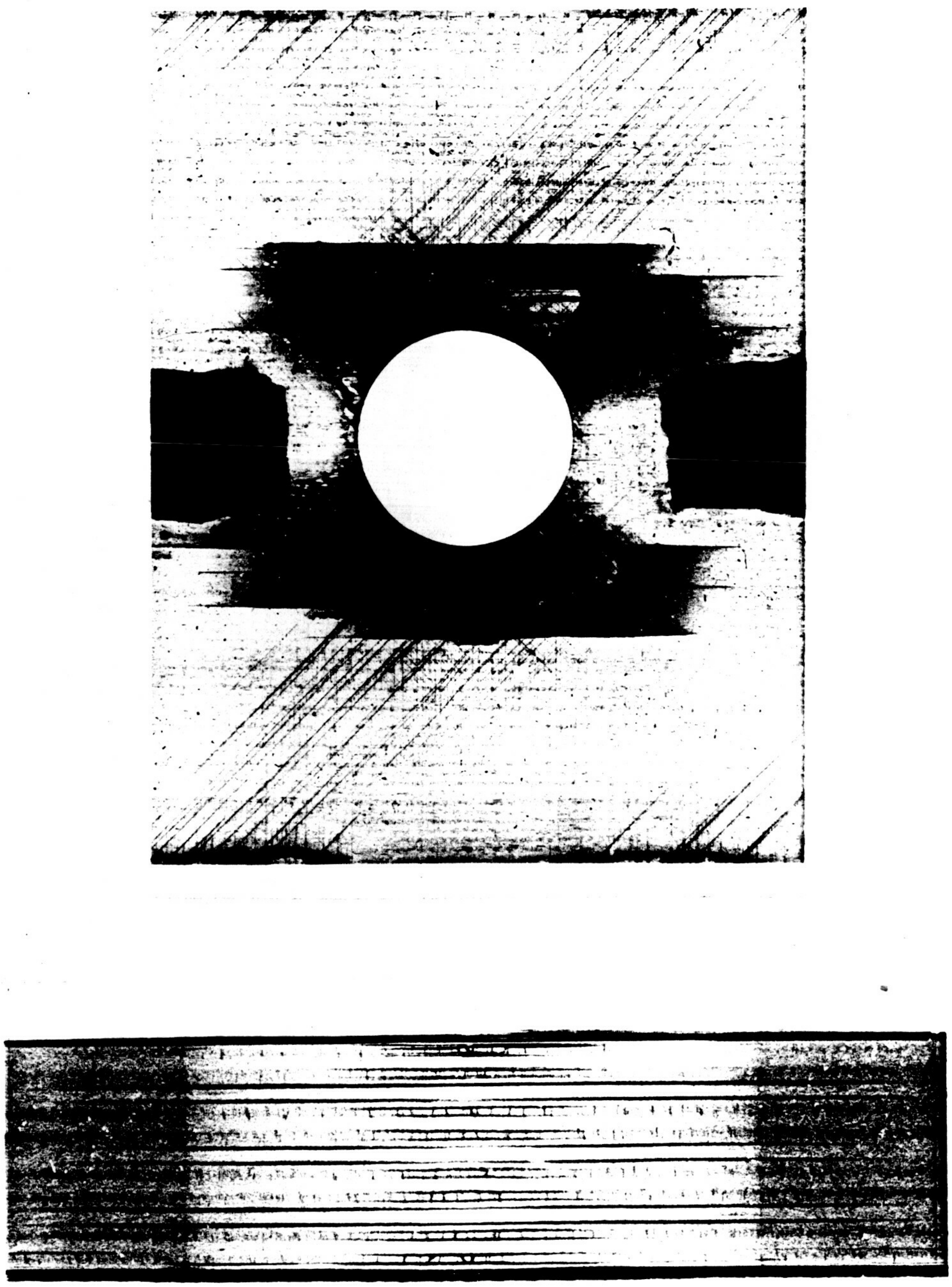

Figure 34: Radiographs, Middle Stage II, High Level

very similar to those given in Figure 26 for the low level test. The delaminations underneath both surface plies still favored the second and fourth quadrants over the first and third.

At 80 to 95 percent of life, delamination growth begins to accelerate as transverse matrix cracks continue to grow in all off-axis plies. In the 0 deg. plies, only the tangent cracks and the surface splits on top of the underlying delamination grow. The outermost 0/45 delaminations approach the straight edge of the specimen near the end of stage II (Figure 35, specimen 1-5, 76K cycles). Delaminations extend continuously from the hole to the straight edge by about 95 percent of life, which is the beginning of stage III. At this time, the normalized tension stiffness is 80 to 85 percent and the compression stiffness is 65 to 80 percent.

A pair of laminates were cycled at the high load level to the second half of stage II (mean tensile and compressive stiffnesses equal to 86 and 80 percent of initial values, respectively) for residual tensile strength measurement and deply. Relative to mean initial values, residual tensile strength was about 130 percent, strain at the hole and edge were 150 and 120 percent, respectively, and the ratio of hole to edge strain was 2.0, or 130 percent (Figure 28 and

←Load Axis→

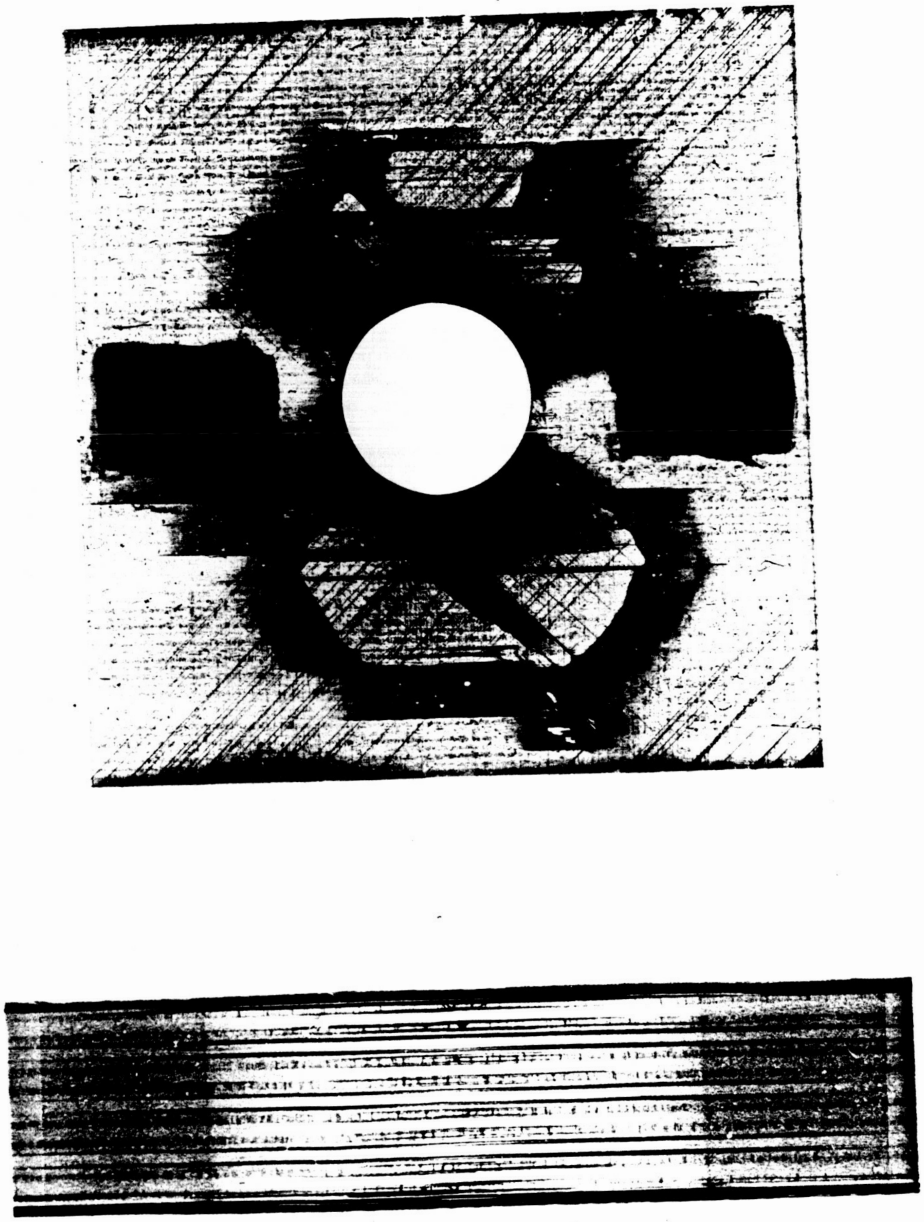

Figure 35: Radiographs, Late Stage II, High Level

Table 1). The strain ratio is noted to increase with increasing damage. Visually, the fracture surface at this stage of life is similar to that earlier in stage II, except for a slightly more irregular appearance. Deply data indicate that most new delamination growth occurs at the first 0/45 interface from each surface. The interior 0/45 delaminations grow slightly laterally and longitudinally in a manner similar to the low level delamination growth. Interior 45/90 and 90/-45 delaminations are only slightly larger than they were at mid-stage II, but are still confined by the adjacent ±45 deg. tangent cracks.

3.4.2.3 Stage III

As in the low level loading, stage III is characterized by rapid delamination growth (Figure 36, specimen 1-5, 93K cycles). The number of cycles at this load level is not very great, and matrix cracks do not grow very much. Several delaminations are growing separately at this time from the hole and the straight edge. Aside from the surface delaminations mentioned earlier, delaminations begin to grow away from the hole along the 45 deg. tangent cracks at the 45/90 interfaces closest to the surface. When the collective state of delamination is such that elastic symmetry in the laminate is disturbed, failure will occur during the compressive portion of the loading. Several cycles may pass before the laminate actually separates into two pieces. At imminent failure, tension stiffness is between 75 and 80 percent and compression stiffness is between 50 and 70 percent of initial values.

The residual tensile strength of a laminate cycled to imminent compressive failure was approximately 120 percent of the mean initial strength (Figure 28). The strains at the hole and edge were 150 and 110 percent of the initial values, and the ratio of these strains was 2.2, or 40 percent greater than the initial value (Table 1). The failure surface involves the large delaminations which developed near the end of life. This suggests that failure at the high load level, as in the low level, is due to a loss of compressive properties. The material in the vicinity of the hole experienced much softening, but this apparently affects the tensile strength favorably.

3.4.3 Positive Load Ratio Fatigue Damage

To complement the fatigue damage information acquired for load ratios equal to -1, one fatigue test was carried out at R=0.1 in tension-tension, and another at R=10 in compression-compression. Intralaminar and interlaminar stresses will thus not undergo the through-zero reversals

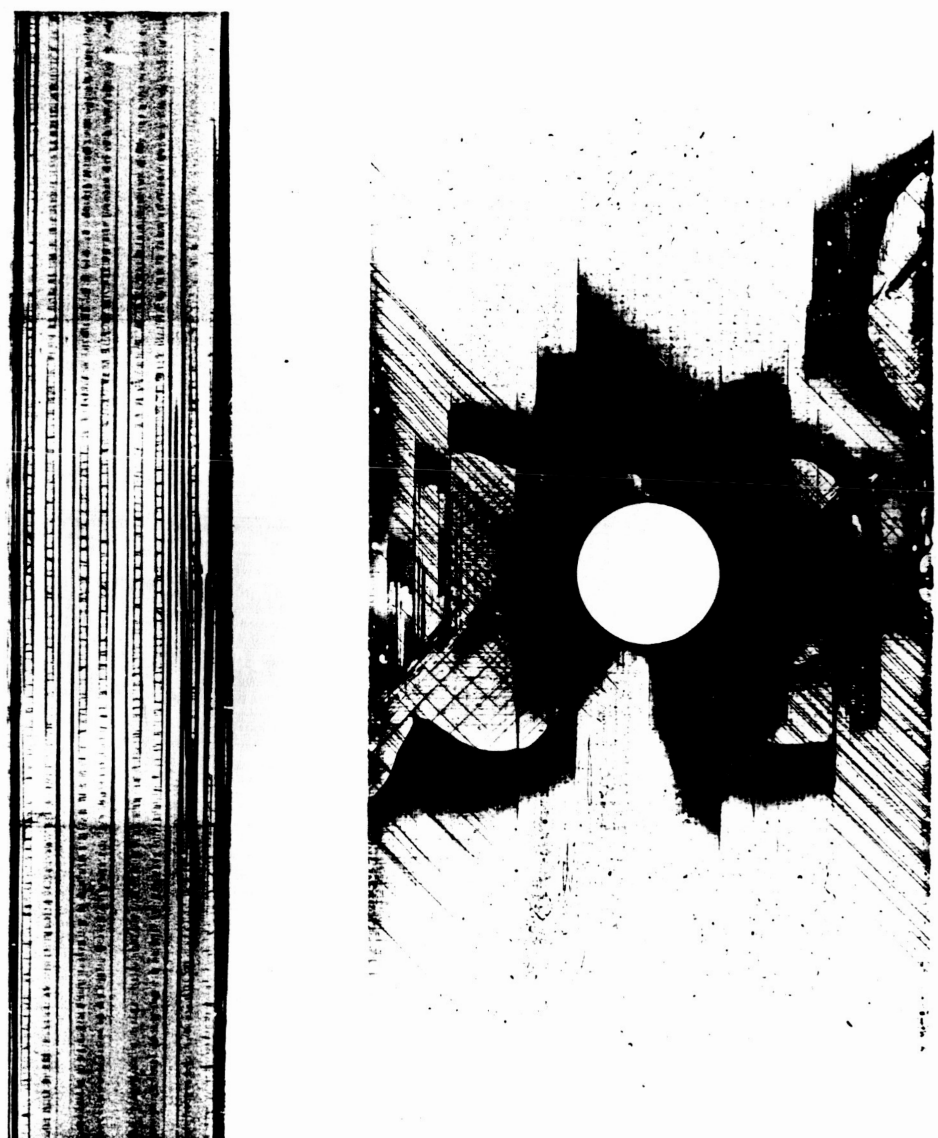

Load Axis

Figure 36: Radiographs at End-of-Life, High Level

that occur during T-C loading. Positive and negative shear stresses should have approximately the same effect on the material, allowing the effect of positive and negative normal stresses to be discerned using T-T and C-C load cycles.

3.4.3.1 Tension-Tension Fatigue Behavior

Several investigators have found that in order to achieve T-T fatigue failures in notched, quasi-isotropic laminates before one million cycles, the maximum load level must be approximately 80 percent of static ultimate. Maximum load amplitude for this T-T fatigue test (R=0.1) was calculated to be about 84 percent (8200 lb., 36.5 kN) of the mean static tensile ultimate, but still no signs of stage III stiffness behavior appeared by one million cycles. Recall that in T-T tests of similar laminates, Ulman, et. al [57] did not achieve T-T fatigue failures at 90 percent of ultimate, while Ryder and Walker [22] did record fatigue failures in T-T at peak loads as low as 73 percent of tensile ultimate. In perspective, the maximum tensile stresses of the two fully reversed load levels (R=-1) in this investigation were 48 and 59 percent of the mean static tensile ultimate.

The end of stage I occurs at about ten thousand cycles when the normalized tension and compression stiffnesses are between 93 and 94 percent of initial values. At this time, there are transverse matrix cracks in all off-axis plies on the right and left side of the hole (Figure 37). Some off-axis cracks that initiated at the hole have reached the straight edge. Shorter cracks initiated at the straight edge and grew inward. In similar fashion as the T-C loading, there are 90 deg. cracks growing with the -45 deg. cracks in adjacent plies. The 90 deg. cracks also appear first at the straight edge, followed by -45 and +45 deg. cracks in adjacent plies. Cracks in the -45 deg. plies initiate away from the hole boundary in the second and fourth quadrants. Cracks in +45 deg. plies initiate away from the hole boundary in the first and third quadrants. There are triangles of 45/90 and 90/-45 interface delamination in the region between the hole boundary and the ±45 deg. tangent cracks. The edge view radiograph suggests that only the first two 45/90 and 90/-45 interfaces from each surface are delaminated along the hole near the 90 and 270 deg. positions. The remaining 90 deg. plies in the interior of the laminate delaminate only at the 45/90 interfaces, and at the same polar positions. The largest delaminations are under the surface 0 deg. plies. These initiate outside of the 0 deg. tangents and grow along the underlying +45 deg. tangents and the surface 0 deg. tangent crack tips. The region at the intersection of the 0 deg. tangents and the hole boundary which served as a delamination initiation site for T-C loading shows very slight delaminations in the second and fourth quadrants. This gives a skewed appearance to the surface delaminations in the radiograph. Other 0/45 delaminations through the thickness are uniform in size, but smaller than the 0/45 delaminations nearest to the surface. In a random manner, the interior 0/45 delaminations grow outside of the 0 deg. tangents.

At 200 thousand cycles, the tension stiffness (87 percent) has degraded more than the compression stiffness (90 percent). This type of behavior was rarely seen in the tests run with R=-1. Off-axis transverse matrix cracks appear over the entire gage length of the specimen except for narrow strips above and below the hole isolated by the surface 0 deg. tangent cracks. Recall that the specimens cycled at R=-1 did develop matrix cracking in this region. The regions immediately above and below the hole are subject to lateral tension during compressive load, and lateral compression during tensile load. The longitudinal stress in these regions is relatively low because of the proximity to the hole. Hence, the stress state suggests that transverse

←Load Axis→

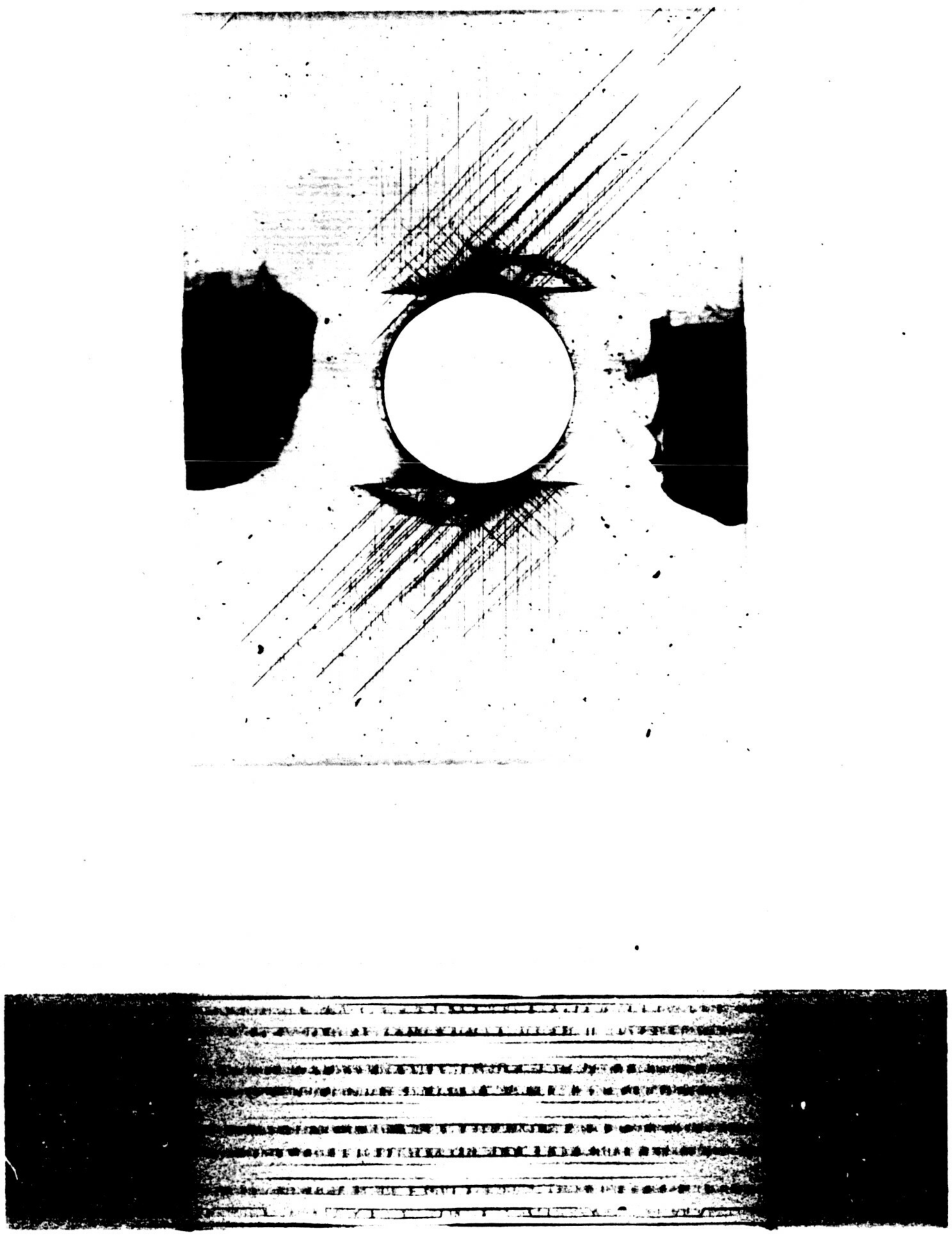

Figure 37: Radiographs, T-T Fatigue, 10K Cycles

matrix cracking is more likely to occur during compressive loading in the region above and below the hole. The density of matrix cracks is much greater than was seen with either R=-1 load case. Considering that the maximum tensile load is close to 50 percent higher than the high level at R=-1, this is not very surprising. Delaminations at this point in life continue to grow laterally and longitudinally and continue to favor interfaces nearer to the surface. New delaminations appear between the 0 deg. tangents in the first and third quadrants between the surface 0 deg. and the underlying +45 deg. ply. The 45/90 interfaces through the thickness are delaminated uniformly between the hole boundary and the ±45 deg. tangent cracks in the edge-view radiograph. Several 90/-45 interfaces, however, still do not show delamination indications in the edge radiograph.

The test was halted after one million cycles and no signs of impending failure were detected. Stiffness retention continued to be less in tension (81 percent) than in compression (87 percent). Transverse matrix cracks approached a saturation spacing over the entire gage length except for the region between the 0 deg. tangents and close to the hole (Figure 38). Off-axis matrix cracking developed below the surface delaminations between the 0 deg. tangent cracks. The largest of these surface delaminations were in the second and fourth quadrants, as in T-C fatigue. Damage growth was also occurring in regions distant from the hole boundary. This was in the form of ±45 deg. cracks initiating in regions of dense cracks that originated at the hole. Also, surface delaminations continued to grow laterally along the underlying +45 deg. tangent cracks. Straight edge delaminations initiated in regions of dense off-axis cracking. The "X" pattern formed by dense cracks and edge delaminations is evident in Figure 38. Through the thickness, all 0/45, 45/90 and 90/-45 interfaces have delaminated with a growth rate favoring the surface.

In summary, the principle differences in the damage development of T-T and T-C loaded coupons, for the imposed test conditions, are:

- Denser transverse matrix cracking in the off-axis plies and less surface 0/45 delamination in T-T, as opposed to T-C.
- Increased frequency of matrix crack initiation away from the hole, and increased density of matrix cracking overall in T-T.
- More isolation in T-T of the strip of material above and below the hole, between the 0 deg. tangent cracks.
- Delaminations under the surface plies grow along the underlying +45 deg. tangent crack in an anti-symmetric

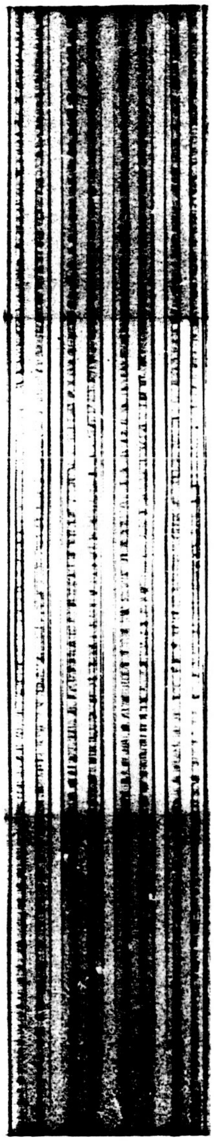

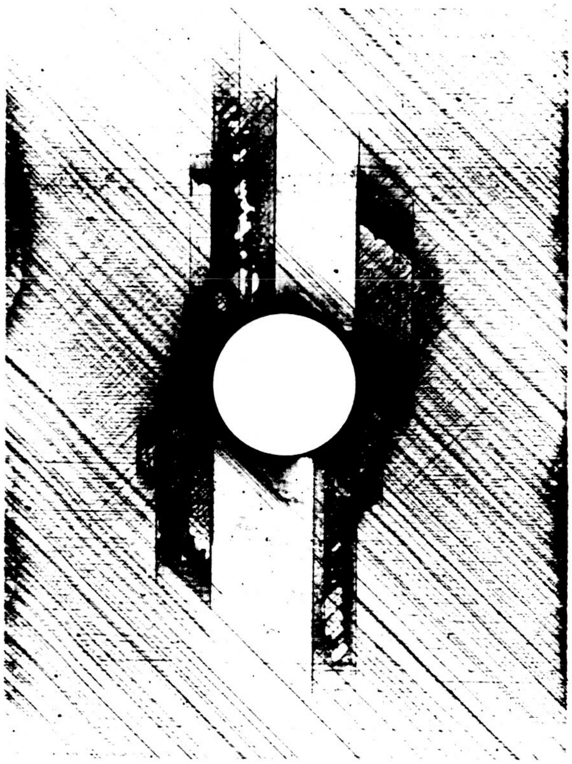

Load Axis

Figure 38: Radiographs, T-T Fatigue, 1M Cycles

manner with respect to the center of the hole in T-T, whereas in T-C these grow in both longitudinal directions.

- There is less tendency to delaminate on either side of 90 deg. plies at the hole boundary or the straight edge. The 90/-45 interfaces delaminate after the +45/90 interfaces, whereas in T-C they delaminate almost simultaneously.

3.4.3.2 Compression-Compression Fatigue Behavior

A C-C fatigue test was run to isolate the effect of only the compressive component of the high level tests previously completed with R=-1. With R=10, the maximum load amplitude was -5500 lb. (-24.5 kN), and the minimum was -550 lb. (-2.5 kN). At this loading, the specimen did not show a large amount of damage by one million cycles, so the test was considered a run-out.

The first form of damage to appear is 0 deg. transverse matrix cracks tangent to the hole, which are uniform through the thickness. Delaminations soon form at the 0/45 interfaces in the region bounded by these cracks and the hole boundary, with those delaminations beneath the surface having later initiation and slower growth. Cracks in the ±45 deg. plies tangent to the hole eventually initiate, but do not cross by the time a single surface delamination appears outside the 0 deg. tangents (Figure 39a). No other off-axis cracks were seen at 200K cycles. Stiffness retention in tension and compression were each 98 percent at this time.

At 500K cycles, the surface delaminations were following the tips of the 0 deg. tangent cracks. This was true of those both inside and outside of the region bounded by the 0 deg. tangents. Interior 0/45 delaminations continued to favor interfaces closer to the surface. All 90/-45 interfaces developed delaminations of similar size at the 90 deg. and 270 deg. positions around the hole boundary. The first and last 45/90 interfaces through the thickness are the only such interfaces with delamination (also at 90 and 270 deg.). Aside from the extension of the 0 and ±45 degree tangent cracks, no other matrix cracks initiated or grew. Stiffness was practically unchanged from that at 200K cycles.

When the test was stopped at 1M cycles, all forms of damage growth had slowed markedly (Figure 39b). The surface delaminations had appeared at all four locations around the hole, but grew only longitudinally. No new transverse cracking occurred except for the growth of the ±45 deg. tangents and some initiation of second generation +45 deg.

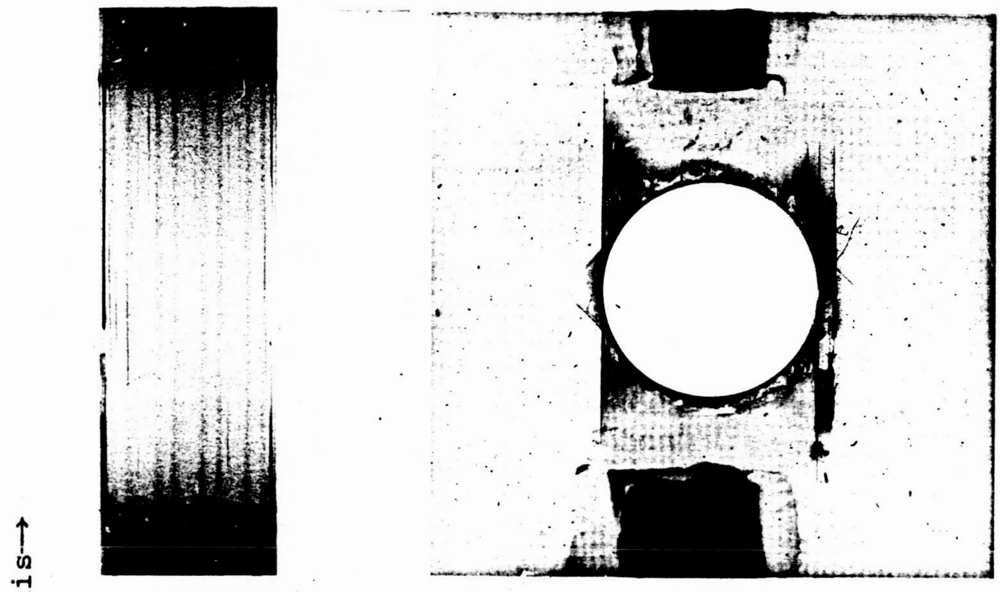

a) 200 Thousand Cycles

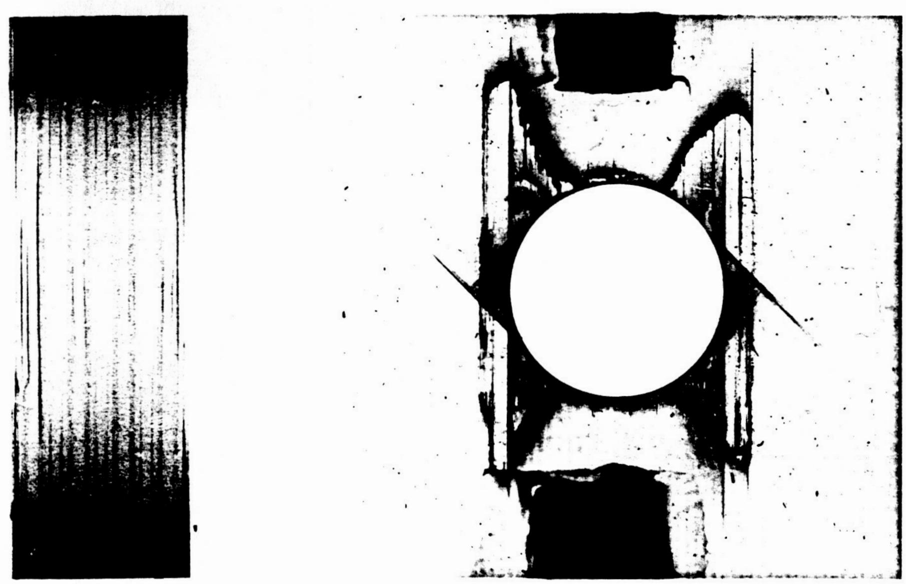

b) One Million Cycles

Figure 39: Radiographs, C-C Fatigue

cracks along the 0 deg. tangents. Existing interior delaminations grew slightly, but no new 45/90 delaminations appeared to complete delamination of all similar interfaces in the laminate. There was little change in stiffness, as both tension and compression values were 97 percent of their initial values.

Contrasting this loading with the T-C loading that involved the same peak compressive load, the C-C loading itself did not induce significant damage or stiffness change in this laminate. No significant traverse cracking occurred away from the hole, and the cracking and delaminations associated with the hole had very slow growth rates. This agrees well with C-C tests in [57], where higher load levels caused fatigue failures by delamination. The load level in this test apparently was not high enough to complete the delamination process through the thickness of the laminate. Delaminations adjacent to 90 deg. plies favored the -45 deg. interfaces. In T-T, the opposite side was favored, and in T-C, both sides delaminated at approximately the same time.

3.4.4 Mixed Load Ratio Fatigue Behavior

Recalling that the fatigue tests run with R=-1 resulted in fatigue lives of 100K cycles or more, the results of the positive load ratio tests at comparable load amplitudes suggest that T-T or C-C loading is not nearly as debilitating as T-C loading. Several additional tests at various load ratios were conducted to investigate this matter more thoroughly.

3.4.4.1 C-C Followed by T-T Fatigue

The specimen that was cycled in C-C at -5500 lb. peaks (R=10) to 1M cycles was subjected to T-T at +5500 lb. peaks (R=0.1) to determine whether or not it was the number of stress reversals or simply the number of peak stress excursions that determined fatigue behavior. It is already known that the specimens tested at this same peak load with R=-1 failed at approximately 100K cycles. This can be interpreted as 100K stress reversals, 100K tension peaks, 100K compression peaks, or some combination of these. Individually, the second and third interpretations can be ruled out based on the T-T and C-C tests that did not cause fatigue failures within a million cycles at peak loads meeting or exceeding ±5500 lb.

Results of this test indicate that the sum of damage introduced by separate blocks of C-C and T-T is less than the total damage produced by an equal number of positive and negative load peaks in a T-C test. The specimen survived an additional million cycles of T-T, with only a moderate increase in delamination and transverse matrix cracking (Figure 40). The +45/90 interfaces that did not delaminate after 1M cycles of C-C are all delaminated at this point. Stiffnesses were between 96 and 97 percent at the time the test was halted, which represents no significant change from the start of this loading block. The importance of stress reversal in fatigue damage development is therefore reinforced by these observations.

3.4.4.2 Block Load Ratios with Initial R=-1

The objective of this series of tests is to determine the combined effects of a high tensile load and various magnitudes and signs of minimum load on the laminate's fatigue response. In particular, it was desired to see whether a tensile mode of failure could be realized with some load ratio between -1 and zero. Recall that up to this point, all T-C fatigue failures were caused by the loss of compressive stiffness and stability. Three specimens were cycled to 200K cycles at the low load level of ±4500 lb. (±20.0 kN) to establish a base of damage that could be compared to previous results. Tension and compression stiffnesses at this point were nominally between 80 and 85 percent of initial values, which are representative of mid-stage II damage. Typical radiographs were similar to

←Load Axis→

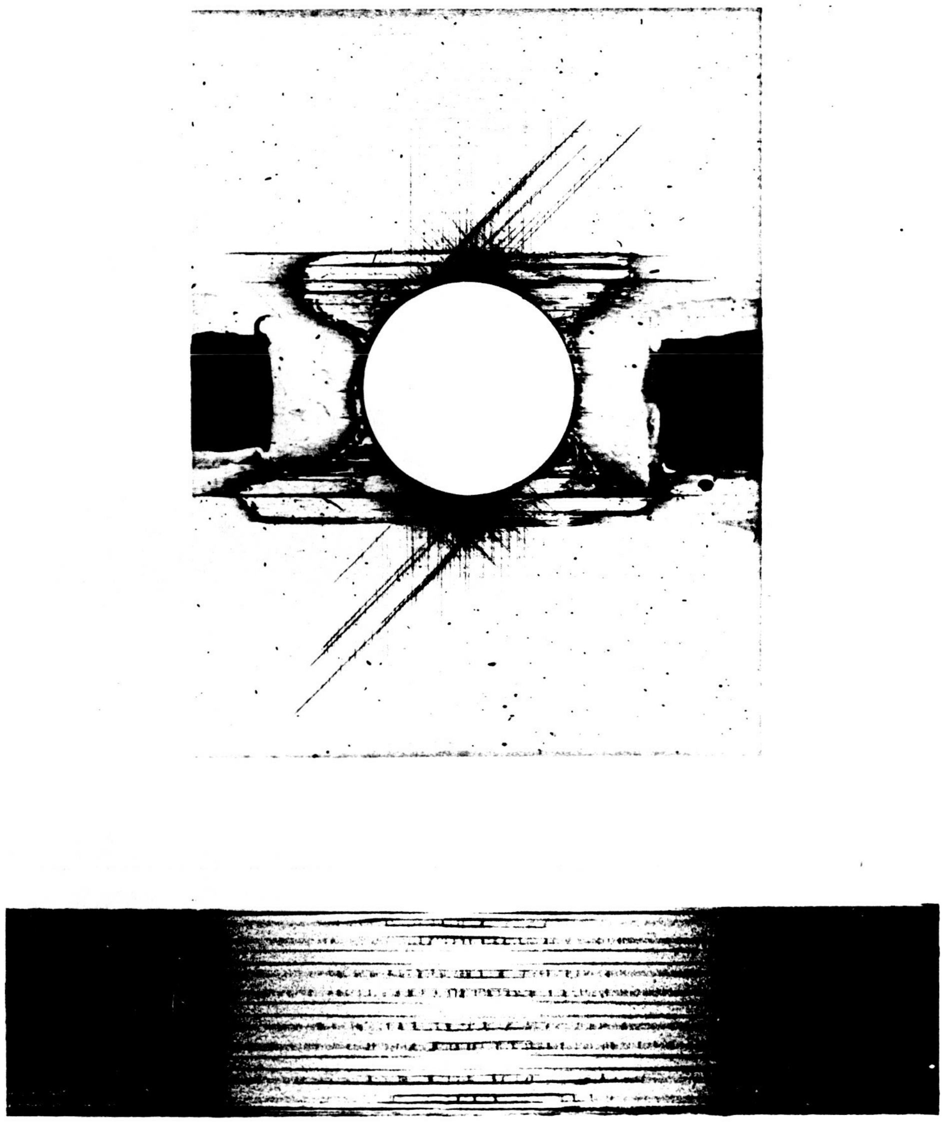

Figure 40: Radiographs, C-C Followed by T-T, 2M Cycles

that shown in Figure 24b. After this first block of loading, the maximum tensile load was raised to 7500 lb. (33.4 kN), which was calculated to cause a remote strain of 6000$\mu\varepsilon$ in undamaged material. (This strain level is representative of projected limit strains that are desired in the design of high-performance structures.) The minimum load amplitudes for the three tests were -4500, -2250 and +750 lb. (-20.0, -10.0, +3.3 kN).

The first specimen (no. 5-8) was cycled at min/max load peaks of -4500/7500 lb. (-20.0/33.4 kN) during the second load block, which is a load ratio of -0.6. With the higher tensile load, off-axis matrix cracks initiated and grew over a large area of the laminate. These were denser than the cracks seen at ±4500 lb (±20.0 kN), and covered a larger area as well. Figure 41 is the X-ray image of damage at the end of life for this specimen. All delaminations through the thickness that were initiated in the first block of loading grew in area. Straight edge delaminations appeared near the end of life at the positions of densest matrix cracking (the region bounded by ±45 deg. tangents to the hole). The stiffness declined rapidly and in a linear manner with respect to cycles during the second load block. Imminent failure at 245K cycles was characterized by a rapidly accelerating compression stiffness loss (Figure 42).

The test was stopped at this time for a measurement of residual tensile strength. The tension and compression tangent stiffnesses were 71 and 70 percent, respectively. Recalling that compression stiffness was generally significantly less than tensile stiffness in tests with R=-1 at the end of life, it was noted in this case that the higher tensile load caused a more rapid tensile stiffness loss. Despite this fact, the impending failure mode was one of compression, suggesting that damage caused by high tensile loads degrades the compressive properties faster than low tensile loads in the presence of equal compressive cyclic loads. The tensile strength at the end of life was 120 percent of the mean initial strength, which is about the same as the residual strengths in the R=-1 tests from early stage II to the end of life. Information on load and strain data from the tensile strength test is given in Table 1. The especially high value of the hole-to-edge strain ratio (2.3, or 140 percent of the undamaged value) is an indication of the increased amount of tensile compliance induced in the material close to the hole, as compared to the fatigue tests with R=-1.

The appearance of the fracture surface is shown in Figure 43a. In contrast with most residual tensile failures at R=-1, and some of the static tensile failures, the double

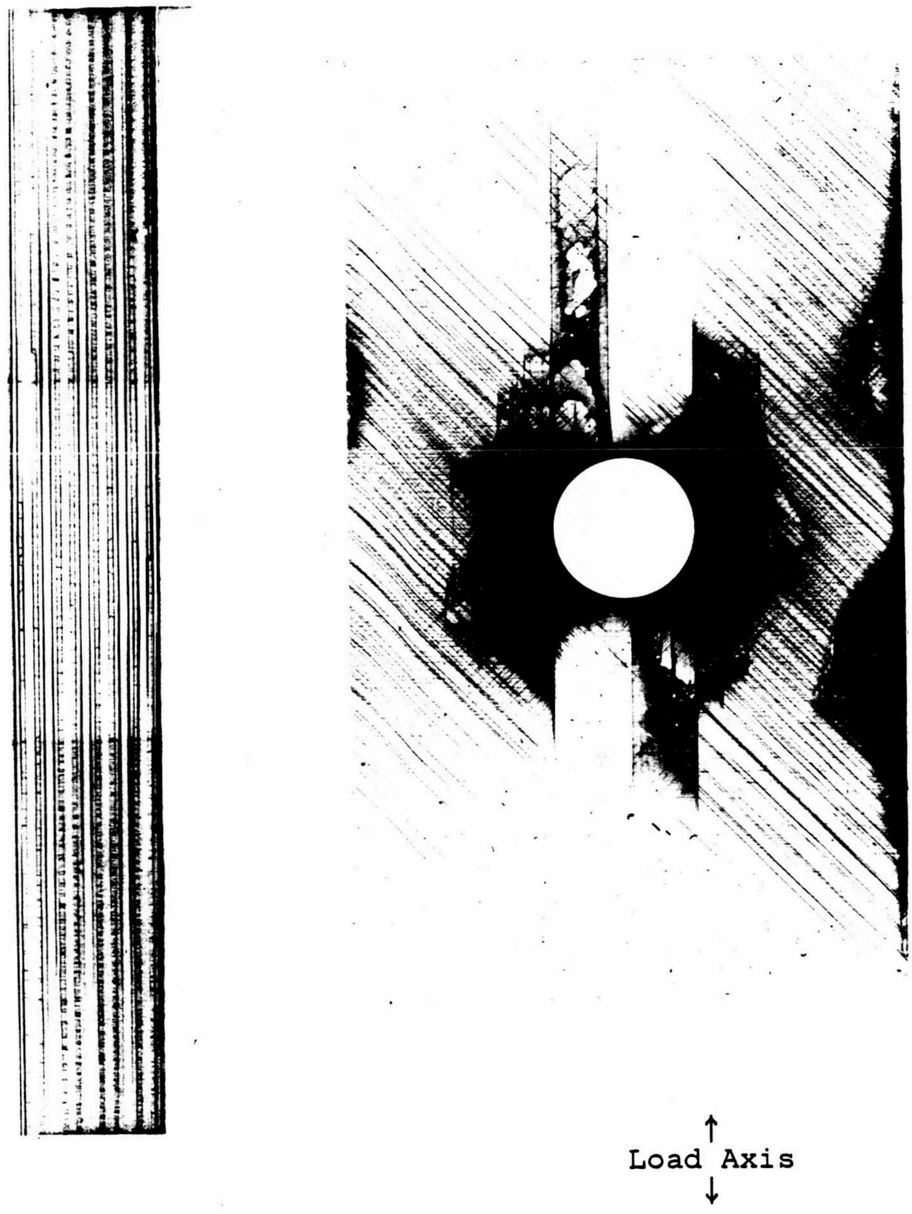

Figure 41: Radiographs of Specimen 5-8, Block Loading

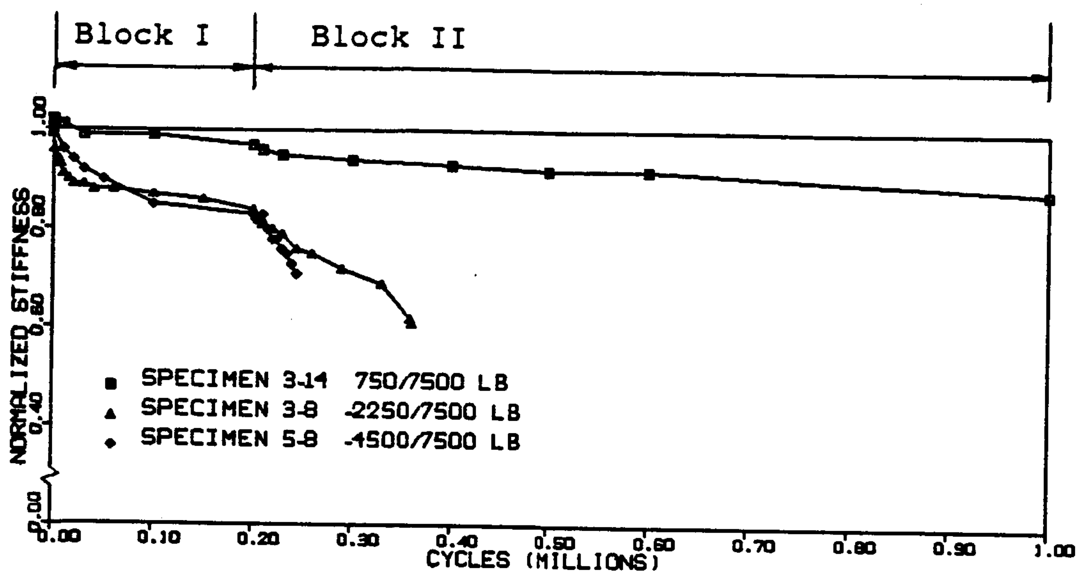

a) Tension Stiffness

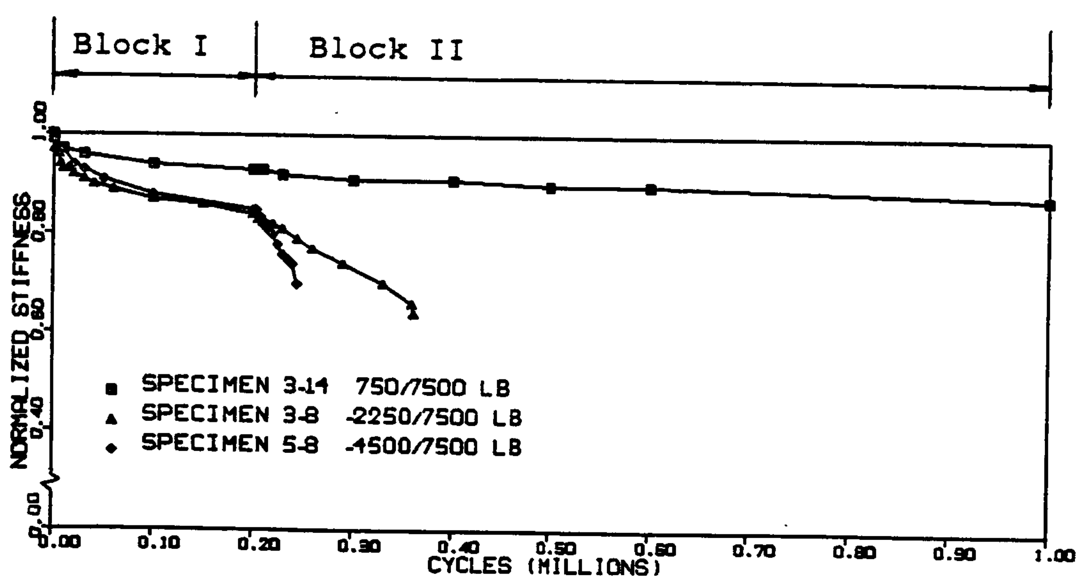

b) Compression Stiffness

Figure 42: Tangent Stiffness Degradation, Block Loadings

-45 deg. plies exhibited fiber fractures. A large delamination caused by the cyclic loading caused the fracture surface to deviate from the hole centerline. The fracture surface of the ligaments to the left and right of the hole resembled those of the unnotched laminates in [22] subjected to residual tensile strength measurement.

The second test imposed a min/max cyclic load of -2250/+7500 lb. (-10.0/+33.3 kN) during the second load block (specimen 3-8), which is a load ratio of -0.3. X-ray radiographs at the end of life (361K), shown in Figure 44, resembled those of specimen 5-8. There was a large increase of matrix cracks in off-axis plies, and the delaminations extended away from the hole. Straight edge delaminations appeared at the same densely cracked areas along the ±45 deg. tangent cracks, and favored the interfaces on either side of the 90 deg. plies nearest to the surface. Stiffness behavior, shown in Figure 42, suggests the existence of a second set of stages I, II and III during the second load block. The first stage of the second set involves a rapid, but slowing stiffness drop of about 5 to 10 percent. The second stage is a more uniform drop of an additional 5 to 10 percent. Stiffness dropped an additional 5 to 10 percent in stage III. Tangent stiffnesses at the end of life were 61 percent in tension and 64 percent in compression, which

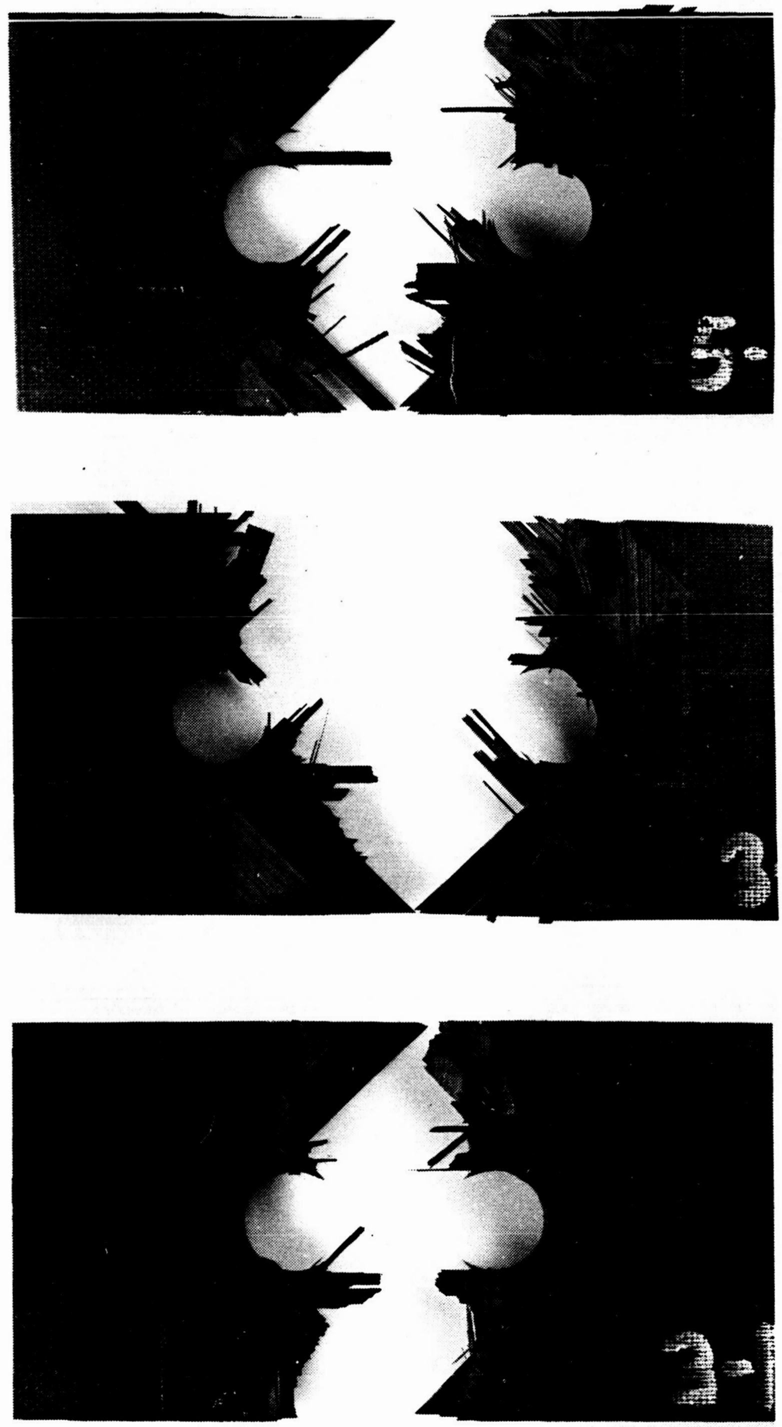

a) Specimen 5-8
-4500/7500 lb.

b) Specimen 3-8
-2250/7500 lb.

c) Specimen 3-14
750/7500 lb.

Figure 43: Tensile Fracture Surfaces, Block Loadings

means that the degradation of tensile stiffness exceeded that for the compression stiffness. As in most previous tests involving compressive loads, the compression stiffness degraded faster than tension stiffness near the end of life. This test was stopped when failure seemed imminent. The residual tensile strength was then measured to be 130 percent of the initial strength. Therefore, even though the tensile stiffness has degraded more than the compression stiffness, there was no obvious degradation of tensile strength, and laminate instability was still the mode of failure. As can be seen in Table 1, the strain increases at the hole and edge were substantial. The ratio of hole strain to edge strain was 140 percent of the mean initial value. In a manner similar to specimen 5-8, the fracture surface was shifted off the center of the hole by delaminations caused by the fatigue loading (Figure 43b).

The third test (specimen 3-14) contained no compressive loading in the second load block. This was intended to force a change of tensile strength at the end of life. The maximum load was +7500 lb. (+33.3 kN), and the minimum was +750 lb. (+3.3 kN), which is a load ratio of 0.1. The stiffness degradation was only about five percent in both compression and tension from 200K to 1M cycles. The most rapid stiffness drop occurred within 100K cycles of the

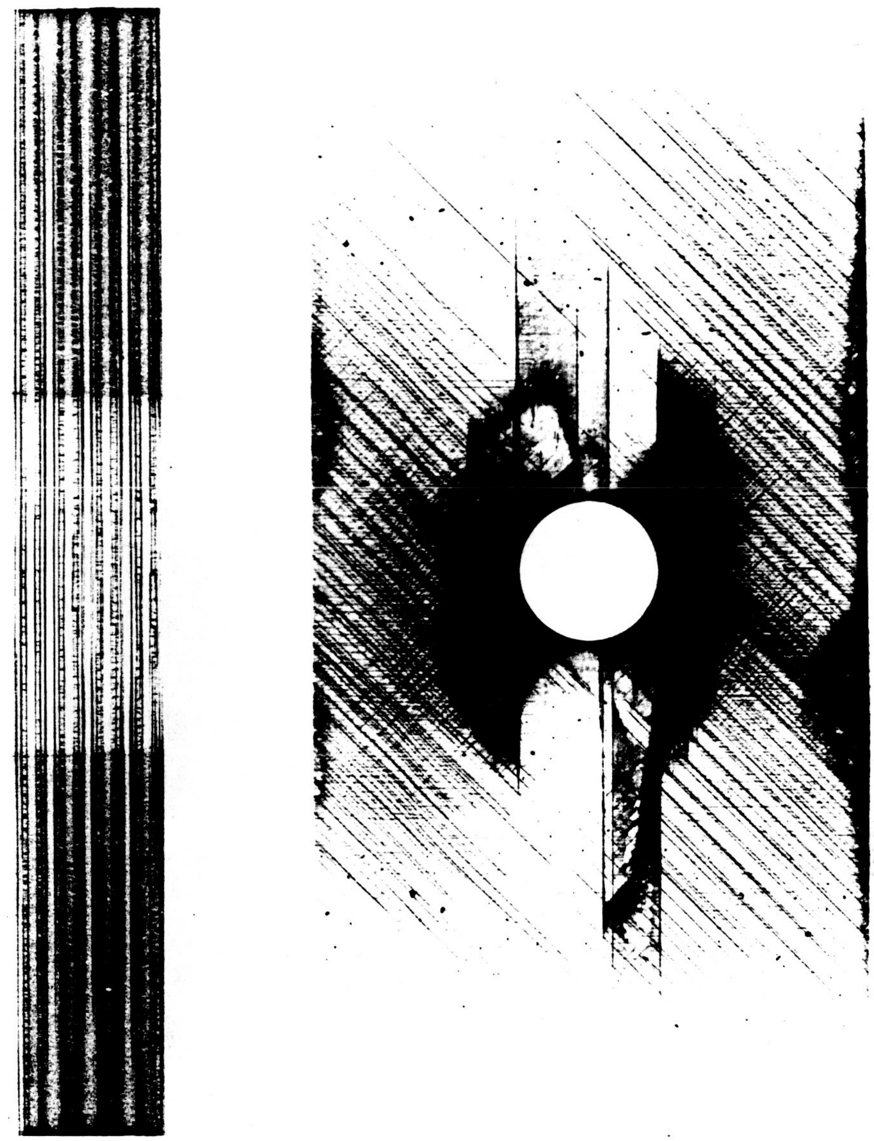

Load Axis

Figure 44: Radiographs of Specimen 3-8, Block Loading

start of the second load block (Figure 42). At one million cycles, the test was stopped for X-ray inspection (Figure 45). The state of damage in the radiograph and the lack of stiffness degradation suggest that this load level was insufficient to cause fatigue failure. The surface delaminations did not grow much laterally, but did grow in the region between the 0 deg. tangents. Matrix cracking and straight edge delaminations were also of lesser extent than the previous two cases. As can be seen in the stiffness plot in Figure 42, the stiffness behavior of this specimen was atypical from the start. At 200K cycles, the tension and compression tangent stiffnesses were 97 and 93 percent, respectively, or roughly 10 percent higher than usual at that load level. After 800K additional cycles of the second block of T-T loading, both normalized tension and compression tangent stiffnesses were 88 percent, which is still higher than the other tests were at the end of the first block. This may have been caused by the lack of test interruptions for NDE. Residual tensile strength measured at the end of the test was 125 percent of initial strength. The ratio of hole strain to edge strain increased to 110 percent of the value for undamaged specimens, which is a negligible change, considering the scatter of data. In this case, neither tensile nor compressive properties were degraded sufficiently to make any conclusions on the mode of failure if the laminate were to be subjected to both tensile and compressive loads again. The fracture surface, shown in Figure 43c, contains less delamination shearout than usual.

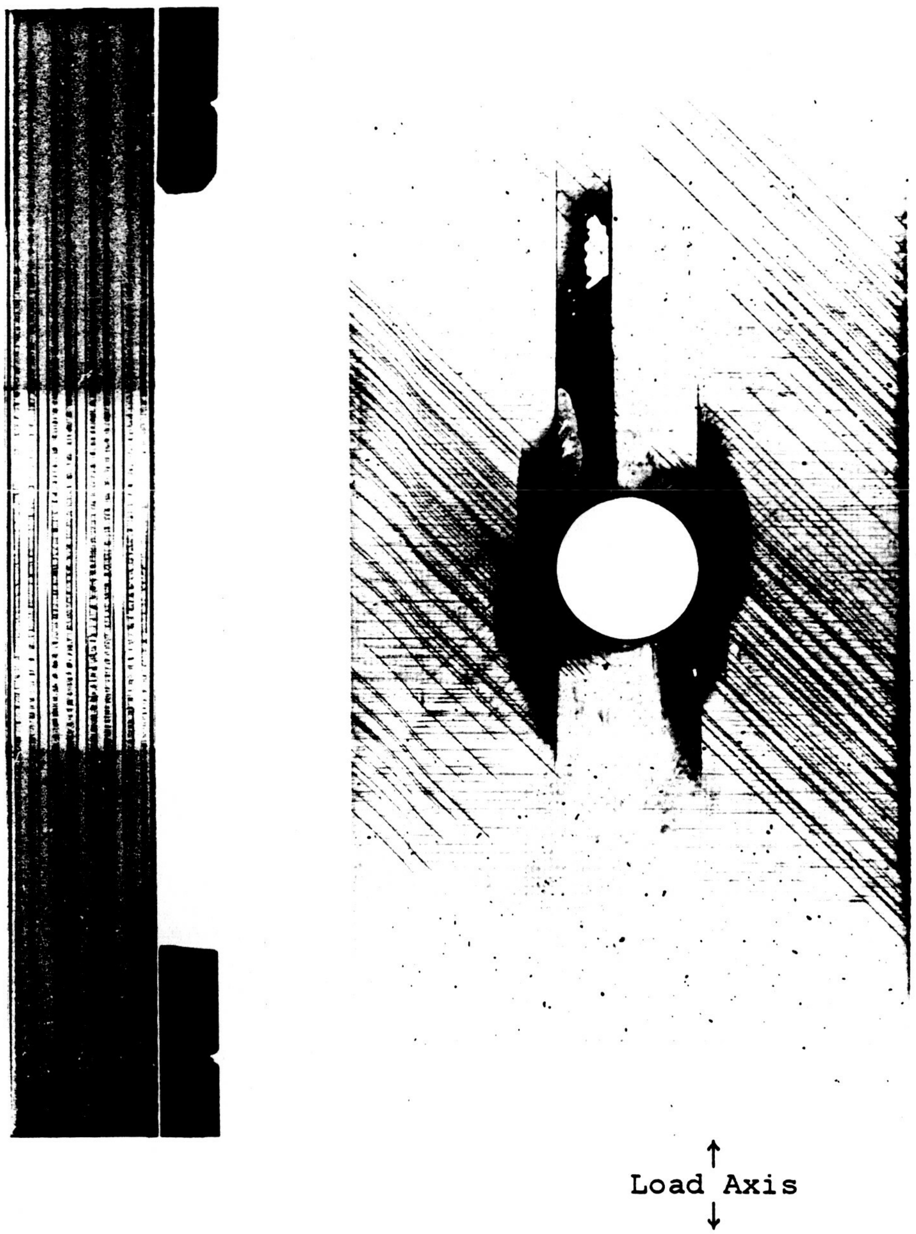

Figure 45: Radiographs of Specimen 3-14, Block Loading

Chapter IV

THEORETICAL TREATMENT OF DELAMINATION

4.1 PREFACE

Delamination has been shown to significantly effect the strength, stiffness and life of composite laminates. When a laminate is subjected to compressive loading, as in this investigation, a delaminated ply or sublaminate can precipitate structural instability. It is therefore of great engineering importance to develop techniques that model and predict delamination initiation and growth. To date, most successful delamination models have concerned the initiation process. The growth process is more difficult to model because of the continuously changing state of stress and geometry in the vicinity of the delamination. The present analysis investigates the feasibility of combining features from several models of delamination and transverse matrix cracks into a single scheme that can predict the delamination initiation sites observed experimentally in a laminate containing a circular hole.

4.2 STRAIGHT EDGE DELAMINATION

Reasonably accurate predictions of the location of delamination onset have been achieved with three-dimensional analyses of the stress state along a discontinuity, such as a free edge. O'Brien's incorporation of the strain-energy-release rate concept of classical fracture mechanics has enabled good prediction of the strain level for delamination onset as well (see Section 1.3). A brief summary of this delamination prediction technique [50] will be presented next to establish a foundation for the modifications performed herein.

The underlying hypothesis of the energy approach to delamination prediction is that a delamination is likely to occur at the ply interface where the strain-energy release rate of incremental delamination growth is maximum. Other considerations, such as the contribution of each of the three modes of delamination (one normal and two shear) and the stress state at the ply interface, are also important in delamination prediction. An equation for the total rate of strain energy release associated with straight edge delamination is

$$G_T = \frac{\varepsilon^2 t}{2m}(E_{LAM} - E^*) \quad , \qquad (4.1)$$

where G_T = Total strain energy release rate

ε = Nominal strain

t = Total laminate thickness

m = Number of delaminations formed

E_{LAM} = Laminate modulus before delamination

E^* = Laminate modulus after delamination.

All moduli and strain values are measured along the load (X) axis of the laminate. Equation 4.1 actually represents the steady-state value of the strain energy release rate once the delamination has grown away from the edge. Finite element modelling of delamination initiation suggests that this steady-state rate occurs within three or four ply thicknesses from the edge [51]. E^* is calculated using a simple rule of mixtures with laminated plate theory as

$$E^* = \frac{1}{t} \sum_{k=1}^{m+1} E_k t_k \ , \qquad (4.2)$$

where the quantity (m+1) equals the number of sublaminates formed by m delaminations through the width of a laminate, and E_k and t_k are the modulus and thickness of the k-th sublaminate, respectively.

When calculating the value of E^*, the effect of bending-extension coupling should be considered. The relation between the loads (N_x, N_y, N_{xy}, M_x, M_y, M_{xy}) and the strain and curvature (ε_x, ε_y, γ_{xy}, κ_x, κ_y, κ_{xy}) at the laminate or sublaminate midplane is stated in classical laminated plate theory as:

$$\begin{Bmatrix} \varepsilon_x^o \\ \varepsilon_y^o \\ \gamma_{xy}^o \\ \kappa_x \\ \kappa_y \\ \kappa_{xy} \end{Bmatrix} = \begin{bmatrix} A_{11} & A_{12} & A_{13} & B_{11} & B_{12} & B_{13} \\ A_{21} & A_{22} & A_{23} & B_{21} & B_{22} & B_{23} \\ A_{31} & A_{32} & A_{33} & B_{31} & B_{32} & B_{33} \\ B_{11} & B_{12} & B_{13} & D_{11} & D_{12} & D_{13} \\ B_{21} & B_{22} & B_{23} & D_{21} & D_{22} & D_{23} \\ B_{31} & B_{32} & B_{33} & D_{31} & D_{32} & D_{33} \end{bmatrix}^{-1} \begin{Bmatrix} N_x \\ N_y \\ N_{xy} \\ M_x \\ M_y \\ M_{xy} \end{Bmatrix}, \tag{4.3}$$

where A_{ij}, B_{ij} and D_{ij} are the extensional, extension-bending coupling, and bending stiffness matrices, respectively [2]. Once the midplane strain and curvature are known, the strain at any distance (z) perpendicular to the midplane can be calculated using the relation

$$\begin{Bmatrix} \varepsilon_x \\ \varepsilon_y \\ \gamma_{xy} \end{Bmatrix} = \begin{Bmatrix} \varepsilon_x^o \\ \varepsilon_y^o \\ \gamma_{xy}^o \end{Bmatrix} + z \begin{Bmatrix} \kappa_x \\ \kappa_x \\ \kappa_{xy} \end{Bmatrix} . \tag{4.4}$$

For a symmetric laminate (B_{ij}=0), the calculation of E_k becomes

$$E_k = 1/(X_{11} t_k) , \tag{4.5}$$

where X_{11} is the (1,1) element of the inverse extensional stiffness matrix (A_{ij}) of the k-th sublaminate. It is not quite clear how E^* is to be calculated for unsymmetric sublaminates that may result from delamination. Using eq. 4.5 to model the stiffness of certain delaminated laminates is sufficiently accurate when compared to experimental data, as shown by O'Brien in [50]. In the $[\pm30/\pm30/90_3/\pm30/\pm30]$ laminate used as his example, the delamination frequently jumps across the 90 plies via transverse matrix cracks so that both -30/90 interfaces are partially delaminated. Consequently, to compute the strain energy release rate, both -30/90 interfaces were modelled as delaminated, and the bending-extension coupling was ignored.

In cases where the bending-extension coupling is too large to ignore, a different type of approximation should be used. Whitcomb and Raju [59] assumed a known force N_x^o applied to the laminate, with the remaining five boundary conditions given by

$$N_y = N_{xy} = M_y = \kappa_x = \kappa_{xy} = 0 \ . \tag{4.6}$$

The effective modulus for the k-th sublaminate is then

$$E_k = N_x^o/(t\varepsilon_x) \ , \tag{4.7}$$

with longitudinal strain, ε_x, constant through the thickness of the sublaminate. This set of boundary conditions simulates a specimen gripped in a testing machine, or localized delamination in a large, symmetric plate under uniform extension. The curvatures along the X-axis (load axis) are eliminated by constraints applied by the grips or surrounding material. In a section of the material away from the constraint, curvature κ_y is allowed since M_y and N_y vanish at the free edge (Saint-Venant's Principle). Using eqs. 4.2, 4.6 and 4.7 to calculate E^* has resulted in good predictions of delamination location in thick laminates [59].

4.3 NOTCH DELAMINATION

To supplement the published literature concerning straight-edge delamination, O'Brien and Raju [51] presented a technique based on previous work that treats the boundary of a circular hole as a series of short, discrete segments of straight edges. The straight edge formulation can then be used as an approximation of the more complicated curved edge problem. Correlation of predictions with results from quasi-static tension tests of two eight-ply, quasi-isotropic laminates revealed that reliable predictions of initial delamination location were possible. Predicted strain levels for delamination initiation, however, were about 30 percent higher than experimental values. It was suggested that this difference is caused by extensive matrix cracking parallel to the fibers in the off-axis plies. A separate study on the effect of transverse matrix cracks on straight-edge delamination initiation supports this suggestion [44].

A brief summary of the notch delamination scheme is necessary at this point. The derivation is valid only for a material with isotropic in-plane elastic properties. Recall the relations for the stress state along an unloaded hole in an isotropic plate of infinite extent subjected to a uniform load, σ_∞, as [64]:

$$\sigma_\theta = \sigma_\infty(1 - 2\cos 2\theta) \tag{4.8}$$

$$\sigma_r = \tau_{r\theta} = 0 \,, \tag{4.9}$$

where θ is measured from the load axis in a clockwise direction (see Figure 3). Making use of Hooke's law at the hole boundary, the state of strain is

$$\varepsilon_\theta = \varepsilon_\infty(1 - 2\cos 2\theta) \tag{4.10}$$

$$\varepsilon_r = \gamma_{r\theta} = 0 \,, \tag{4.11}$$

where ε_∞ is the remote strain along the load direction. If the equation for circumferential strain, ε_θ, is substituted into the relation for the strain energy release rate (eq. 4.1), one arrives at

$$G_T(\theta) = (1 - 2\cos 2\theta)^2 \varepsilon_\infty^2 \frac{t}{2m}[E_{LAM} - E^*(\theta)] \,, \tag{4.12}$$

which is an approximate total strain energy release rate of a delamination growing perpendicular to the hole boundary at some angular position, θ. The value of $E^*(\theta)$ is computed as in the straight edge problem, with the ply angles rotated for a particular position, θ, on the hole boundary. The in-plane modulus, E_{LAM}, remains constant at any angle of rotation for a quasi-isotropic laminate. In [51], this equation is nondimensionalized with respect to the remote strain, laminate thickness and lamina modulus in the fiber direction to facilitate comparison of different layups:

$$\frac{G(\theta)}{E_{11}\varepsilon_{\infty}^{2}t} = \frac{(1 - 2\cos 2\theta)^{2}}{2m\ E_{11}}[E_{LAM} - E^{*}(\theta)] \ . \qquad (4.13)$$

If all other parameters relevant to delamination were the same, delamination initiation is hypothesized to occur when the configuration of variables in eq. 4.13 yields the highest non-dimensionalized strain energy release rate, G_{nd}.

4.4 THICKNESS AND CRACKING EFFECTS

The analysis of thick laminates by Whitcomb [59] was derived for straight edge delamination, while the analysis by O'Brien [51] pertained to thin, notched laminates with isotropic in-plane elastic properties. An effort was made to combine the good qualities of both of these analytical treatments into a single scheme appropriate for the thick, notched laminate used in the present experimental investigation, and to account for the extensive matrix cracking that has been shown experimentally to precede delamination at the notch.

In the interest of obtaining the most accurate model of damage in a material, all modes of damage should be accounted for. This turns out to be a very difficult task with fiber-reinforced composite materials due to the complexity of damage development. Often, degradation of this type of material is caused by the initiation and growth of many separate damage modes, such as matrix cracks, which interact in some, as yet, unpredictable manner. Neither of the delamination models discussed to this point account for damage in the laminate that often precedes delamination. The present analytical effort incorporates a simple technique, called "ply discount", to model the elastic disturbance caused by transverse matrix cracks.

Ply discount has been used in the past to successfully model the degradation of material stiffness in fiber-reinforced composite laminates [36]. Briefly, the procedure involves reducing (discounting) the elastic properties of a particular ply in a laminate to reflect the state of damage in that ply. Since a transverse matrix crack effectively blocks transmission of transverse and shear load in a ply at some localized area, the transverse and shear stiffness at that area could be considered small or nearly zero. Thus, in the presence of a densely cracked lamina, a reasonable modelling for laminate analysis can be achieved by reducing these stiffnesses by a factor of one thousand.

As used here, the ply discount technique assumes homogeneity at the lamina level. That is, a ply's elastic properties are the same at any location in the laminate. Two important consequences of this assumption are that: 1) the effect of cracks at the microscopic level is not included; and 2) the macroscopic distribution of cracks near the notch is not accurate. The first consequence is important if delamination initiation or growth is directly associated with the preceding crack(s). Experimental evidence presented in Chapter 3 strongly suggested that delaminations often do initiate at the crossings of matrix cracks in adjacent plies, but whether or not these delaminations precede free edge delamination is not known. In any case, this type of delamination is not included in the formulation given by eq 4.1, and hence cannot be predicted. If the second consequence is important, the non-uniform nature of cracking at the notch (and whether or not the crack is elastically "visible" during all parts of T-C loading) adds uncertainty to the ideal strain distributions for which closed-form solutions exist. With the above limitations in mind, the ply discount technique is proposed as a first-cut model of pre-delamination damage in a laminate.

It was learned from the fatigue tests previously performed that dense transverse matrix cracks in all off-axis plies preceded delamination. Cracks in the 0 deg. plies were not as extensive and were located primarily at the two tangents to the hole. To obtain the most accurate distribution of strain along the entire hole boundary with a minimum of computational effort, the transverse and shear stiffnesses in only the off-axis plies were discounted. This is a compromise that is felt to be the best model of material behavior in an overall sense. The laminate elastic properties before and after this procedure were:

Property	Before Discounting	After Discounting
E_{xx}	7.64 Msi (52.7 GPa)	6.50 Msi (44.8 GPa)
E_{yy}	7.64 Msi (52.7 GPa)	6.80 Msi (46.8 GPa)
G_{xy}	2.93 Msi (20.2 GPa)	2.64 Msi (18.2 GPa)
ν_{xy}	.305	.332

The strain distribution around the hole can then be easily modified to reflect the orthotropy of the material. Lekhnitskii [17] gives the circumferential stress distribution on the boundary of a circular hole in an infinite orthotropic plate as

$$\sigma_\theta = \sigma_\infty \frac{E_\theta}{E_x}[\mu_1\mu_2\cos^2\theta + (1+n)\sin^2\theta] \ , \qquad (4.14)$$

where $$n = -i(\mu_1 + \mu_2) \qquad (4.15)$$

$$\frac{1}{E_\theta} = \frac{\sin^4 r}{E_x} + [\frac{1}{G_{xy}} - \frac{2\nu_{xy}}{E_x}]\sin^2\theta\cos^2\theta + \frac{\cos^4 r}{E_y} \qquad (4.16)$$

σ_∞ is the remote stress, $i = \sqrt{-1}$, and μ_i are the complex roots of the characteristic equation:

$$\mu^4 + (\frac{E_x}{G_{xy}} - 2\nu_{xy})\mu^2 + \frac{E_x}{E_y} = 0 \ . \qquad (4.17)$$

While there are actually four roots to this equation, they occur as two conjugate pairs for an orthotropic material. Hence, μ_1 and μ_2 represent the two roots with a positive imaginary part. The circumferential strain is then given by

$$\varepsilon_\theta = \varepsilon_\infty[\mu_1\mu_2\cos^2\theta + (1+n)\sin^2\theta] \ , \qquad (4.18)$$

where ε_∞ is the remote strain. When this equation for strain around the hole is substituted into the strain energy release rate equation (4.1) in place of the isotropic strain distribution, and the roots μ_1 and μ_2 are expressed in terms of the elastic properties, the result (normalized as before) is:

$$\frac{G(\theta)}{E_{11}\varepsilon_\infty^2 t} = \{- \frac{E_x}{E_y}\cos^2\theta + [1 + (\frac{E_x}{G_{xy}} - 2\nu_{xy} + 2\frac{E_x}{E_y})^{.5}]\sin^2\theta\}^2$$

$$\times [E_{LAM}(\theta) - E^*(\theta)](\frac{1}{2m\ E_{11}}) \ . \qquad (4.19)$$

In the orthotropic case, the in-plane modulus, E_{LAM}, is a function of θ on the hole boundary. Equation 4.19 is actually a more general case of equation 4.13, and thus can be used to calculate G_{nd} for isotropic materials as well.

A comparison of the effects of off-axis discounting on the global laminate properties reveals some noteworthy information. The effective laminate longitudinal modulus, E_x, of an equivalent unnotched material is reduced by 15 percent of the its value before discounting, while the transverse modulus, E_y, is reduced only 11 percent. The stress concentration factor is reduced by six percent at the 90 deg. position on the hole boundary, while at the 0 deg. position it increases by two percent. The stress distribution along the hole boundary is thus redistributed so that the peak magnitude is reduced. In practical situations, however, the same damage that causes this reduction of "macro" stress concentration could also raise the "micro" stress concentration near crack tips.

As part of an estimation of delamination onset (along with a three dimensional stress solution), the nondimensional strain energy release rate given by eq. 4.19 could be evaluated on a comparative basis at each interface through the thickness of a laminate and at various positions along the hole boundary. Such a parametric study is illustrated in Figures 46 and 47 for half of the $[(0/45/90/-45)_s]_4$ laminate. Results for the second half of the laminate are a mirror image of the first half. Separate curves were drawn for the isotropic and orthotropic (off-axis discount) cases to note the effects of the proposed discounting scheme on the nondimensional strain energy release rate. When comparing G_{nd} for two different laminates, however, one must consider the particular non-dimensionalizing scheme used. In this case, the strain energy release rate is normalized to the remote strain (a variable) and other factors which are identical for either laminate. Hence, G_{nd} represents the relative tendency of the two laminates to delaminate when the same axial strain is being applied. For convenience in labelling the axes, the calculated value of G_{nd} was multiplied by 50 before plotting. The loading direction in Figures 46 and 47 is vertical. Equations 4.6 and 4.7, which are appropriate for thick laminates, were used to calculate the effective modulus (E^*) for the sublaminates via eq. 4.2. The trend of decreasing G_{nd} at interfaces farther from the surface is evident for this laminate configuration, particularly in the first ply group (8 plies). Hence, for a particular axial strain, delamination onset is predicted to prefer locations nearer to the surface. Recall from Section 1.4 that Whitcomb and Raju [59] observed a similar surface effect on G_{nd} for thick, unnotched laminates with $[(45/0/-45/90)_s]_n$ stacking sequences (n = 2,4,8).

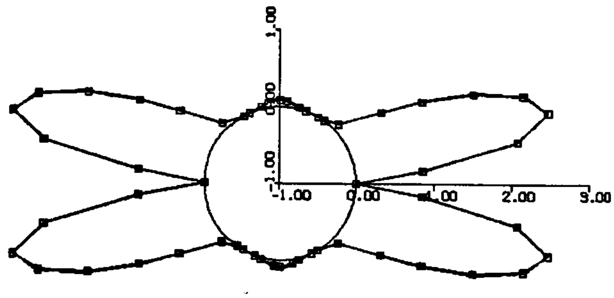

INTERFACE 1 0/45

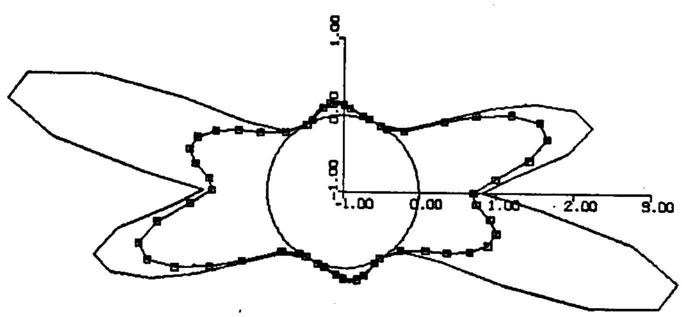

INTERFACE 2 45/90

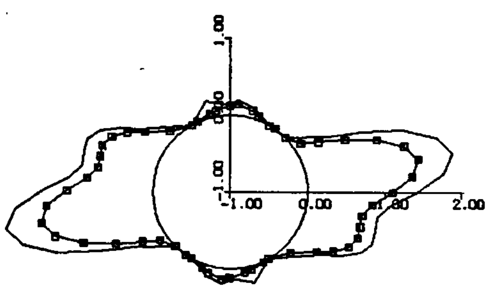

INTERFACE 3 90/-45

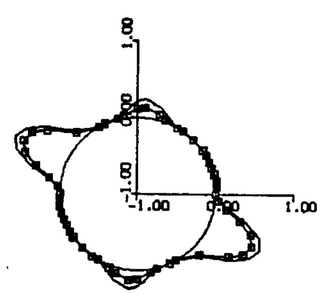

INTERFACE 4 -45/-45

↑
LOAD AXIS
↓

NO DISCOUNT —□—□—

OFF-AXIS DISCOUNT ———

Figure 46: Nondimensional Strain Energy Release Rate on Hole Boundary (Interfaces 1 - 4)

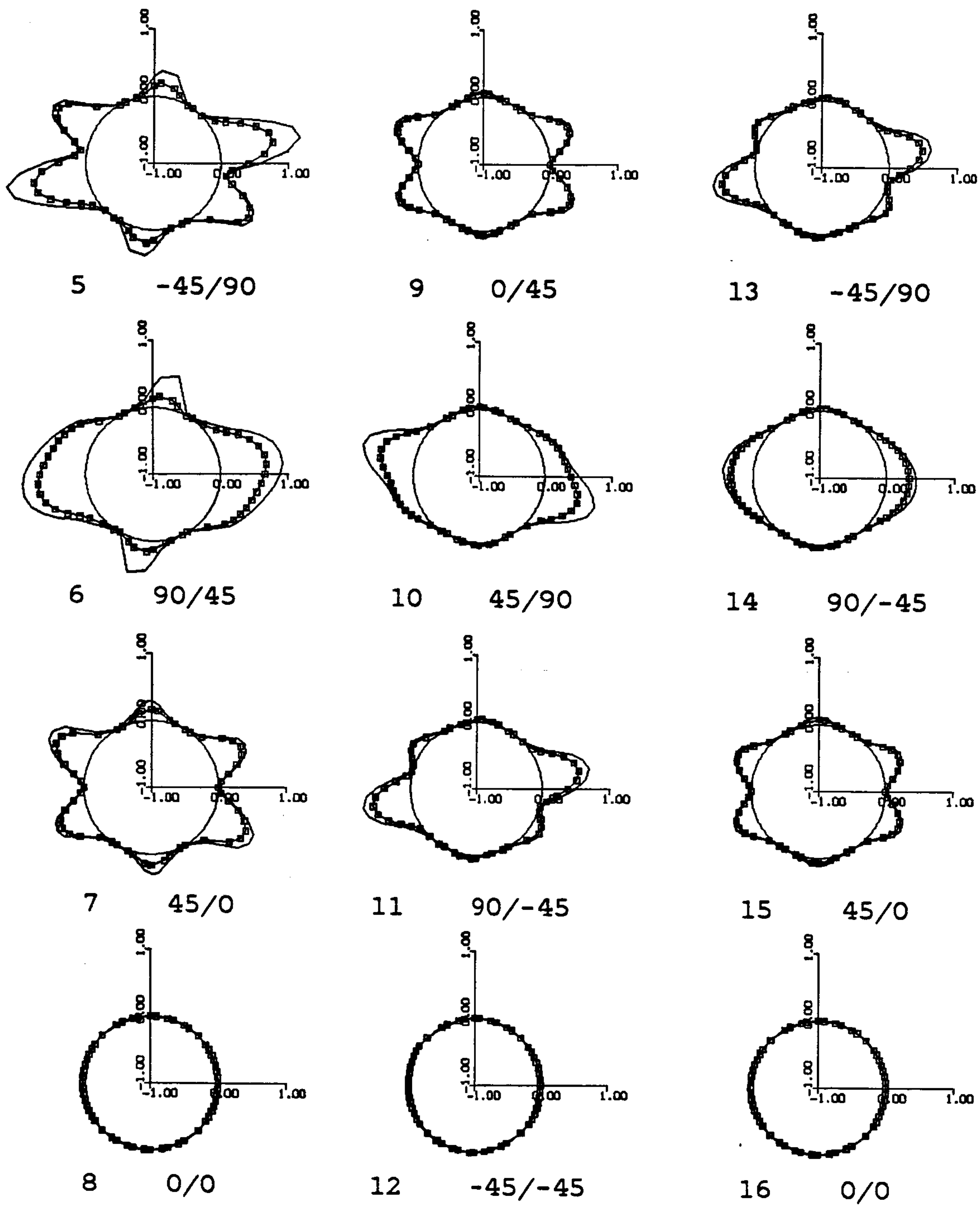

Figure 47: Nondimensional Strain Energy Release Rate on Hole Boundary (Interfaces 5 - 16)

Other parameters entering into the delamination prediction process for brittle materials, such as T300-5208 graphite-epoxy, is the amount of the total strain energy release rate contributed by mode I crack opening (G_I), and the state of stress at the ply interfaces. The calculation of these parameters requires a three-dimensional stress analysis that enables quantification of the energy released by the normal opening motion of incremental delamination growth. A finite element mesh with a nodal release scheme is sufficient for this purpose. Such a calculation, however, is beyond the scope of this investigation. Instead, a simple approximation of the interlaminar shear forces, $F_{\theta z}$ and F_{rz}, and the interlaminar normal stress, σ_z, based on two-dimensional laminated plate theory [7], were computed to obtain qualitative information on the interlaminar stress state near the free edge. The forces, shown in Figure 48a, represent an integration of interlaminar shear stresses near the free-edge of a tensile specimen of uniform cross-section under uniaxial extension, and are calculated through consideration of force equilibrium at the ply level. For analysis of a circular hole, the force at a particular interface must be calculated in polar coordinates by using the same discretization scheme used in the development of the strain energy release rate along the boundary of a hole. For example, the interlaminar shear forces acting on the k-th interface and at a particular angular position, θ, on the hole boundary can be calculated by summing the forces on all plies above that interface in the laminate caused by the in-plane stresses $\sigma_r(\theta)$ and $\tau_{\theta r}(\theta)$ as follows:

$$[F_{rz}(\theta)]_k = \sum_{i=k}^{N} [\sigma_r(\theta)t]_i \qquad (4.20)$$

$$[F_{\theta z}(\theta)]_k = \sum_{i=k}^{N} [\tau_{\theta r}(\theta)t]_i \ , \qquad (4.21)$$

where N is the total number of plies in the laminate, and t_i is the thickness of the i-th ply. The in-plane forces above the k-th interface also cause a moment about the longitudinal axis (circumferential axis in polar coordinates) that must be balanced by the interlaminar normal stress along the free edge. An approximation for the peak value of this stress is given by the relation

$$[\sigma_z(\theta)]_k = 90M_k(\theta)/[7T^2] \ , \qquad (4.22)$$

where $M_k(\theta)$ is the moment on the k-th interface at an angular position of θ on the hole boundary (Figure 48), and T is the total laminate thickness. A more detailed development of the approximate interlaminar stress analogues summarized here is available in [7].

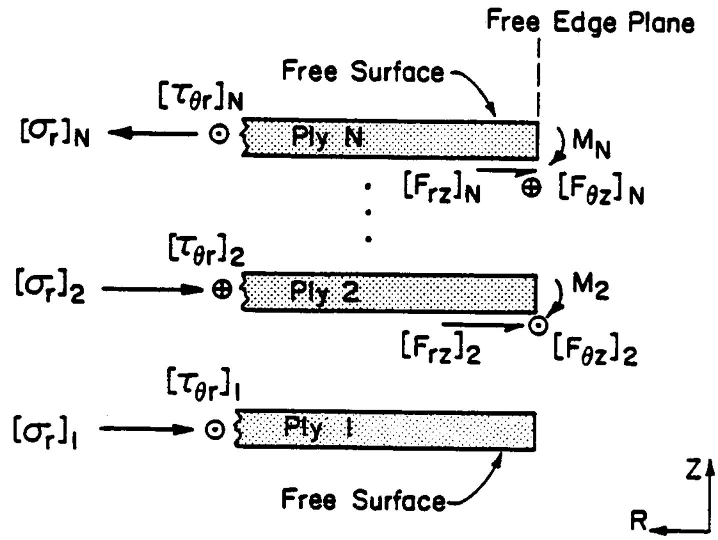

a) Force and Moment Resultants at a Free Edge

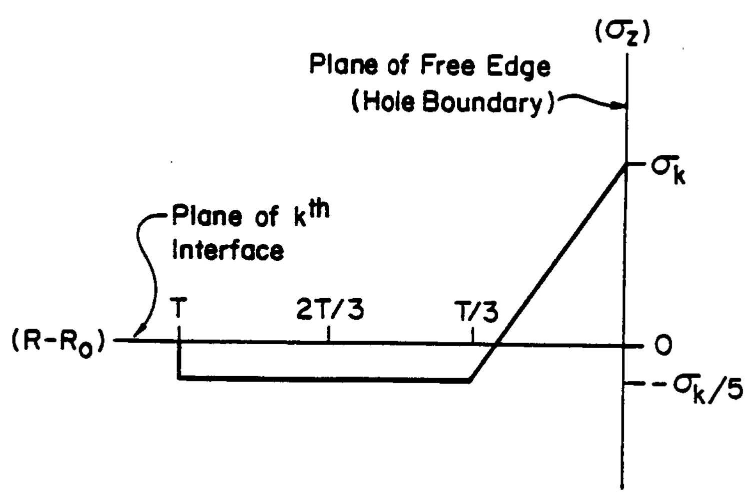

b) Assumed Interlaminar Normal Stress Distribution

Figure 48: Interlaminar Forces and Stresses by Pipes [7] in Polar Coordinates

There are, of course, gross approximations being made in order to use the above stress and force relations in the present application. These schemes were developed for the purpose of quickly and qualitatively comparing the magnitude of interlaminar stresses in parallel-sided laminates under uniform load. However, even a more sophisticated stress analysis would not be able to fully account for the complex distribution of damage around the hole. Therefore, the use of approximate schemes such as these is a practical and economical alternative, if only for qualitative information in a small region along the hole boundary.

Figures 49 and 50 illustrate all the unique distributions of σ_z, $F_{\theta z}$ and F_{rz} in the laminate. As in the previous plots, both the isotropic and discounted curves are drawn for comparison, and the load axis is vertical. All values in these figures are nondimensionalized by the applied longitudinal load (σ_x for Figure 49 and N_x for Figure 50), rather than the applied strain as in Figures 46 and 47. For plotting convenience, the values of σ_z were pre-multiplied by a factor of 70 before plotting, and the shear forces were pre-multiplied by a factor of 15. Note that at the middle of the double -45 deg. plies, there is a significant interlaminar normal force, but no interlaminar shear force. Based on the approximate stress and force formulation used, there would be no surface effect in delamination initiation. All of these parameters are calculated from the in-plane stresses of each ply derived from classical laminated plate theory, and thus simply repeat at similar interfaces through the thickness. A fully three dimensional stress analysis would reveal that the interlaminar stresses perhaps do vary with location through the thickness. More detail on the plots of strain energy release rate and interlaminar stress and force will be presented next so that comparisons may be made with experimental results.

4.5 RESULTS

Cursory examination of the polar G_{nd} plots (Figures 46, 47) reveals an interesting consequence of invoking the off-axis ply discount condition. All interfaces through the thickness had an increased G_{nd}, suggesting that merely the change in elastic properties of transversly cracked plies increases the likelihood of delamination. Stress concentration and additional cracking modes believed to be caused by the matrix cracks do not enter into the calculation. The most obvious change in G_{nd}, and perhaps the most important from the standpoint of delamination initiation, occurred in the first two interfaces. Before discounting, the sites of highest G_{nd} were at the 75, 105,

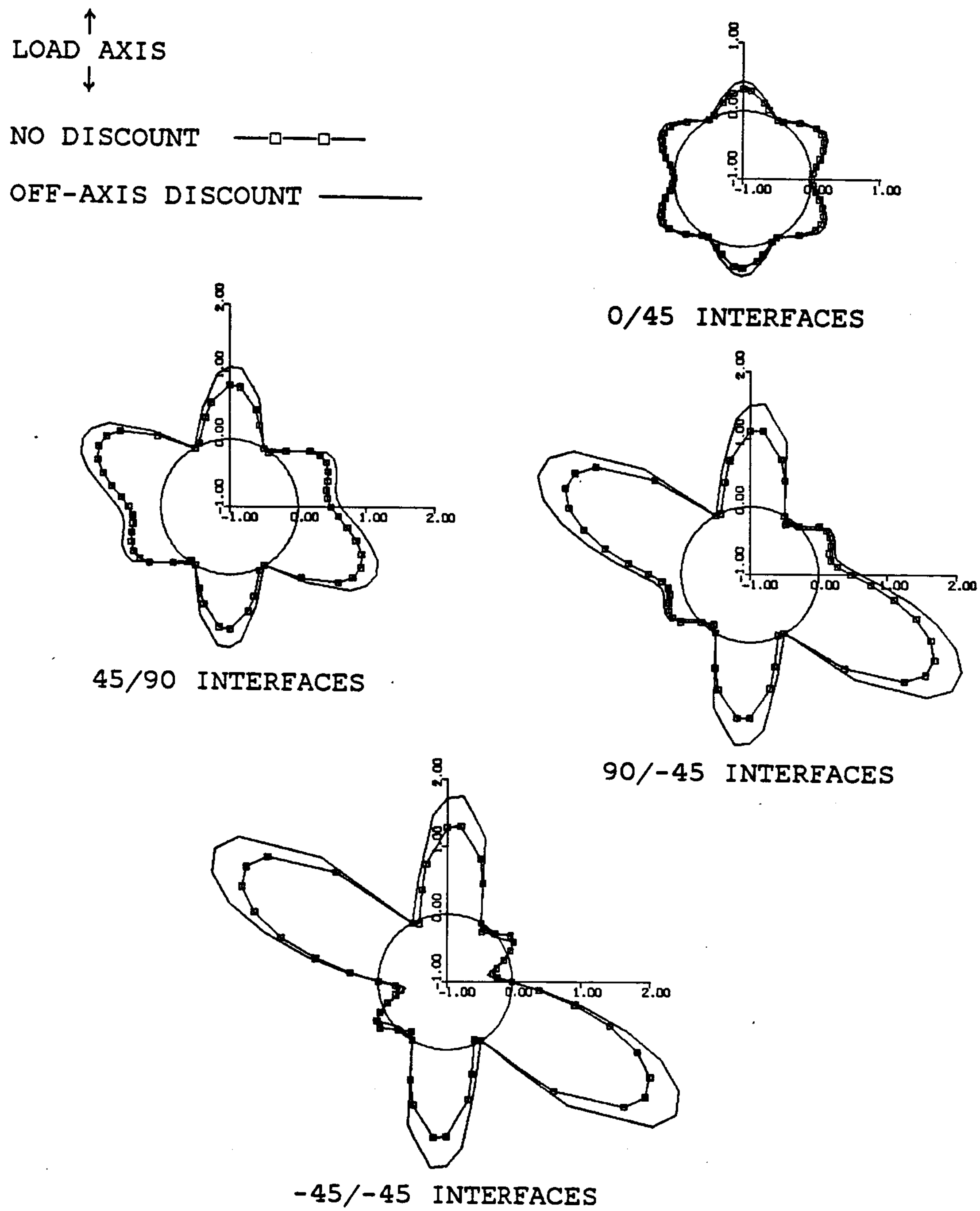

Figure 49: Normalized Interlaminar Normal Stress on Hole Boundary

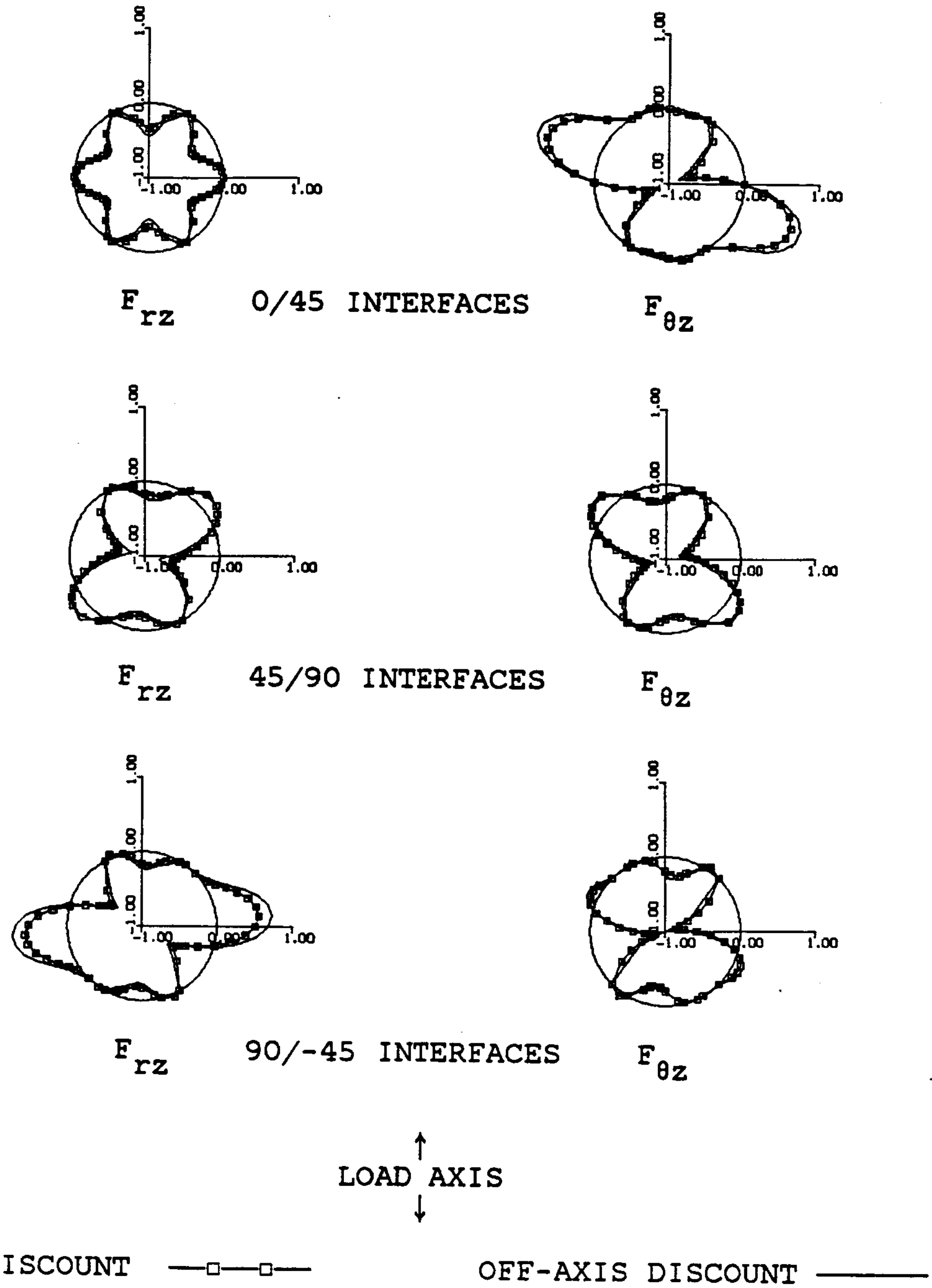

Figure 50: Normalized Interlaminar Shear Forces on Hole Boundary

255 and 285 deg. positions at the first 0/45 interface below each surface. The next highest G_{nd} were about 30 percent lower in magnitude, and were located at the next interface below the surface (45/90) at the 75 and 255 deg. positions. After discounting, the site of highest G_{nd} shifted to the second interface (45/90) such that its magnitude exceeded the maximum non-discounted case by about 35 percent. The effect of discounting on G_{nd} at the second interface was to shift the peak from the first and third quadrants to the second and fourth, and increase the magnitude of this peak by a factor of two. No other interface except the second experienced such a drastic change. The magnitude and location of the peak G_{nd} at the first interface was not affected significantly by discounting. Examining the other interfaces through the thickness, it becomes apparent that interfaces involving a 90 deg. ply are affected the most by off-axis ply discount. This is a reasonable result, considering that both plies at these interfaces were discounted. The only other interfaces of interest in the laminate involved 0 deg. plies, which were not discounted. Overall, the highest strain energy release rate occured with off-axis ply discount at the second interface from the surface (45/90) at the 105 and 285 deg. positions along the hole boundary. Supposing that delamination had indeed

initiated at one of these locations, further delamination growth and new initiation could not be predicted with Figures 46 and 47 since the first delaminations alter the analytical formulation.

Interlaminar stress and forces in Figures 49 and 50 indicate that a relatively small, but significant, change did occur as a result of the discounting. Both parameters increased overall in amplitude, which is twice as important in T-C fatigue loading because of the stress reversal. Recalling that these parameters repeat at similar interfaces through the thickness, the highest interlaminar normal stress, σ_z, occurred between the -45/-45 interfaces at the 110 and 290 deg. positions on the hole. The effect of discounting was to increase most peaks of σ_z by about 20 percent. The highest magnitudes of F_{rz} and $F_{\theta z}$ were at the 105 and 285 deg. positions on the 45/90 interfaces, and the 75 and 255 deg. positions on the 90/-45 interfaces, respectively. After discounting, the peak F_{rz} increased by nearly 30 percent, while the peak $F_{\theta z}$ increased by less than 20 percent.

The regions of maximum G_I were not available to use in actual delamination prediction; therefore, G_{nd} was used instead. The highest G_{nd} shifted between the first two occurrences of 0/45 and 45/90 interfaces for the two extreme cases of no discounted plies and essentially 100 percent off-axis ply discounting. Both of these interfaces have tensile σ_z at some point of the load cycle in the regions of high G_{nd}, and are therefore likely candidates for delamination. Thus, delamination is predicted to initiate at either of the following locations:

- The outermost 0/45 interfaces at the 75, 105, 255 and 285 deg. positions on the hole boundary.
- The outermost 45/90 interfaces at the 105 and 285 deg. positions on the hole boundary.

No prediction of strain level for delamination onset was attempted without knowledge of the mode I component of G_{nd}.

4.6 COMPARISON OF THEORY AND EXPERIMENT

4.6.1 Fatigue Loading

In the fully reversed T-C fatigue tests (R=-1), recall that delamination intiation at both load levels involved the outermost 0/45 interfaces in the region bounded by the 0-deg. tangents and the hole boundary. Frequently, this occurred in the second and fourth quadrants before the first and third. The outermost 45/90 interface was seen to delaminate coincidently or shortly after this same time near the 90 and 270 deg. positions on the hole boundary. This compares favorably with predictions based on the energy analysis. Additional support of the analysis is gained by comparing the extent of delamination revealed by the deply process in Figure 26 with the overall appearances of Figures 46 to 50, keeping in mind that the latter pertain only to delamination initiation, not growth. The favoring of the second and fourth quadrants at the outermost 0/45 interface was not predicted, but could have been caused by factors not incorporated into the analysis. For example, the crossing of adjacent 0 and +45 deg. transverse matrix cracks that are tangent to the hole occurs in the second and fourth quadrants at a very small distance away from the hole. The stress concentration at these two crossings may have precipitated local delamination, and was not considered in the strain energy release rate equation. Interlaminar normal stresses and shear forces at the 0/45 interfaces do not lend any additional insight to this anomaly, since they also are roughly equal in all four quadrants.

To emphasize the importance of not placing too much faith in the use of G_{nd} alone to predict initial and subsequent delamination locations, one may consider the non-zero value of this parameter at the outermost -45/-45 "interface". There was no indication of delamination within these two plies during any fatigue tests. Here, G_{nd} is far from the maximum in the laminate, but comparable to values at locations where delamination did occur. Therefore, other factors, such as the local stress state (which may be altered by preceding damage), should also be considered to predict delamination events. By similar reasoning, it is apparent that σ_z alone is not sufficient to predict delamination either. The -45/-45 interface just mentioned has the highest interlaminar normal stress in the entire laminate, according to the approximate method, yet delaminations involving this double-thick ply remained confined to the two interfaces shared by 90 deg. plies. The magnitude of the interlaminar shear forces within and surrounding the double -45 deg. plies may have influenced this behavior.

At the 45/90 interfaces, the position of local delamination initiation coincides with high G_{nd}, F_{rz}, $F_{\theta z}$, and moderate σ_z. At the 90/-45 interfaces, the position of local delamination initiation coincides with high G_{nd}, F_{rz} and $F_{\theta z}$, but low σ_z. Thus, it is possible that interlaminar shear forces may have had a more important role in delamination than σ_z in these fatigue tests. In conclusion, a sound approach to delamination onset prediction should involve both the energy method and a three-dimensional stress analysis.

The strain energy release rate formulation just presented is applicable to any axial loading, such as those used in this experimental investigation. Therefore, differences in the mechanisms of delamination initiation with various loadings must be attributable to the stress state alone, or some other factor not considered in this analysis (such as out-of-plane deformation). The delamination initiation sequences in T-T and C-C fatigue were not investigated thoroughly enough to make a definitive comparison with the analysis. Still, from the several radiographs obtained at various stages of life, it was apparent that delamination initiation under either of these loadings was the same as those for T-C fatigue. That is, the outermost 0/45 interfaces in the second and fourth quadrants were always part of delamination initiation. It could thus be said with a certain amount of caution that the delamination prediction scheme works for T-T, T-C and C-C fatigue tests with the laminate at hand. The emphasis here is on caution, recalling the different effects that T-T and C-C fatigue had on late-life delamination sites bounding 90 deg. plies in the laboratory. This type of behavior was most likely due to the different stress distributions under tension and compression load that develop after the introduction of damage around the hole. No explanation for this behavior could be found by examining Figures 46 - 50, but none should be expected since this not a matter of delamination initiation on the laminate level.

4.6.2 Quasi-Static Tension Loading

A single test was performed to evaluate the laminate's response to incrementally higher tensile load until failure was reached. The objective of the test was to pinpoint the location of delamination onset around the hole under static tension load. The procedure is to subject the specimen to some load that is suspected to initiate damage, perform NDE to record that state of damage, and repeat at a higher peak load until specimen failure. The NDE technique used was X-ray radiography, which necessitated the unloading and removal of the specimen from the testing machine after each load segment. In this respect, the quasi-static test resembles a low cycle, increasing amplitude fatigue test.

At what turned out to 82 percent of ultimate load, the face view radiograph appeared similar to the low cycle radiographs of fatigue-damaged specimens, with numerous transverse matrix cracks in off-axis plies surrounding the hole. Cracks in 0 deg. plies were limited to the locations tangent to the hole. It was very difficult to detect any delamination at this point, so there is no doubt that dense matrix cracking preceded delamination. A small region of either very dense matrix cracking or delamination initiation was visible at the intersection of the 0 deg. tangent crack and the hole boundary in the fourth quadrant, but could not be distinguished from drill-induced damage in the edge-view radiograph. During the subsequent load increment, the specimen failed at 9300 lb. (41 kN) before any sign of impending failure could be seen with the strain monitoring devices used (see Table 1), so no additional damage development data was obtained. If the questionable region in the radiograph at 82 percent of ultimate was indeed delamination onset, the implication would be that the damage initiation sequence is the same in quasi-static tension as in cyclic loading. Furthermore, the strain energy release rate scheme as modified in this chapter for discounted plies is reasonably accurate for predicting delamination onset in the current laminate under any of the load histories discussed.

Chapter V

SUMMARY AND CONCLUSIONS

Test Design and Methodology

- With proper design, T-C cyclic loading of thick laminates can be accommodated without large out-of-plane deflection in unsupported coupons for at least 90 percent of fatigue life. Circular holes drilled with an ultrasonic drill bit provide a consistent stress concentration that enables observation of unbiased damage development along a curved boundary in the interior of laminates.
- X-ray radiography, continuous stiffness monitoring, and C-scan are complementary and mutually consistent techniques for nondestructively evaluating damage development in graphite-epoxy laminates. Some evidence suggests that the liquid X-ray penetrant may accelerate matrix degradation.
- The deply technique provides valuable information regarding the nature and location of delamination through the thickness of a laminate. Matrix cracks, especially in the interior of the laminate, were not clearly visible with this technique.

The following conclusions pertain to the $[(0/45/90/-45)_s]_4$ graphite-epoxy laminate used in the experimental portion of this investigation:

Static Properties

- Mean tensile and compressive strengths of undamaged coupons loaded monotonically to failure were 9400 and 10000 lb. (42 and 45 kN), respectively, or 38 and 41 ksi (260 and 280 MPa) computed on the mean unnotched area.
- Strain at failure measured across the hole with a one inch extensometer was 7300 $\mu\varepsilon$ in tension and approximately 8000 $\mu\varepsilon$ in compression (extrapolated).
- Dense matrix cracks in off-axis plies and tangent to the hole in 0 deg. plies preceded delamination in quasi-static tension loading. Many of the off-axis cracks are concentrated along the 0 deg. tangents.
- The tensile fracture surface revealed that all plies except the -45 deg. plies had failed along a section through the hole and transverse to the loading axis. The -45 deg. plies were often without fiber fractures, in which case they sheared out of the adjoining 90 deg. plies. This was the only significant delamination visible at the fracture surface.

- The compression fracture surface indicated a crushing mode of failure. Many delaminations were visible, but plies were fractured roughly along a section transverse to the loading axis and through the hole. The largest delaminations were along 0 deg. plies.

Tension-Compression Fatigue

- For the fully reversed load ratios (R=-1), fatigue life at high level (5500 lb., 22.2 ksi, or 24.5 kN, 143 MPa) was about 100K cycles. At the low level (4500 lb., 18.3 ksi, or 20.0 kN, 125 MPa), fatigue life varied from 451K cycles to run-outs at 2.6M cycles. Remote axial strains in undamaged material at the high and low load levels were 2900 and 2400 $\mu\varepsilon$, respectively.
- Continuous monitoring of stiffness degradation suggested the classification of life into three stages. The first stage, lasting about 10 percent of finite fatigue life, consisted of rapid stiffness loss and initiation of most unique modes of damage. The second stage lasted about 80 to 85 percent of life, and consisted of relatively slow stiffness loss and damage growth. The last stage spanned the last 10 to 15 percent of life, and coincided with the accelerating rate of damage events and stiffness loss that preceded failure. Damage development was seen to correlate

better with tensile or compressive stiffness degradation than with a simple cycle count.

- For R=-1 loading, compression stiffness degradation measured across the hole was as much as 60 percent of the initial value by the end of life. Tension stiffness degradation was not as dramatic.
- For load ratios greater than -1 but less than 0, the tension stiffness degraded as rapidly as or more rapidly than the compression stiffness. The failure mode, though, was always delamination-induced instability of the laminate during the compressive portion of the load cycle. For equal maximum tensile loads, higher compressive stresses shorten T-C fatigue life. Higher tensile load with equal compressive load also shortens life.
- Damage caused by T-C loading began as transverse matrix cracking in off-axis plies around the hole, and 0 deg. cracks tangent to the hole. Delamination initiation and growth was affected by the presence of prominent matrix cracks at the hole. Zero degree cracks and their associated delaminations grew faster near the surface of the laminate. Delamination growth along the 90 deg. plies was arrested by large cracks at the hole, and was not strongly affected by distance from the surface for much of the fatigue life.

- Load level at R=-1 did not affect the delamination initiation sequence significantly. The typical specimen delaminated first at the outermost 0/45 interface in the second and fourth quadrants around the hole, and soon after at the outermost 45/90 interface near the 90 and 270 deg. positions around the hole. Delaminations later filled in the first and third quadrants at 0/45 interfaces, and initiated in similar fashion at all interior interfaces. Toward the end of life, delamination growth accelerated, especially at interfaces near the laminate's surface.
- Micro-delamination initiation was seen away from the hole at the crossing of transverse matrix cracks in adjacent plies, especially near the surface. The leading edge of a growing delamination was sometimes uniform and bounded by a large matrix crack. Other times it appeared irregular due to scattered micro-delaminations.
- The fatigue fracture surface at the end of life for T-C loading revealed more delamination than the undamaged tensile fractures, but less than undamaged compression fractures. Surface 0 deg. plies had a shredded fracture appearance along the entire gage length. Except for a few double-thick -45 deg. plies that

exhibited no fiber fractures, most plies fractured along a transverse section through the hole.

- Peak loads applied cyclically in C-C followed by T-T induced less damage than an equal number of identical load peaks applied cyclically in T-C.
- Fatigue damage initiated by T-C or C-C loading does not grow readily under T-T fatigue.

Residual Tensile Strength

- In T-C fatigue ($-1 \le R < 0$), residual tensile strength increased during the first 10 to 40 percent of life to a maximum of 140 percent of the undamaged strength. After this, the tensile strength remained approximately constant to near the end of life, when the coupons were unable to sustain the compressive load.
- The fracture surface of coupons with fatigue damage involved delaminations that formed during cycling. In general, all plies except the double -45's fractured along transverse surface through the center of the hole. Many of the -45 deg. plies did not fail across fibers.

Theoretical Treatment of Delamination

- The strain energy release rate scheme originally developed for straight edge delamination modelling can be successfully modified to predict delamination initiation along a circular hole in a thick laminate.

- The strain energy release rate of a single delamination in the laminate decreases in an overall sense as the distance between that delamination and the laminate's surface increases. The most rapid decrease occurs within the outer ply group (8 plies) of the laminate.
- Selectively reducing lamina elastic properties (ply discount) to reflect pre-delamination damage (transverse matrix cracking) reduces the predicted delamination resistance of the laminate, without accounting for new modes of delamination that may result from such damage. It also shifts the location of highest delamination-induced strain energy release rate from the outermost ply interface to the second interface below the surface of the laminate.
- Experimentally observed delamination onset sites under quasi-static tension or T-T, T-C, and C-C cyclic load histories coincide with regions of high strain energy release rate and high interlaminar shear forces. Sign and magnitude of interlaminar normal stress did not strongly affect delamination onset.

REFERENCES

1. Dastin, S.J., "Composites for Aerospace Applications," Composite Materials: Testing and Design (Fifth Conference), ASTM STP 674, S.W. Tsai, Ed., American Society for Testing and Materials, 1979, pp. 5-13.

2. Jones, R.M., Mechanics of Composite Materials, Scripta Book Co., Washington D.C., 1975.

3. Liechti, K.M., Reifsnider, K.L., Stinchcomb, W.W. and Ulman, D.A., Miller, H.R., "Cumulative Damage Model for Advanced Composite Materials," Phase II Final Report, AFWAL-TR-84-4007, Materials Laboratory, Air Force Wright Aeronautical Laboratories, Air Force Systems Command, Wright-Patterson AFB, OH, March 1984. (General Dynamics Corp., Fort Worth Division, Fort Worth TX.)

4. Herakovich, C.T., "Influence of Layer Thickness on the Strength of Angle-Ply Laminates," J. Composite Materials, Vol. 16, May 1982, pp. 216-227.

5. Pagano, N.J. and Pipes, R.B., "The Influence of Stacking Sequence on Laminate Strength," J. Composite Materials, Vol.5, Jan. 1971, pp. 50-57.

6. Stalnaker, D.O. and Stinchcomb, W.W., "Load History - Edge Damage Studies in Two Quasi-Isotropic Graphite Epoxy Laminates," Composite Materials: Testing and Design (Fifth Conference), ASTM STP 674, S.W. Tsai, Ed., American Society for Testing and Materials, 1979, pp. 620-641.

7. Pagano,N.J. and Pipes, R.B., "Some Observations on the Interlaminar Strength of Composite Laminates," Int. J. Mechanical Sciences, Vol. 15, 1973, pp. 679-688.

8. Herakovich, C.T., "On the Relationship Between Engineering Properties and Delamination of Composite Materials," J. Composite Materials, Vol. 15, July 1981, pp. 336-348.

9. Pipes, R.B. and Pagano, N.J., "Interlaminar Stresses in Composite Laminates - An Approximate Elasticity Solution," J. Applied Mechanics, Vol. 41, 1974, p. 668.

10. Pipes, R.B. and Pagano, N.J. "Interlaminar Stresses in Composite Laminates Under Uniform Axial Extension," J. Composite Materials, Vol. 4, Oct. 1970, pp. 538-548.

11. Herakovich, C.T., "On Thermal Edge Effects in Composite Laminates," Int. J. Mechanical Sciences, Vol. 18, 1976, pp. 129-134.

12. Wang, A.S.D., Crossman, F.W., "Some New Results on Edge Effect in Symmetric Composite Laminates," J. Composite Materials, Vol. 11, January 1977, pp. 92-106.

13. Wang, A.S.D., Slomiana, M. and Bucinell, R., "A Three Dimensional Finite Element Analysis of Delamination Growth in Composite Laminates. Part I, The Energy Methods and Case-Study Problems," NADC-84017-60, Naval Air Development Center, Warminster PA, September 1983.

14. Wilkins, D.J., Eisenmann, J.R., Canim, R.A., Margolis, W.S. and Benson, R.A., "Characterizing Delamination Growth in Graphite-Epoxy," Damage in Composite Materials, ASTM STP 775, K.L. Reifsnider, Ed., American Society for Testing and Materials, 1982, pp. 168-183.

15. Rosenfeld, M.S. and Gause, L.W., "Compression Fatigue Behavior of Graphite/Epoxy in the Presence of Stress Raisers," Fatigue of Fibrous Composite Materials, ASTM STP 723, American Society for Testing and Materials, 1981, pp. 174-196.

16. Konish, H.J. and Whitney, J.M., "Approximate Stresses in an Orthotropic Plate Containing a Circular Hole," J. Composite Materials, Vol. 9, April 1975, pp. 157-166.

17. Lekhnitskii, S.G., Anisotropic Plates, translated from the second Russian edition by Tsai, S.W. and Cheron, T., Gordon and Breach Science Publishers Inc., New York NY, 1968.

18. Kress, G.R. and Stinchcomb W.W., "Fatigue Response of Notched Graphite Epoxy Laminates," Recent Advances in Composites in the United States and Japan, ASTM STP 864, American Society for Testing and Materials, 1985.

19. Black, N.F. and Stinchcomb, W.W., "Compression Fatigue Damage in Thick, Notched Graphite/Epoxy Laminates," Long-Term Behavior of Composites, ASTM STP 813, T.K. O'Brien, Ed., American Society for Testing and Materials, Philadelphia, 1983, pp. 95-115.

20. Whitcomb, J.D., "Experimental and Analytical Study of Fatigue Damage in Notched Graphite/Epoxy Laminates," Fatigue of Fibrous Composite Materials, ASTM STP 723, American Society for Testing and Materials, 1981, pp. 48-63.

21. Chang, F.H., Gordon, D.E., Gardner, A.H., "A Study of Fatigue Damage in Composites by Nondestructive Testing Techniques," Fatigue of Filamentary Composite Materials, ASTM STP 636, K.L. Reifsnider and K.N. Lauraitis, Eds., American Society for Testing and Materials, 1977, pp. 57-72.

22. Ryder, J.T. and Walker, E.K., "The Effect of Compressive Loading on the Fatigue Lifetime of Graphite/Epoxy Laminates," AFML-TR-79-4128, Final Technical Report, Air Force Materials Laboratory, Air Force Systems Command, Wright-Patterson AFB, OH, October 1979. (Lockheed-California Co., Burbank CA.)

23. Ramani, S.V. and Williams, D.P., "Notched and Unnotched Fatigue Behavior of Angle-Ply Graphite/Epoxy Composites," Fatigue of Filamentary Composite Materials, ASTM STP 636, K.L. Reifsnider and K.N. Lauraitis, Eds., American Society for Testing and Materials, 1977, pp. 27-46.

24. Reifsnider, K.L., Stinchcomb, W.W., O'Brien, T.K., "Frequency Effects on a Stiffness-Based Fatigue Failure Criterion in Flawed Composite Specimens," Fatigue of Filamentary Composite Materials, ASTM STP 636, K.L. Reifsnider and K.N. Lauraitis, Eds., American Society for Testing and Materials, 1977, pp. 171-184.

25. Roderick, G.L. and Whitcomb, J.D., "Fatigue Damage of Notched Boron/Epoxy Laminates Under Constant-Amplitude Loading," Fatigue of Filamentary Composite Materials, ASTM STP 636, K.L. Reifsnider and K.N. Lauraitis, Eds., American Society for Testing and Materials, 1977, pp. 73-88.

26. Ratwani, M.M. and Kan, H.P., "Effect of Stacking Sequence on Damage Propagation and Failure Modes in Composite Laminates," Damage in Composite Materials, ASTM STP 775, K.L. Reifsnider, Ed., American Society for Testing and Materials, 1982, pp. 211-228.

C-3

27. Rybicki, E.F. and Schmueser, D.W., "Effect of Stacking Sequence and Lay-Up Angle on Free Edge Stresses Around a Hole in a Laminated Plate Under Tension," J. Composite Materials, Vol. 12, July 1978, pp. 300-313.

28. Whitney, J.M. and Kim, R.Y., "Effect of Stacking Sequence on the Notched Strength of Laminated Composites," Composite Materials: Testing and Design, (Fourth Conference), ASTM 617, American Society for Testing and Materials, 1977, pp. 229-242.

29. Daniel, I.M., Rowlands, R.E. and Whiteside, J.B., "Effects of Material and Stacking Sequence on Behavior of Composite Plates with Holes," Experimental Mechanics, Vol. 14, No. 1, January 1974, pp. 1-9.

30. Harris, C.E. and Morris, D.H., "An Evaluation of the Effects of Stacking Sequence and Thickness on the Fatigue Life of Quasi-Isotropic Graphite/Epoxy Laminates," NASA Contractor Report 172169, April 1983.

31. Whitney, J.M. and Nuismer, R.J., "Stress Fracture Criteria for Laminated Composites Containing Stress Concentrations, J. Composite Materials, Vol. 8, July 1974, pp. 253-265.

32. Poe, C.C. Jr., Sova, J.A., "Fracture Toughness of Boron/Aluminum Laminates With Various Proportions of 0° and ±45° Plies," NASA Technical Paper 1707, 1980.

33. Cruse, T.A., "Tensile Strength of Notched Composites," J. Composite Materials, Vol. 7, April 1973, pp. 218-229.

34. Lo, K.H., Wu, E.M. and Konishi, D.Y., "Failure Strength of Notched Composite Laminates," J. Composite Materials, Vol. 17, Sept 1983, pp. 384-398.

35. Reifsnider, K.L., Henneke, E.G. II, Stinchcomb, W.W. and Duke, J.C., "Damage Mechanics and NDE of Composite Laminates," Mechanics of Composite Materials, Z. Hashin and C.T. Herakovich, Eds., Proceedings of the IUTAM Symposium on Mechanics of Composite Materials, Blacksburg VA, 1982, pp. 399-420.

36. Reifsnider, K.L., Schulte, K. and Duke, J.C., "Long-Term Fatigue Behavior of Composite Materials," Long Term Behavior of Composites, ASTM STP 813, T.K. O'Brien, Ed., American Society for Testing and Materials, Philadelphia, 1983, pp. 136-159.

37. Kriz, R.D. and Stinchcomb, W.W., "Effects of Moisture, Residual Thermal Curing Stresses, and Mechanical Load on the Damage Development in Quasi-Isotropic Laminates," Damage in Composite Materials, ASTM STP 775, K.L. Reifsnider, Ed., American Society for Testing and Materials, 1982, pp. 63-80.

38. Sun, C.T. and Chan, W.S., "Frequency Effect on the Fatigue Life of a Laminated Composite," Composite Materials: Testing and Design (Fifth Conference), ASTM STP 674, S.W. Tsai, Ed., American Society for Testing and Materials, 1979, pp. 418-430.

39. Jamison, R.D., Highsmith, A.L. and Reifsnider, K.L., "Strain Field Response of 0-deg. Glass/Epoxy Composites Under Tension," Composites Technology Review, Vol. 3, No. 4, pp. 158-159.

40. Reifsnider, K.L. and Highsmith, A.L., "Stress Redistribution in Composite Laminates," Composites Technology Review, Vol. 3, No. 1, 1981, pp. 32-34.

41. Jamison, R.D. and Reifsnider, K.L., "Advanced Fatigue Damage Development in Graphite Epoxy Laminates," AFWAL-TR-82-3103, Flight Dynamics Laboratory (FIBE), Air Force Wright Aeronautics Laboratories (AFSC), Wright-Patterson AFB, OH, December 1982. (VA Polytechnic Institute and State University, Blacksburg, VA.)

42. Talug, A. and Reifsnider, K.L., "Analysis of Stress Fields in Composite Laminates with Interior Cracks," VPI-E-78-23, College of Engineering Report, Virginia Polytechnic Institute and State University, 1978.

43. Crossman, F.W. and Wang A.S.D., "The Dependence of Transverse Cracking and Delamination on Ply Thickness in Graphite/Epoxy Laminates," Damage in Composite Materials, ASTM STP 775, K.L. Reifsnider, Ed., American Society for Testing and Materials, 1982, pp. 118-139.

44. O'Brien, T.K., "Analysis of Local Delamination and Their Influence on Composite Laminate Behavior," NASA TM 85728, 1984.

45. Wang, A.S.D., Kishore, N.N. and Li, C.A., "On Crack Development in Graphite-Epoxy $[0_2/90_n]_s$ Laminates under Uniaxial Tension," presented at the International Symposium on Composites: Materials and Engineering, University of Delaware, September 1984.

46. O'Brien, T.K., "Stiffness Change as a Nondestructive Damage Measurement," Mechanics of Nondestructive Testing, W.W. Stinchcomb, Ed., Plenum Press, New York, 1980, pp. 101-121.

47. Camponeschi, E.T. and Stinchcomb, W.W., "Stiffness Reduction as an Indicator of Damage in Graphite/Epoxy Laminates," Composite Materials: Testing and Design (Sixth Conference), ASTM STP 787, I.M. Daniel, Ed., American Society for Testing and Materials, 1982, pp. 225-246.

48. Reifsnider, K.L., Henneke, E.G. II, and Stinchcomb, W.W., "Defect-Property Relationships in Composite Materials," AFML-TR-76-81, Part IV, Final Report, Air Force Materials Laboratory (MBM), Wright-Patterson AFB, OH, June 1979. (VA Polytechnic Institute and State University, Blacksburg VA.)

49. Wang, A.S.D. and Lau, C.E., "An Energy Method for Multiple Transverse Cracks in Graphite-Epoxy Laminates," Modern Developments in Composite Materials and Structures, presented at the ASME Winter Meeting, New York, 1979.

50. O'Brien, T.K., "Characterization of Delamination Onset and Growth in a Composite Laminate," Damage in Composite Materials, ASTM STP 775, K.L. Reifsnider, Ed., American Society for Testing and Materials, 1982, pp. 140-167.

51. O'Brien, T.K. and Raju, I.S., "Strain-Energy-Release Rate Analysis of Delamination Around An Open Hole in Composite Laminates," presented at the 25th AIAA/ASME/ASCE/AHS Structures, Structural Dynamics and Materials Conference, May 14-16, 1984, Palm Springs, CA.

52. O'Brien, T.K., "Mixed Mode Strain-Energy-Release Rate Effects on Edge Delamination of Composites," Effects of Defects in Composite Materials, ASTM STP 836, American Society for Testing and Materials, 1984, p. 125.

53. Phillips, E.P., "Effects of Truncation of a Predominantly Compression Load Spectrum on the Life of a Notched Graphite/Epoxy Laminate," Fatigue of Fibrous Composite Materials, ASTM STP 723, American Society for Testing and Materials, 1981, pp. 197-212.

54. Saff, C.R., "Compression Fatigue Life Prediction Methodology for Composite Structures - Literature Survey," NADC-78203-60, Interim Report, Commander Naval Air Development Center, Warminster PA, June 1980. (McDonnell Aircraft Co., St. Louis MI.)

55. Ryder, J.T. and Walker, E.K., "Effect of Compression on Fatigue Properties of a Quasi-Isotropic Graphite/Epoxy Composite," Fatigue of Filamentary Composite Materials, ASTM STP 636, K.L. Reifsnider and K.N. Lauraitis, Eds., American Society for Testing and Materials, pp. 3-26.

56. Clark, R.K. and Lisagor, W.B., "Effects of Method of Loading and Specimen Configuration on Compressive Strength of Graphite/Epoxy Composite Materials," NASA TM 81796, April 1980.

57. Ulman, D.A., Bruner, R.D., Reifsnider, K.L., Stinchcomb, W.W, and Henneke, E.G., "Damage Accumulation in Composites," Semi-Annual Progress Report No. 2, 15 March 1982 to 15 September 1982, Contract No. F33615-81-C-3226, Prepared for Air Force Wright Aeronautical Laboratories, FDL, AFSC, Wright-Patterson AFB, OH. (General Dynamics, Fort Worth Division, Fort Worth TX.)

58. Harris, C.E. and Morris, D.H., "Fracture Behavior of Thick, Laminated Graphite/Epoxy Composites," NASA Contractor Report 3784, March 1984, (VA Polytechnic Institute and State Univ., Blacksburg, VA.)

59. Whitcomb, J.D. and Raju, I.S., "Analysis of Interlaminar Stresses in Thick Composite Laminates With and Without Edge Delamination," NASA TM 85738, January 1984.

60. Ratwani, M.M and Kan, M.P., "Compression Fatigue Analysis of Fiber Composites," NADC-78049-60, Naval Air Development Center, Warminster PA, September 1979. (Northrop Corp., Hawthorne CA.)

61. Whitney, J.M., "A Residual Strength Degradation Model for Competing Failure Modes," Long-Term Behavior of Composites, ASTM STP 813, T.K. O'Brien, Ed., American Society for Testing and Materials, Philadelphia, 1983, pp. 225-245.

62. Walter, R.W., Johnson, R.W., June, R.R., and McCarty, J.E., "Designing for Integrity in Long-Life Composite Aircraft Structures," Fatigue of Filamentary Composite Materials, ASTM STP 636, K.L. Reifsnider and K.N. Lauraitis, Eds., American Society for Testing and Materials, 1977, pp. 228-247.

63. ASTM working document, proposed additions to ASTM D3878, Definitions of Terms Relating to High-Modulus Reinforcing Fibers and Their Composites.

64. Timoshenko, S.P. and Goodier, J.N., Theory of Elasticity, Third Edition, McGraw-Hill Book Co., New York, 1970.

65. Reddy, J.N., Finite Element Program "FEM2D," in An Introduction to the Finite Element Method, McGraw-Hill Book Co., New York, 1984.

66. Gibbins, M.N. and Stinchcomb, W.W., "Fatigue Response of Composite Laminates with Internal Flaws," Composite Materials: Testing and Design (Sixth Conference), ASTM STP 787, I.M. Daniel, American Society for Testing and Materials, 1982, pp. 305-322.

67. Sendeckyj, G.P., Maddux, G.E. and Porter, E., "Damage Documentation in Composites by Stereo Radiography," Damage in Composite Materials, ASTM STP 775, K.L. Reifsnider, Ed., American Society for Testing and Materials, 1982, pp. 16-26.

68. Rummel, W.D., Tedrow, T., Brinkerhoff, H.D., "Enhanced X-Ray Stereoscopic NDE of Composite Materials," AFWAL-TR-80-3053, Final Report, June 1980, FDL, AFSC, Air Force Wright Aeronautical Laboratories, Wright-Patterson AFB, OH. (Martin Marietta Corp., Denver CO.)

69. Freeman, S.M., "Characterization of Lamina and Interlaminar Damage in Graphite/Epoxy Composites by the Deply Technique," Composite Materials: Testing and Design (Sixth Conference), ASTM STP 787, I.M. Daniel, Ed., American Society for Testing and Materials, 1982, pp. 50-62.

70. Freeman, S.M., "Damage Progression in Graphite-Epoxy by a Deplying Technique," AFWAL-TR-81-3157, Final Report, December 1981, FDL, Air Force Wright Aeronautical Laboratories, AFSC, Wright-Patterson AFB, OH. (Lockheed-Georgia Company, Marietta GA.)

VIRGINIA TECH CENTER FOR COMPOSITE MATERIALS AND STRUCTURES

The Center for Composite Materials and Structures is a coordinating organization for research and educational activity at Virginia Tech. The Center was formed in 1982 to encourage and promote continued advances in composite materials and composite structures. Those advances will be made from the base of individual accomplishments of the forty members who represent ten different departments in two colleges.

The Center functions through an Administrative Board which is elected yearly and a Director who is elected for a three-year term. The general purposes of the Center include:

- collection and dissemination of information about composites activities at Virginia Tech,
- contact point for other organizations and individuals,
- mechanism for collective educational and research pursuits,
- forum and agency for internal interactions at Virginia Tech.

The Center for Composite Materials and Structures is supported by a vigorous program of activity at Virginia Tech that has developed since 1963. Research expenditures for investigation of composite materials and structures total well over seven million dollars with yearly expenditures presently approximating two million dollars.

Research is conducted in a wide variety of areas including design and analysis of composite materials and composite structures, chemistry of materials and surfaces, characterization of material properties, development of new material systems, and relations between damage and response of composites. Extensive laboratories are available for mechanical testing, nondestructive testing and evaluation, stress analysis, polymer synthesis and characterization, material surface characterization, component fabrication, and other specialties.

Educational activities include eight formal courses offered at the undergraduate and graduate levels dealing with the physics, chemistry, mechanics, and design of composite materials and structures. As of 1984, some 43 Doctoral and 53 Master's students have completed graduate programs and several hundred Bachelor-level students have been trained in various aspects of composite materials and structures. A significant number of graduates are now active in industry and government.

Various Center faculty are internationally recognized for their leadership in composite materials and composite structures through books, lectures, workshops, professional society activities, and research papers.

MEMBERS OF THE CENTER

Aerospace and Ocean Engineering
Raphael T. Haftka
William L. Hallauer, Jr.
Eric R. Johnson
Rakesh K. Kapania

Chemical Engineering
Donald G. Baird

Chemistry
James E. McGrath
Thomas C. Ward
James P. Wightman

Civil Engineering
R. M. Barker
Raymond H. Plaut

Electrical Engineering
Ioannis M. Besieris
Richard O. Claus

Engineering Science and Mechanics
Hal F. Brinson
Robert Czarnek
David Dillard
Norman E. Dowling
John C. Duke, Jr.
Daniel Frederick
O. Hayden Griffin, Jr.
Zafer Gurdal
Robert A. Heller
Edmund G. Henneke, II
Carl T. Herakovich
Robert M. Jones
Alfred C. Loos
Don H. Morris
Ali H. Nayfeh
Marek Pindera
Daniel Post
J. N. Reddy
Kenneth L. Reifsnider
C. W. Smith
Wayne W. Stinchcomb

Industrial Engineering and Operations Research
Joel A. Nachlas

Materials Engineering
David W. Dwight
D. P. H. Hasselman
Robert E. Swanson
W.J. van Ooij

Mathematics
Werner E. Kohler

Mechanical Engineering
Charles E. Knight
S. W. Zewari

Inquiries should be directed to:

Center for Composite Materials and Structures
College of Engineering
Virginia Tech
Blacksburg, VA 24061
Phone: (703) 961-4969

VIRGINIA POLYTECHNIC INSTITUTE AND STATE UNIVERSITY

UT PROSIM